UNCLASSIFIED

AFCRL- 70-0882

(1)

ANALYSIS AND ELEMENT PATTERN DESIGN OF PERIODIC ARRAYS OF CIRCULAR APERTURES ON CONDUCTING CYLINDERS

AD717199

Giorgio V. Borgiotti
Quirino Balzano

RAYTHEON CO. MISSILE SYSTEMS DIVISION
BEDFORD LABORATORIES
Hartwell Rd. Bedford, Massachusetts 01730

CONTRACT NO. F19628-70-C-0226
PROJECT NO. 4600
TASK NO. 460010
UNIT NO. 46001001

SCIENTIFIC REPORT NO. 1
NOVEMBER 1970

CONTRACT MONITOR: ALLAN SCHELL
MICROWAVE PHYSICS LABORATORY

JAN 29 1971

This document has been approved for public release and sale; its distribution is unlimited.

Prepared for
AIR FORCE CAMBRIDGE RESEARCH LABORATORIES
AIR FORCE SYSTEMS COMMAND
UNITED STATES AIR FORCE
Bedford, Massachusetts 01730

Reproduced by
NATIONAL TECHNICAL
INFORMATION SERVICE
Springfield, Va. 22151

UNCLASSIFIED

AFCRL- 70-0882

ANALYSIS AND ELEMENT PATTERN DESIGN OF PERIODIC ARRAYS OF CIRCULAR APERTURES ON CONDUCTING CYLINDERS

Giorgio V. Borgiotti
Quirino Balzano

RAYTHEON CO. MISSILE SYSTEMS DIVISION
BEDFORD LABORATORIES
Hartwell Rd. Bedford, Massachusetts 01730

CONTRACT NO. F19628-70-C-0226
PROJECT NO. 4600
TASK NO. 460010
UNIT NO. 46001001

SCIENTIFIC REPORT NO. 1
NOVEMBER 1970

CONTRACT MONITOR: ALLAN SCHELL
MICROWAVE PHYSICS LABORATORY

This document has been approved for public release and sale; its distribution is unlimited.

Prepared for
AIR FORCE CAMBRIDGE RESEARCH LABORATORIES
AIR FORCE SYSTEMS COMMAND
UNITED STATES AIR FORCE
Bedford, Massachusetts 01730

ABSTRACT

The analysis and the design of the elements of a large array of circular apertures on a triangular grid is approached by modeling the antenna as an infinite structure rotationally symmetric and periodic along the cylinder axis. Because of this particular symmetry every possible excitation is the superposition, with suitable weights, of a set of fundamental excitations having uniform magnitude and linear phase progression in the azimuthal direction and in the direction of the cylinder axis ("eigenexcitations"). Thus, by invoking superposition the electromagnetic analysis of the array is reduced to the solutions of the simpler boundary value problems pertinent to the set of eigenexcitations. This is done by expanding the field in normal modes in the region exterior to the cylinder and in the waveguides feeding the apertures, followed by a field matching at the cylinder surface (obtained approximately through Galerkin's method). The realized gain pattern of the radiators can be modified to a considerable extent by using an "element pattern shaping network" (in the radiator waveguides), serving the purpose of matching the array for a selected eigenexcitation. Criteria for the network design are given. A series of numerical examples illustrates the technique and shows that a "flat" element pattern can be thus obtained with a gain fall off with respect to the peak of less than 6 db at 80 degrees.

TABLE OF CONTENTS

	Page
ABSTRACT	iii
LIST OF ILLUSTRATIONS	vii
LIST OF SYMBOLS	xi
1. INTRODUCTION	1
2. THEORY OF INFINITE PERIODIC CYLINDRICAL ARRAYS	5
2.1 Structure Geometry	5
2.2 Array Eigenexcitations	6
2.3 Patterns and Reflection Coefficients for Arbitrary Excitations	8
3. THE ELECTROMAGNETIC PROBLEM FOR CYLINDRICAL ARRAYS OF CIRCULAR APERTURES	11
3.1 Aperture Field Match	11
3.2 Eigenpatterns	16
3.3 Remarks	20
4. ELEMENT PATTERN DESIGN	23
5. SELECTED NUMERICAL EXAMPLES AND DISCUSSION	27
6. CONCLUDING REMARKS	33
APPENDIX A - ORTHONORMALIZED EIGENEXCITATIONS	105
APPENDIX B - EXPRESSION OF TRANSFORMS OF VECTOR MODE FUNCTIONS	107
APPENDIX C - DERIVATION OF THE EXPRESSIONS FOR THE REFLECTION AND MODE CROSS COUPLING COEFFICIENTS	109
APPENDIX D - COMPUTATION OF CYLINDRICAL FUNCTIONS AND SPACE HARMONICS SERIES	113
REFERENCES	115

LIST OF ILLUSTRATIONS

Figure		Page
1	Geometry of the Structure	38
2	Element Pattern Shaping Network	38
3	Lattice 1	39
4	Reciprocal Lattice of Cylindrical Array	40
5	"Continuous" Cut-off of Floquet-Bessel Harmonics	41
6	Realized Gain Pattern. Circumferential Plane. Circumferential Polarization. Equiphase Match (R = 99.23λ)	42
7	Realized Gain Pattern. Circumferential Plane. Axial Polarization. Equiphase Match (99.23λ)	43
8	Realized Gain Pattern. Axial Plane. Equiphase Match (R = 99.23λ)	44
9	Realized Gain Pattern. Conical Section θ = 60°. Axial Polarization Excited. Equiphase Match (R = 99.23λ)	45
10	Realized Gain Pattern. Conical Section θ = 60°. Circumferential Polarization Excited. Equiphase Match (R = 99.23λ)	46
11	Realized Gain Pattern. Circumferential Plane. Circumferential Polarization. Equiphase Match (R = 49.62λ)	47
12	Realized Gain Pattern. Circumferential Plane. Axial Polarization. Equiphase Match (R = 49.62λ)	48
13	Realized Gain Pattern. Axial Plane. Equiphase Match (R = 49.62λ)	49
14	Realized Gain Pattern. Conical Section θ = 60°. Axial Polarization Excited. Equiphase Match (R = 49.62λ)	50
15	Realized Gain Pattern. Conical Section θ = 60°. Circumferential Polarization Excited. Equiphase Match (R = 49.62λ)	51
16	Realized Gain Pattern. Circumferential Plane. Circumferential Polarization. (R = 11.57λ)	52
17	Realized Gain Pattern. Circumferential Plane. Axial Polarization. Equiphase Match (R = 11.57λ)	53
18	Realized Gain Pattern. Axial Plane. Equiphase Match (R = 11.57λ)	54
19	Realized Gain Pattern. Conical Section θ = 60°. Axial Polarization Excited. Equiphase Match (R = 11.57λ)	55

LIST OF ILLUSTRATIONS (Cont.)

Figure		Page
20	Realized Gain Pattern. Conical Section θ = 60°. Circumferential Polarization Excited. Equiphase Match (R = 11.57λ)	56
21	Lattice 2	57
22	Realized Gain Pattern. Circumferential Plane. Circumferential Polarization (R = 49.33λ)	58
23	Realized Gain Pattern. Axial Plane. Axial Polarization. (R = 49.33λ)	59
24	Realized Gain Pattern. Conical Section θ = 60°. Axial Polarization Excited. Equiphase Match (R = 49.33λ)	60
25	Realized Gain Pattern. Conical Section θ = 30°. Axial Polarization Excited. Equiphase Match (R = 49.33λ)	61
26	Realized Gain Pattern. Conical Section θ = 60°. Circumferential Polarization Excited. Equiphase Match (R = 49.33λ)	62
27	Realized Gain Pattern. Conical Section θ = 30°. Circumferential Polarization Excited. Equiphase Match (R = 49.33λ)	63
28	Realized Gain Pattern. Conical Section θ = 60°. Axial Polarization Excited. Match for w = k sin 80°. (R = 49.33λ)	64
29	Realized Gain Pattern. Conical Section θ = 30°. Axial Polarization Excited. Match for w = k sin 80°. (R = 49.33λ)	65
30	Realized Gain Pattern. Conical Section θ = 60°. Circumferential Polarization Excited. Match for i/R = k sin 80°. (R = 49.33λ)	66
31	Realized Gain Pattern. Conical Section θ = 30°. Circumferential Polarization Excited. Match for i/R = k sin 80°. (R = 49.33λ)	67
32	Realized Gain Pattern. Circumferential Plane. Axial Polarization (R = 49.33λ)	68
33	Realized Gain Pattern. Circumferential Plane. Circumferential Polarization (R = 11.61λ)	69
34	Realized Gain Pattern. Axial Plane. Axial Polarization. (R = 11.61λ)	70
35	Realized Gain Pattern. Conical Section θ = 60°. Axial Polarization Excited. Equiphase Match (R = 11.61λ)	71
36	Realized Gain Pattern. Conical Section θ = 30°. Axial Polarization Excited. Equiphase Match (R = 11.61λ)	72

LIST OF ILLUSTRATIONS (Cont.)

Figure		Page
37	Realized Gain Pattern. Conical Section θ = 60°. Circumferential Polarization Excited. Equiphase Match (R = 11.61λ)	73
38	Realized Gain Pattern. Conical Section θ = 30°. Circumferential Polarization Excited. Equiphase Match (R = 11.61λ)	74
39	Realized Gain Pattern. Conical Section θ = 60°. Axial Polarization Excited. Match for w = k sin 80° (R = 11.61λ)	75
40	Realized Gain Pattern. Conical Section θ = 30°. Axial Polarization Excited. Match for w = k sin 80° (R = 11.61λ)	76
41	Realized Gain Pattern. Conical Section θ = 60°. Circumferential Polarization Excited. Match for i/R = k sin 80° (R = 11.61λ)	77
42	Realized Gain Pattern. Conical Section θ = 30°. Circumferential Polarization Excited. Match for i/R = k sin 80°. (R = 11.61λ)	78
43	Realized Gain Pattern. Frequency Sensitivity	79
44	Realized Gain Pattern. Frequency Sensitivity	80
45	Maximum Angular Extension of Array Aperture	81
46	Array Pattern. Circumferential Plane. Circumferential Polarization. Number of Array Elements 37	82
47	Array Pattern. Circumferential Plane. Circumferential Polarization. Number of Array Elements 313	83
48	Array Scan Coverage. Circumferential Plane. Circumferential Polarization. Equiphase Match. Number of Array Elements 37	84
49	Array Scan Coverage. Axial Plane. Axial Polarization. Equiphase Match. Number of Array Elements 37	85
50	Array Scan Coverage. Circumferential Plane. Circumferential Polarization Match for i/R = k sin 80°. Number of Array Elements 37	86
51	Array Scan Coverage. Axial Plane. Axial Plane Match for w = k sin 80°. Number of Array Elements 37	87
52	Array Scan Coverage. Circumferential Plane. Circumferential Polarization. Equiphase Match. Number of Array Elements 313	88
53	Array Scan Coverage. Axial Plane. Axial Polarization. Equiphase Match. Number of Array Elements 313	89

LIST OF ILLUSTRATIONS (Cont.)

Figure		Page
54	Array Scan Coverage. Circumferential Plane. Circumferential Polarization Match for $1/R = k \sin 80°$. Number of Array Elements 313	90
55	Array Scan Coverage. Axial Plane. Axial Polarization Match for $w = k \sin 80°$. Number of Array Elements 313	91
56	Array Scan Coverage. Circumferential Plane. Circular Polarization. Equiphase Match. Number of Array Elements 37	92
57	Array Scan Coverage. Conical Section $\theta = 60°$. Circular Polarization. Equiphase Match. Number of Array Elements 37	93
58	Array Scan Coverage. Conical Section $\theta = 30°$. Circular Polarization. Equiphase Match. Number of Array Elements 37	94
59	Array Scan Coverage. Circumferential Plane. Circular Polarization. Number of Array Elements 37	95
60	Array Scan Coverage. Conical Section $\theta = 60°$. Circular Polarization. Number of Array Elements 37	96
61	Array Scan Coverage. Conical Section $\theta = 30°$. Circular Polarization. Number of Array Elements 37	97
62	Array Scan Coverage. Circumferential Plane. Circular Polarization. Equiphase Match. Number of Array Elements 313	98
63	Array Scan Coverage. Conical Section $\theta = 60°$. Circular Polarization. Equiphase Match. Number of Array Elements 313	99
64	Array Scan Coverage. Conical Section $\theta = 30°$. Circular Polarization. Equiphase Match. Number of Array Elements 313	100
65	Array Scan Coverage. Circumferential Plane. Circular Polarization. Number of Array Elements 313	101
66	Array Scan Coverage. Conical Section $\theta = 60°$. Circular Polarization. Number of Array Elements 313	102
67	Array Scan Coverage. Conical Section $\theta = 30°$. Circular Polarization. Number of Array Elements 313	103

LIST OF SYMBOLS

r, θ, ϕ	Spherical coordinates
ρ, ϕ, z	Cylindrical coordinates
$\underline{s}_1, \underline{s}_2$	Lattice basis vectors
d	Circumferential spacing of elements
h	Axial spacing of elements
$\underline{t}_1, \underline{t}_2$	Reciprocal vectors of $\underline{s}_1, \underline{s}_2$
ξ	Circumferential coordinate over cylinder surface
(u, w)	Coordinates of wave number plane
$\underline{u}_{opq}$	Vector representative of a point of reciprocal lattice
$\underline{e}(\underline{u}_o)$	Array eigenexcitation
N	Number of elements in one ring
R	Cylinder radius
i	Eigenexcitation azimuthal number
$\underline{a}$	Array excitation column vector
$c(i, w_o)$	Projection of $\underline{a}$ on $\underline{e}$ ($\underline{u}o$)
$\underline{b}$	Reflected wave column vector
$\Gamma(i, w_o)$ and $\Gamma(\underline{u}_o)$	Reflection coefficient of eigenexcitation $\underline{e}(\underline{u}_o)$
$\vec{F}(\theta, \phi)$	Radiation pattern for arbitrary excitation
$\vec{f}_o(\theta, \phi)$	Realized gain pattern for the reference element
$\vec{g}(i, w_o, \gamma, \theta, \phi)$	Far field for eigenexcitation $e(\underline{u}_o)$
$\underline{s}$	Position vector over cylinder surface
$\underline{e}_a(s)$	Axial mode function
$\underline{e}_c(s)$	Circumferential mode function
$\underline{\mathcal{E}}_a(s)$	Fourier Transform of $\underline{e}_a(s)$
$\underline{\mathcal{E}}_c(s)$	Fourier Transform of $\underline{e}_c(s)$
B_{ao}	Shunt susceptance at element axial polarization port
B_{co}	Shunt susceptance at element circumferential polarization port

LIST OF SYMBOLS (Cont.)

Y_o	Circular waveguide modal admittance for TE_{11} mode
$\sqrt{\frac{G_{ao}}{Y_o}} = \frac{n_1}{n_2}$	Turn ratio of perfect transformer at element axial polarization port
$\sqrt{\frac{G_{co}}{Y_o}} = \frac{n_1}{n_2}$	Turn ratio of perfect transformer at element circumferential polarization port
$Y_a(\underline{u}_o)$	Active admittance
$\underline{E}_t(s)$	Transverse electric field
$A(\underline{u}_{opq})$	Bessel-Floquet's expansion coefficient
$\underline{H}_t(s)$	Transverse magnetic field
C	Element all area
λ	Free space wavelength
$k = 2\pi/\lambda$	Free space propagation constant
η	Free space impedance
$L_{aa}(\underline{u}_o)$	Self-admittance of axially polarized mode for eigenexcitation $\underline{e}(\underline{u}_o)$
$L_{cc}(\underline{u}_o)$	Self-admittance of circumferentially polarized mode for eigenexcitation $\underline{e}(\underline{u}_o)$
$L_{ac}(\underline{u}_o)$	Mutual admittance between modes for eigen-excitation $\underline{e}(\underline{u}_o)$
a	Radiating aperture radius
J_1	Bessel function of first order and king
J_1'	Derivative of J_1
x_{11}'	First solution of $J_1'(x) = 0$

1. INTRODUCTION

It is the purpose of this report to present certain recent developments in conformal array theory and design. Some results are of a theoretical nature, that is, they establish effective methods of analysis for practical structures thus allowing a better insight of their electromagnetic behavior. Other results are of direct relevance for the design. In fact a technique is introduced which allows the modification of the realized gain pattern of an element via a control of the mutual coupling mechanism, simply by placing a matching network in the element waveguides. Through this method it is possible to tailor the element pattern to meet the scan coverage requirement of the array: if for example the array is designed for wide angle performance, the radiation at direction near grazing incidence can be enhanced at the expense of broadside gain.

Conformal array theory has significantly advanced during the last two to three years. Methods of analysis for cylindrical arrays, taking into account mutual coupling, have been developed for idealized structures consisting of infinite slits fed by parallel plate waveguides [1-3]. More recently cylindrical infinite arrays of rectangular apertures, polarized in circumferential direction, have been studied by Gladman [4] and Sureau and Hessel [5] who considered elements in a rectangular grid. A mutual coupling analysis of an array consisting of a finite number of rings of rectangular axially polarized apertures in triangular arrangement has also been performed by Borgiotti and Balzano [6], who showed dependence of the element pattern upon its distance from the edge of the array.[1]

In this report arrays of flush mounted circular apertures are considered. The apertures are arranged in a triangular lattice, as it is in most modern arrays, to save on the number of elements. The structure investigated is

[1] Some of the results presented in this paper have been already presented by the authors at the U.R.S.I Fall Meeting 1970, Ohio State University, Columbus, Ohio, Sept. 15-17, 1970.

infinite and periodic along the cylinder axis and in the circumferential sense. This model is accurate except for the elements in the proximity of the array edge. The technique for the analysis is based on a systematic exploitation of the translational and rotational symmetry of the structure. Every arbitrary "free" array excitation [7] is decomposed into a set of elementary special excitations matching the symmetry of the structure, in the sense of being eigenvectors of the symmetry operators representing the congruences of the structure [8]. The analysis of the structure for these "eigenexcitations" is much simpler than in the general case, which on the other hand can be studied by applying superposition [1-3].

The usefulness of the analysis and design technique introduced here is illustrated by a number of numerical examples. Two cylinders with radii equal to approximately 11 λ and 50 λ with two different element spacings have been studied in detail. The effect of different matching conditions on the wide angle scan performance has been investigated. It has been shown that element patterns can be obtained which are "flat" within a fraction of db up to 60 degrees from broadside and with a gain fall-off of less than 6 db up to 80 degrees in the principal planes. It has also been checked that these favorable characteristics are preserved in a frequency band of several percent around the center frequency. Also for each cylinder a number of curves of gain vs. scan angle for two arrays having broadside gains of approximately 20 and 30 db have been calculated, for different match conditions, showing the effectiveness of the technique in improving the scan coverage of the array.

The report is organized in the following way. In Section 2 the geometry of the structure is defined and certain general results are established depending only upon the special symmetry of the structure. It is shown how remarkably far one can go in the development of the theory on the basis of pure symmetry considerations without specifying the physical details of the antenna. In Section 3 the method of solution of the boundary value problem for the particular structure under study is outlined briefly (most of the analytical details being confined in the Appendices). Section 4 shows how the analytic technique developed here is not only valuable for the analysis of a

given structure, but can also be used as an effective design tool. Element pattern design criteria are observed. Finally in Section 5 selected numerical examples are presented.

2. THEORY OF INFINITE PERIODIC CYLINDRICAL ARRAYS

2. Structure Geometry

For the developments of this section there is no need to specify the nature of the radiating elements, all the results being a mere consequence of the axial and circumferential periodicity of the structure. However, since in later sections the attention will be focused on aperture arrays, it is this type of structures which will be indicated in the illustrations.

To specify the geometric reference the axis of the cylinder is assumed to be coincident with the z axis of a system of rectangular coordinates. A polar system r, θ, φ and a cylindrical system ρ, z, φ are associated in the usual way with the rectangular system. With reference to Figure 1 the symmetry of the structure is conveniently defined by the pair of column vectors:

$$\underline{s}_1 = \begin{bmatrix} d \\ 0 \end{bmatrix} \qquad \underline{s}_2 = \begin{bmatrix} \frac{d}{2} \\ h \end{bmatrix} \tag{1}$$

In analogy with the planar case [9-11], the reciprocal (row) vectors $\underline{t}_i$ are defined by the equations:

$$\underline{t}_i \cdot \underline{s}_k = 2\pi\delta_{ik} \qquad (i, k = 1, 2) \tag{2}$$

where δ_{ik} is Kronecker's delta. From (2):

$$\underline{t}_1 = \left[\frac{2\pi}{d}, -\frac{\pi}{h}\right] \qquad \underline{t}_2 = \left[0, \frac{2\pi}{h}\right] \tag{3}$$

In addition to the angular coordinate φ, it is convenient to introduce a coordinate ξ on the array perimeter defined as:

Preceding page blank

$$\xi = R\varphi \tag{4}$$

where R is the cylinder radius. Thus a point of the cylinder surface can be individuated by the position column vector:

$$\underline{s} = \begin{bmatrix} \xi \\ z \end{bmatrix} \tag{5}$$

The radiator whose center is located at $z = 0$ and $\xi = \varphi = 0$ will be called "reference" element. All the array elements will occupy the positions defined by the vectors:

$$\underline{s}_{mn} = m\underline{s}_1 + n\underline{s}_2 \tag{6}$$

where n indicates the ring and m the position inside it.

2.2 Array Eigenexcitations

Array "free" excitation is always considered in this paper (i. e. defined as the set of incident waves in the transmission lines feeding the elements). Without loss of generality each radiator will be assumed to have only a single excited port. If the elements are excited at two input ports (as it occurs for circularly polarized antennas) the response[2] of the array in this situation can be obtained by superposition from the solution of the two partial problems relative to the excitation of a port at a time, the other being terminated in the impedance of its (equivalent) generator. Every array excitation is represented by the infinite dimensional column vector $\underline{a}$, belonging to the array "input space". Each of its component a_{mn} clearly indicates the excitation of the element in the position defined by m and n.

[2] The set of reflected waves at the input ports and the array far field pattern are concisely indicated as the "response" of the array (for a given excitation).

The interactions among the array elements can be described by the scattering (or mutual coupling) matrix $\underline{\underline{S}}$ (of infinite order). Its eigenvectors are the "eigenexcitations" of the array [3], namely those sets of incident waves producing identical active reflection coefficients at each element input port. As discussed in Appendix A, they are given by the infinite dimensional vectors (suitably normalized):

$$\underline{e}(u_o, v_o) = \underline{e}(\underline{u}_o) = \sqrt{\frac{h}{2\pi N}} \left| \exp \left[-j\underline{u}_o (m\underline{s}_1 + n\underline{s}_2) \right] \right| \tag{7}$$

where m is an integer between 0 and N-1, n any integer and $\underline{u}_o$ is a row vector representing the ordered pair of numbers:

$$\underline{u}_o = \left[u_o, w_o \right] \tag{8}$$

with $u_o = i/R$. Each eigenexcitation is individuated by the azimuthal number i (indicating that the phase progression between two adjacent elements in a ring is $2\pi i/N$) and by the longitudinal number w_o (corresponding to a phase progression $w_o h$ between two contiguous rings). All the eigenvectors are obtained by having i to take all the integers values from -N to N-1 and w all the real values from $-\pi/2h$ to $\pi/2h$ (Appendix A).

In view of the further developments it is convenient to associate to each bidimensional vector $\underline{u}_o$, a regular lattice of points in the u, w plane defined by the set of vectors (reciprocal lattice):[3]

$$\underline{u}_{opq} = \underline{u}_o + p\underline{t}_1 + q\underline{t}_2 \tag{9}$$

with p and q arbitrary integers, and $\underline{t}_1$ and $\underline{t}_2$ given by (3). The rectangular coordinates of the points (9) are given explicitly by:

[3] The geometry of the reciprocal lattices is shown in Figure 4 for a particular case.

$$u_{opq} = \frac{i}{R} + p\frac{2\pi}{d} \qquad w_{opq} = w_o + (2q-p)\frac{\pi}{h} \tag{10}$$

In Section 3 the responses of the array to the set of eigenexcitations will be determined through approximate solutions of the appropriate boundary value problems. For an arbitrary excitation the reflection coefficients at each input port and the radiation pattern of the array are then obtained, through superposition, from the set of active reflection coefficients $\Gamma(\underline{u}_o)$ and far field $\vec{g}(i, w_o, r, \theta, \varphi)$. A general account of the philosophy of the method has been already given elsewhere [3]. Thus only the features peculiar to the geometry at hand will be discussed in some detail in this paper.

2.3 Patterns and Reflection Coefficients for Arbitrary Excitations

By using the set of vectors (7) as an orthonormal basis for the array input space the excitation $\underline{a}$ is expressed through the following expansion:

$$\underline{a} = \sum_{i=-N}^{N-1} \int_{\frac{-\pi}{2h}}^{\frac{\pi}{2h}} c(i, w_o)\, \underline{e}\left(\frac{i}{R}, w_o\right) dw_o \tag{11}$$

whose coefficients $c\left(i, w_o\right)$ are the projections of $\underline{a}$ on the basis vectors (7), i.e. are given by the scalar products:

$$c(i, w_o) = \underline{e}^{+}(\underline{u}_o) \cdot \underline{a} \tag{12}$$

where the cross denotes the conjugate transpose. Explicitly

$$c(i, w_o) = \sqrt{\frac{h}{2\pi N}} \sum_m \sum_n a_{mn} \exp\left[j\underline{u}_o(m\underline{s}_1 + n\underline{s}_2)\right] \tag{13}$$

where the summations are extended to those values of m and n corresponding to the elements belonging to the finite excited sector of the infinite structure.

The power reflected back into the input ports is represented by the infinite dimensional column vector $\underline{b}$, which from the representation (11) for $\underline{a}$ is promptly found to be given by the expression:

$$\underline{b} = \sum_{i=-N}^{N-1} \int_{-\frac{\pi}{2h}}^{\frac{\pi}{2h}} \Gamma(i, w_o)\, \underline{e}\left(\frac{i}{R}, w_o\right) c(i, w_o)\, dw_o \qquad (14)$$

Similarly, the array radiation pattern $\vec{F}(\theta, \varphi)$ for an arbitrary excitation is a linear combination of the eigenpatterns with the weights $c(i, w_o)$, as it follows ($k = 2\pi/\lambda$ being the free space propagation constant):

$$\frac{e^{-jkr}}{r} \vec{F}(\theta, \varphi) = \sum_{i=-N}^{N-1} \int_{-\frac{\pi}{2h}}^{\frac{\pi}{2h}} \vec{g}(i, w_o, r, \theta, \varphi)\, c(i, w_o)\, dw_o \qquad (15)$$

It will be shown in Section 3.2 that the integration in (15) is readily performed through an application of stationary phase method. The use of (14) is instead less immediate, requiring a numerical integration. It is stressed however that (15) alone provides all the relevant information about the radiative properties of the array (including for example the variation of gain with scan angle). If in particular a single radiator (e.g. the reference element located at m = n = 0) is excited, because of (11), equation (15) takes the form:

$$\frac{e^{-jkr}}{r} \vec{f}_o(\theta, \varphi) = \sqrt{\frac{h}{2\pi N}} \sum_{i=-N}^{N-1} \int_{-\frac{\pi}{2h}}^{\frac{\pi}{2h}} \vec{g}(i, w_o, r, \theta, \varphi)\, dw_o \qquad (16)$$

Equation (16) yields the realized gain pattern of the reference element.

3. THE ELECTROMAGNETIC PROBLEM FOR CYLINDRICAL ARRAYS OF CIRCULAR APERTURES

3.1 Aperture Field Match

In this section the input properties of the array (reflection coefficient and cross coupling between aperture modes) will be determined (for the structure eigenexcitations), by solving approximately the appropriate boundary value problem. The results derived here will be used in next section to establish expressions for the array eigenpatterns.

The idealized model of the array consists of a regular grid of circular apertures of radius a on an infinite cylindrical surface having radius R, fed by waveguides with the same cross-sections as the apertures. The elements may be filled with dielectric. Only the two orthogonal TE_{11} fundamental modes, circumferentially and axially polarized, are assumed to be above cutoff in the feeding waveguide. A matching network, whose physical nature is such not to create coupling between the two propagating modes (located at a sufficient distance from the aperture not to interfere with evanescent modes) can be present to modify the element realized gain pattern.

The cylinder radius is supposed to be large in terms of wavelengths. Thus the waveguide aperture can be considered planar with negligible error. To simplify the treatment the element aperture transverse electric field distribution will be assumed to be represented with good accuracy as the superposition of the two TE_{11} modes. This approximation gives good accuracy for the planar case [12], for comparable element and lattice size, and it is reasonable to assume that the same will occur for the present geometry (see Section 3.3). The vector mode functions for the mode polarized in the axial and circumferential directions will be denoted by $\underline{e}_a(\underline{s})$ and $\underline{e}_c(\underline{s})$, respectively, $\underline{s}$ being the position vector defined by (5).

A technique to design the matching network to modify the scan coverage characteristics of the array will be discussed in Section 4. For the purpose of the analysis we only need here to assume that two shunt susceptances

Preceding page blank

$-B_{ao}$ and $-B_{co}$ (one for each mode and such not to produce mode cross coupling) are positioned at half wavelengths from the apertures, and that in the transmission lines immediately prior to them two perfect transformers are located, having the turn ratios $n_1:n_2 = \sqrt{G_{ao}:Y_o}$ and $n_1:n_2 = \sqrt{G_{co}:Y_o}$, respectively, where G_{ao} and G_{co} are two suitable conductances and Y_o is the characteristic admittance of the waveguide.

Let the element ports of the axial mode (say) be excited by the eigen-excitation $\underline{e}(\underline{u}_o)$, i.e. by a set of incident waves, of equal magnitude, and having a phase given by $-\frac{2\pi i}{N}\left(p + \frac{q}{2}\right) - w_o qh$. The transverse aperture electric field of the reference element is represented, under the two modes approximation, by the combination of the selected modes as follows:

$$\underline{E}_t(\underline{s}) = \sqrt{2}\, G_a^{-1/2} \sqrt{\frac{h}{2\pi N}} \left| \left[1 + \Gamma_a(\underline{u}_o)\right] \underline{e}_a(\underline{s}) + \Gamma_{ac}(\underline{u}_o)\, \underline{e}_c(\underline{s}) \right| \tag{17}$$

where $\Gamma_a(\underline{u}_o)$ is the reflection coefficient of the excited mode, and $\Gamma_{ac}(\underline{u}_o)$ is a cross coupling coefficient representing the passive excitation of the cross polarized mode. It can be convenient, in view of further developments, to introduce the simple equivalent circuit in Figure 2 for the admittance viewed at the input port of the excited mode. The active admittance $Y_a(\underline{u}_o)$ evidently includes also the effects of coupling with the cross polarized mode passively excited. Paralleling the treatment for the planar case [10] the transverse electric field on the cylinder surface can be represented through the following Floquet's double series, (consequence of the skew symmetry of the structure):

$$\underline{E}_t(\underline{s}) = \sum_{q=-\infty}^{+\infty} \sum_{p=-\infty}^{+\infty} \underline{A}(\underline{u}_{opq})^{-j\underline{u}_{opq}\underline{s}} \tag{18}$$

whose coefficients are bidimensional vectors

$$\underline{A}(\underline{u}_{opq}) = A_z(\underline{u}_{opq})\hat{z} + A_\varphi(\underline{u}_{opq})\ \hat{\varphi} \tag{19}$$

The continuity of the transverse electric field on the cylinder surface will be approximately enforced, by requiring that the difference between $\underline{E}_t(\underline{s})$, eq. (17), and the exterior mode expansion (18) (on the fundamental array cell of the reference element) have zero projection (in the Hilbert space sense) on each Floquet's harmonic. By following this procedure, discussed in detail for the formally similar planar case in Ref. [10], the following set of equations is obtained (one for each of the points (9)):

$$\sqrt{2}\, G_a^{-1/2} \sqrt{\frac{h}{2\pi N}} \left| [1 + \Gamma_a(\underline{u}_o)]\ \underline{\mathcal{E}}_a(\underline{u}_{opq}) + \Gamma_{ac}(\underline{u}_c)\ \underline{\mathcal{E}}_c(\underline{u}_{opq}) \right|$$

$$= \frac{C}{2\pi}\, \underline{A}(\underline{u}_{opq}) \tag{20}$$

where C is the area of the elementary cell and $\underline{\mathcal{E}}_a(\underline{u})$ and $\underline{\mathcal{E}}_c(\underline{u})$ are the Fourier transforms of the vector mode functions $\underline{e}_a(\underline{s})$ and $\underline{e}_c(\underline{s})$, whose explicit expressions are given in Appendix B.

The continuity of the transverse magnetic field on the radiator aperture is approximately enforced through a similar procedure. Under the two mode approximation, the magnetic transverse field on the reference element is given by (Appendix C):

$$\underline{H}_t(\underline{s}) = \hat{\rho}_o x \left\{ \left[\left(1 - \Gamma_a(\underline{u}_o)\right) G_{ao} + \left(1 + \Gamma_a(\underline{u}_o)\right) jB_{ao} \right] \underline{e}_a(\underline{s}) + \right.$$

$$\left. - \Gamma_{ac}(\underline{u}_o)\,(G_{co} - jB_{co})\,\underline{e}_c(\underline{s}) \right\} \sqrt{2}\ G_a^{-1/2} \sqrt{\frac{h}{2\pi N}} \tag{21}$$

$\hat{\rho}_o$ being a unit vector having the direction of the reference element waveguide axis, pointing outward of the cylindrical surface. By using vector potential techniques, the z and ϕ components of the magnetic field in the region exterior to the cylinder can be related to the coefficients (19) of Floquet's expansion, obtaining the following expressions (Appendix C):

$$H_z(\rho, \phi, z) = \frac{\sqrt{2}\, G_a^{-1/2}}{jk\eta} \sqrt{\frac{h}{2\pi N}} \sum_{p=-\infty}^{+\infty} \sum_{q=-\infty}^{+\infty} e^{-j\underline{u}_{opq}\underline{s}} \left\{ \frac{\sqrt{k^2 - w_{opq}^2}\, H^{(2)}_{-i-pN}\left(\rho \sqrt{k^2 - w_{opq}^2}\right)}{H^{(2)}_{-i-pN}\left(R \sqrt{k^2 - w_{opq}^2}\right)} \left[A_\phi(\underline{u}_{opq}) + \frac{(i+pN)\, w_{opq}\, A_z(\underline{u}_{opq})}{R\,(k^2 - w_{opq}^2)} \right] \right\} \quad (22)$$

and:

$$H\phi(\rho, \phi, z) = \sqrt{2} G_a^{-1/2} \sqrt{\frac{h}{2\pi N}} \sum_{p=-\infty}^{+\infty} \sum_{q=-\infty}^{+\infty} e^{-j\underline{u}_{opq}\underline{s}} \left\{ \frac{-(i+pN)\, w_{opq}\, H^{(2)}_{-i-pN}(\rho \sqrt{k^2 - w_{opq}^2})}{j\omega u \sqrt{k^2 - w_{opq}^2}\, \rho H^{(2)'}_{-i-pN}(R \sqrt{k^2 - w_{opq}^2})} \left[A_\phi(\underline{u}_{opq}) + \frac{(i+pN)\, w_{opq}\, A_z(\underline{u}_{opq})}{R\,(k^2 - w_{opq}^2)} \right] - \frac{j\omega\epsilon\, A_z(\underline{u}_{opq}) H^{(2)'}_{-i-pN}(\rho \sqrt{k^2 - w_{opq}^2})}{\sqrt{k^2 - w_{opq}^2}\, H^{(2)}_{-i-pN}(R \sqrt{k^2 - w_{opq}^2})} \right\} \quad (23)$$

with $A_z(\underline{u}_{opq})$ and $A_\phi(\underline{u}_{opq})$ given by (19) and (20).

By requiring that the difference between the expression (21) and the expansion (22-23) have zero projections on the modal function $\hat{\rho}_o \times \underline{e}_a(\underline{s})$ and $\hat{\rho}_o \times \underline{e}_c(\underline{s})$, the following expressions for the reflection and mode cross coupling coefficients are derived (Appendix C):

$$\Gamma_a(\underline{u}_o) = \frac{\left\{G_{ao} - \left[L_{aa}(\underline{u}_o) - jB_{ao}\right]\right\}\left\{G_{co} + \left[L_{cc}(\underline{u}_o) - jB_{co}\right]\right\} + L_{ac}^2(\underline{u}_o)}{\left\{G_{ao} + \left[L_{aa}(\underline{u}_o) - jB_{ao}\right]\right\}\left\{G_{co} + \left[L_{cc}(\underline{u}_o) - jB_{co}\right]\right\} - L_{ac}^2(\underline{u}_o)} \tag{24}$$

and

$$\Gamma_{ac}(\underline{u}_o) = \frac{-2L_{ac}(\underline{u}_o)}{\left\{G_{ao} + \left[L_{aa}(\underline{u}_o) - jB_{ao}\right]\right\}\left\{G_{co} + \left[L_{cc}(\underline{u}_o) - jB_{co}\right]\right\} - L_{ac}^2(\underline{u}_o)} \tag{25}$$

where $L_{aa}(\underline{u}_o)$, $L_{ac}(\underline{u}_o)$ and $L_{cc}(\underline{u}_o)$ are rather complicated functions, whose explicit expression is given in Appendix C. They can be however calculated straightforwardly once the Fourier transforms of the vector mode functions are known. Their physical interpretation is that of self and mutual admittances for the axially and circumferentially polarized fundamental modes (for a given eigenexcitation).

Once the transverse electric field distribution (17) on the elements has been determined using (24) and (25), the eigenpatterns are obtained from the solution of the exterior electromagnetic problem. This is discussed in the next section.

So far it has been assumed that only the axial mode is excited. If, on the other hand, the circumferential mode is the one excited (with the same eigenexcitation) a perfectly similar treatment can be done, obtaining the

expression of the reflection coefficient Γ_c ($\underline{u}_o$) of the circumferential mode simply by permuting the subscripts a and c in (24), the expression for the cross coupling coefficient Γ_{ca} ($\underline{u}_o$) still being given by (25). The general case is obtained by superposition.

3.2 Eigenpatterns

The components $\vec{g}$ (i, w_o, r, θ, ϕ) of the far field for an arbitrary excitation are obtained from the Floquet-Bessel expansion (22-23), by using the standard asymptotic expression of Hankel functions for large arguments.

Notice first that only for

$$|w_{opq}| \leq k \tag{26}$$

the terms in (22) and (23) represent waves carrying energy away from the structure. The terms of (22) and (23) for which (26) does not hold represent instead cylindrical evanescent waves. If in particular the distance between two rings h is smaller than $\lambda/2$, the only propagating waves are found to be those for which $p = 2q$, and, if

$$|w_o| > k - \frac{\pi}{h}, \tag{27}$$

those for which one of the two equalities holds:

$$p-2q = \pm 1$$

the upper and lower sign referring to negative and positive w_o, respectively. The asymptotic expressions for H_z and H_ϕ are found to be given by:

$$H_z(\rho, \phi, z) \underset{\rho \to \infty}{=} \sum_{|w_{opq}| \leq k} \frac{2 G_a^{-1/2} \sqrt{\frac{h}{2\pi N}}}{\sqrt{j\pi\rho \, (k^2 - w_{opq}^2)^{1/2}}} \frac{j^{i-1} (k^2 - w_{opq}^2)^{1/2}}{k\eta} e^{-ji\phi}$$

$$e^{-j (w_{opq} z + \rho \sqrt{k^2 - w_{opq}^2})} \frac{j^{pN} e^{-jpN\phi}}{H_{i+pN}^{(2)} (R\sqrt{k^2 - w_{opq}^2})}$$

$$\left[A_\phi (i+pN, w_{opq}) + \frac{(i+pN) w_{opq} A_z (i+pN, w_{opq})}{R (k^2 - w_{opq}^2)} \right] \qquad (28)$$

$$H_\phi(\rho, \phi, z) \underset{\rho \to \infty}{=} - \sum_{|w_{opq}| \leq k} \frac{2 G_a^{-1/2} \sqrt{\frac{h}{2\pi N}}}{\sqrt{j\pi\rho \, (k^2 - w_{opq}^2)^{1/2}}} \frac{k j^i e^{-ji\phi}}{(k^2 - w_{opq}^2)^{1/2}}$$

$$e^{-j (w_{opq} z + \rho \sqrt{k^2 - w_{opq}^2})} \frac{j^{pN} e^{-jpN\phi} A_z (i+pN, w_{opq})}{H_{i+pN}^{(2)} (R\sqrt{k^2 - w_{opq}^2})} \qquad (29)$$

where the summations are extended to w_{opq} satisfying (26).

The series in (28) and (29) are rapidly convergent, since the terms for which

$$|i + pN| >> R\sqrt{k^2 - w_{opq}^2} \qquad (30)$$

can be easily shown to be negligible.

In view of further developments it is convenient to consider the electric far field of the structure and also to use polar coordinates r, θ, ϕ, related to z and ρ by the standard transformations:

$$\rho = r \sin\theta \qquad z = r \cos\theta \qquad (31)$$

From (28) and (29) through straightforward manipulations the following expression of the electric far field of the structure for the eigenexcitation $\underline{e}(\underline{u}_o)$ are established:

$$\vec{g}(i,w_o, r,\theta,\phi) = \frac{2G_a^{-1/2}}{\sqrt{j\pi r \sin\theta}} \sqrt{\frac{h}{2\pi N}} \sum_{|w_{opq}|\leq k} \frac{e^{-jr(w_{opq}\cos\theta + \sin\theta\sqrt{k^2-w_{opq}^2})}}{(k^2 - w_{opq}^2)^{1/4}}$$

$$\left[\hat{\theta}\, g_\theta\ (i,\ w_{opq},\ \phi) + \hat{\phi}\, g_\phi\ (i,\ w_{opq},\ \phi)\right] e^{ji\left(\frac{\pi}{2} - \phi\right)}$$

where:

$$g_\theta\ (i,\ w_{opq},\ \phi) = \frac{k}{\sqrt{k^2 - w_{opq}^2}} \quad \frac{j^{pN} A_z\ (i+pN,\ w_{opq})\, e^{-jpN\phi}}{H_{i+pN}^{(2)}\ (R\sqrt{k^2 - w_{opq}^2})} \tag{32}$$

and

$$g_\phi\ (i,\ w_{opq},\ \phi) = -j \frac{j^{pN} e^{-jpN\phi}}{H_{i+pN}^{(2)'}\ (R\sqrt{k^2 - w_{opq}^2})} \left[A_\phi\ (i+pN,\ w_{opq})\right.$$

$$\left. + \frac{(i+pN)\, w_{opq}\, A_z\ (i+pN,\ w_{opq})}{R\ (k^2 - w_{opq}^2)}\right] \tag{33}$$

The antenna far field pattern, by applying (15) is thus given by:

$$\vec{F}(\theta,\phi) = \frac{h}{2N}\sqrt{\frac{2j}{\pi r \sin\theta}} \sum_m \sum_n \sum_{|w_{opq}|\leq k} \int_{-\frac{\pi}{2h}}^{\frac{\pi}{2h}} \sum_{i=N}^{N-1} e^{ji(\frac{\pi}{2}-\phi)}$$

$$a_{mn}\, e^{j(imd+\frac{nd}{2})}\; e^{jw_o nh}\; \frac{e^{-jr(w_{opq}\cos\theta + \sin\theta\sqrt{k^2-w_{opq}^2})}}{(k^2 - w_{opq}^2)}$$

$$\left[\hat{\theta}\, g_\theta\,(i, w_{opq}, \phi) + \hat{\phi}\, g_\phi\,(i, w_{opq}, \phi)\right] dw_o \qquad (34)$$

where the summation in n and in m are extended to the elements of the finite area excited of the infinite structure. The integral in (34) can be evaluated for $r \to \infty$ through straightforward application of stationary phase method, obtaining finally:

$$\vec{F}(\theta,\phi) = \frac{e^{-jkr}}{r}\;\frac{h\sqrt{2}}{\pi N}\; G_a^{-1/2}\, j^{1/2} \sum_{i=N}^{N-1} e^{ji(\frac{\pi}{2}-\phi)} \sum_{|w_{opq}|\leq k}$$

$$\left[\hat{\theta}\, g_\theta\,(i, w_{opq}, \phi) + \hat{\phi}\, g_\phi\,(i, w_{opq}, \phi)\right]$$

$$\left[\sum_m \sum_n a_{mn}\, e^{ji\frac{2\pi}{N}(m+\frac{n}{2})}\; e^{jknh\cos\theta}\right] \qquad (35)$$

As mentioned in Section 2.3, the realized gain pattern of an element is obtained as a particular application of the general result (35).

3.3 Remarks

In the previous sections in developing the appropriate formalism for the analysis of cylindrical arrays it has been attempted to stress the similarity with planar array theory. In both cases the field outside the cylinder is expanded in an infinite series of Floquet's harmonics, of a general type, each of them conveniently associated with a point of a regular lattice in a "reciprocal" wavenumbers plane. However, certain important differences should be remarked. The most apparent is that in order to calculate one point of the realized gain pattern of a cylindrical array element (or more generally one point of the array pattern for an arbitrary excitation), it is necessary to calculate the array response to the eigenexcitations pertinent to all azimuthal numbers i's. For a planar periodic array all the excitations with uniform magnitude and linear phase taper are eigenexcitations, and the response to only one of them characterizes the realized gain pattern of an element in a certain direction. Another less obvious difference is related to the phenomenon of the "continous" cutoff of the cylindrical functions representing the electromagnetic field. The question is straightforward for uniform cylindrical arrays [1-3] but is relatively complicated for the present structure.

A discussion of this phenomenon by using the concept of reciprocal lattice in the u, w plane gives insight on certain array properties. For the planar case there exists a circle (visible region) within which the reciprocal lattice points represent radiating waves (carrying energy away from the structure). All the other harmonics represent instead evanescent waves associated with the reactive power stored in the neighborhood of the array [9-11]. For a cylindrical array, instead, the waves whose representative points in the u, w plane do not belong to the strip (26) represent evanescent waves. Inside the strip (26) the Floquet Bessel harmonics are associated with both radiating and reactive power. However, from (22-23), by invoking well known properties of cylindrical functions it can be seen that the waves for which

$$\left| i + pN \right| > R \sqrt{k^2 - w_{opq}^2} \tag{36}$$

are "essentially" below cutoff, while the ones for which the inequality (36) is reversed are essentially radiating. The propagation region, (corresponding in planar array theory to the visible circle) has now a blurred boundary, and a transitional zone exists where the harmonics contribute to both active and reactive power. In Figure 5 the edges of this zone have been indicated, conventionally defined as the loci where the ratios between the imaginary and the real parts of the wave admittance are either 0.1 or 10.

A few comments are at this point appropriate about the numerical accuracy of the solution. In both the planar and cylindrical cases the solution of the electromagnetic problem is obtained by expanding the field in the proper modes of the waveguide and of the radiation half space. The modal series are then truncated and through an application of Galerkin's method a system of equations is written for the unknown coefficients. Recently, the question of the accuracy of this procedure has been debated [13-15], and it has been observed that for certain types of waveguide discontinuity problems increasing the number M and N of the modes in the two regions at the two sides of the discontinuity may not make the coefficients of the expansion to tend to their correct values. It has been shown that for certain problems (different from these considered here) M and N must be increased keeping a certain ratio between them [14-15]. These studies have constituted a very useful warning, pointing out that a single convergence test (increase of M and N) is not sufficient to guarantee the accuracy of the solution. However, by no means this implies that the method of solution above described is incorrect or inaccurate. In fact the practical certainty of the correctness of the solution is obtained if several convergence tests are made (increasing M and N, keeping their ratio constant but equal to a different value for each test) checking that the modal coefficients tend in the different tests to the same values. This has been done for the planar configuration, and has been thus checked that for this type of problem (essentially equivalent to a junction between two waveguides with different cross sections) the solution is not sensitive to the way M and N are related. This conclusion is consistent with what found by Lee et al [14]. Extensive numerical computations performed along these lines have shown that for arrays of circular apertures of dimensions and spacings similar to the ones considered in this study, two

modes are sufficient for achieving good accuracy (see for example [12]). In many instances the analytical solutions have compared with experimental data, with consistently excellent agreement. Because of the physical and analytical similarity of the two problems it can be inferred that the same will be true for the cylindrical structures (for radius of curvature sufficiently large).

Certain questions concerning the numerical evaluations of the Floquet-Bessel series are briefly discussed in Appendix D.

4. ELEMENT PATTERN DESIGN

The scattering coefficients among the elements are functions of the parameters of the tuning network of Figure 2. Consider a single excited element. The interference between its direct radiation and the energy scattered by the other elements passively excited, depends upon the turn ratio of the transformer, and the susceptance of Figure 2, and so does the element realized gain pattern. In order to get an insight of the relationship between element pattern and matching network parameters, it is appropriate here to briefly compare the two methods of cylindrical array analysis presently available, from the viewpoint of their suitability for element design.

One of the methods is based on an attempt to determine the passive reradiation of the elements in the situation of a single excited radiator, by establishing thus a formalism which is a direct analytical counterpart of the physical picture given above. To this end the complex waves, solutions of Maxwell equations for the source free structure must be determined [2]. This requires the solution of a transverse resonance equation having as unknowns the complex wave numbers in the longitudinal and azimuthal directions. The idea upon which this approach is based is a valuable aid for the understanding of the phenomena occurring in conformal arrays. However, this approach does not lead to manageable computational procedures except for very simple idealized structures [2]. In addition, it does not seem easily adaptable to efficient element pattern synthesis.

The other approach is the "eigenexcitations method", considered in this paper and described in the previous sections, which naturally leads to a relatively simple procedure for controlling to a considerable extent the element pattern. In this method no direct evaluation of mutual coupling is necessary, the element interaction phenomena being represented by the set of active reflection coefficients $\Gamma(\underline{u}_o)$. Consider the plane tangent to the array surface through the center of the reference element, and on such plane the straight line in the direction of the cylinder axis and its perpendicular. Suppose that one seeks to enhance the radiation into a direction having cosines γ and α

with those axes. To accomplish this purpose, the network if Figure 2 is chosen to match the structure when excited by the eigenexcitation identified by:

$$w_o = k\gamma \quad ; \quad i = kR\alpha \tag{40}$$

The realized gain pattern for obvious symmetry reasons will be the same in the direction $-\alpha$ and $-\gamma$ symmetric to α and γ with respect to broadside. This procedure is easily justified by observing that the realized gain pattern of an element in a conformal array having a large cylinder radius is obviously "similar" to that of the same element (with the same lattice) in a planar array. For the latter case, the element pattern in a direction α, γ is maximized if the array is made transparent (i. e. matched) for a plane wave incident from such a direction, or equivalently if it is matched for steering in the direction α, γ. Thus, for a conformal array, the corresponding condition will be the one mentioned above, for which the same relative phase progression exists among the elements.

For a varipolarization element, it is possible to maximize the gain in two directions (one for each polarization of an orthogonal pair) by using waveguide elements acting on a single polarization (e. g. waveguide posts). These directions can be chosen close to grazing incidence in the axial and circumferential directions (for axial and circumferential polarization, respectively). The use of varipolarization elements allows to eliminate the loss due to the almost complete reflection at large angle from broadside of the energy associated with the field polarized parallel to the surface, simply by suitably choosing the element nominal polarization.[4]

Practically the evaluation of the network parameters will be done by calculating the terminal admittance for the eigenexcitation (40) (following the procedure of sect 3 and Appendix C) for $B_{co} = B_{ao} = 0$ and $G_{co} = G_{ao} = Y_o$. The real and imaginary parts of the admittance so determined provide the

[4] Assuming that the antenna at the other terminal of the communication link is circularly polarized, of course there is still a 3 db loss due to polarization mismatch.

values of G_{ao} and B_{ao} or the values of G_{co} and B_{co} for axially polarized or circumferentially polarized excitation, respectively.

When maximizing the gain in certain directions off broadside it is expected that the broadside gain will decrease. Thus the element pattern will be "flatter" than in the case of broadside match. Resonance notches are in most cases essentially determined by the array lattice (at least in absence of dielectric sheets on the array surface and/or elements having too large apertures). Thus one should choose an element grid for which in a planar array no grating lobes would be present (for any scan condition). The design is not critically frequency sensitive.

Numerical examples of element patterns designed according to the criteria above outlined are discussed in Section 5.

5. SELECTED NUMERICAL EXAMPLES AND DISCUSSION

In this section a number of illustrative examples will be briefly considered with the aim of determining the effects of the structure geometrical parameters (cylinder radius, element size and lattice), and of showing the effectiveness of the design technique discussed in Section 4. A large amount of numerical data have been generated. Three cylinder radii and two different element lattices have been considered. The element aperture radius has been always assumed equal to 0.22 wavelengths (at center frequency for those cases for which a frequency sensitivity study has been performed). The elements waveguides are assumed to be filled by a dielectric with $\epsilon_r = 2.5$ (for $\epsilon_r = 1$ the fundamental modes would have been below cutoff).

A first set of figures refer to arrays with the lattice of Figure 3. A planar array with the same lattice would have grating lobes in the visible space for certain scan conditions. The first array studied has a radius of approximately 100 wavelengths. Circumferential, axial and conical sections of element realized gain patterns have been calculated for nominal axial and circumferential polarizations, the elements being matched for the equiphase condition, conventionally called "broadside", (Figure 6 to 10). For this lattice size and orientation a notch is present (Figure 6) in the circumferential plane for circumferential polarization in a direction approximately corresponding for a planar array to a scan direction for which a grating lobe enters into visible space. Characteristically however, the notch is absent for axial polarization. Also the slope of the realized gain pattern in the shadow region is substantially greater for axial polarization. These patterns are shown here also to point out that the technique of analysis here introduced can be used without any difficulty also for large cylinder radii. In Figures from 11 to 15 similar patterns are shown for an array on a cylinder with a radius approximately equal to 50 wavelengths. The patterns are very similar to those for the array with larger radius. The only differences being, as expected, the less pronounced notch and the lesser slope in the shadow

Preceding page blank

region of the circumferential sections. These trends become even more pronounced for the array with a cylinder radius of approximately 11 wavelengths, (Figure 16 to 20). The resonance notch becomes here a minor perturbation of the pattern. In Figure 16 the realized gain pattern has been shown also for the condition of elements matched for an eigenexcitation corresponding to an azimuthal phase taper which would give origin in a planar array to the beam in the direction of the notch. The improvement of the angular coverage is apparent.

It is worth noticing that in the axial section the element realized gain pattern is very insensitive to the cylinder radius and practically coincident with that for a planar array. It is also of some interest the fact that in the shadow region the cross polarized component of the field can reach values greater than the nominal (see for example Figure 14).

By using a smaller size lattice the patterns do not have resonance notches. A second set of patterns refer to the lattice of Figure 21. For an array with approximately 50 wavelengths of diameter Figure 22 to 31 show the effect of "off broadside" match. Axial and circumferential polarizations are separately matched (as described in Section 4): the array is matched for $i/R = 2\pi \sin 80°/\lambda$ (and $w_o = 0$) for circumferential polarization (in the circumferential plane), and for $w_o = 2\pi \sin 80°/\lambda$ (and $i = 0$) for the axial polarization (in the axial plane). In the circumferential plane matching the elements at 80 degrees from broadside yields a realized gain pattern with a gain decrease at 80 degrees of approximately 6 db with respect to broadside, to be compared with the gain loss of approximately 12 db for the more conventional equiphase match. In the axial plane also the improvement is substantial (Figure 23). A few conical sections are shown in Figure 24 to 31. If the axial polarization is matched in the circumferential plane a pattern almost completely flat up to approximately 80 degrees is obtained (Figure 32).

Similar diagrams have been calculated for three different match conditions for an array with a radius of approximately 11 wavelengths (Figure 33 to 44). The frequency sensitivity of the realized gain pattern has been also investigated (Figure 43 and 44) and show the realized gain pattern variations for ± 5 percent change of frequency with respect to design frequency.

Broadside and 80 degrees off broadside match conditions have been considered. A notch begins to appear at high frequency, and it is interesting to see that the modification of the realized gain pattern with frequency depends substantially upon match conditions, and thus is not due simply to geometrical reasons. In calculating the curves of Figure 43 and 44, the matching susceptance shunting the aperture has been assumed constant with frequency (a reasonable approximation in a ± 5 percent band).

The realized gain patterns of the elements of a conformal array, (unlike the planar case), are only an indirect indication of the scan coverage of the antenna. In order to get direct performance information a "small" and a "large" arrays, with 37 and 313 elements respectively, have been considered.[5] Both the cylinders with radii of 11 and 50 wavelengths have been investigated. The array apertures are circular, gaussianly illuminated with a 10 db edge taper. The lattice is that shown in Figure 21. The angular sectors occupied by the arrays on the smaller radius cylinder are shown in Figure 45. The array pattern is calculated by using expression (35). The "free" array excitation is chosen always in such a way to have the radiative contributions of all elements to add in phase at the peak of the beam. Since the phase patterns of the element realized gains are essentially flat up to 80 degrees from broadside, the phases of the excitations turn out to be practically coincident with those obtained from simple geometrical optics considerations. Figure 46 depicts the circumferential section of the array pattern for the small array on the small cylinder with circumferential nominal polarization (equiphase match) with the beam scanned at broadside (i.e., in the direction perpendicular to the cylinder axis and passing through the array center). The array realized gain is approximately 20.8 db (Table 3). In Figure 47 the realized gain pattern of the array with 313 elements is shown, for broadside scan. Two different matching conditions have been considered: broadside and for $i/R = 2\pi \sin 80°/\lambda$ (and $w_o = 0$). Thus in the second case the element realized gain pattern is that of Figure 33. The two patterns are

[5] According to the discussion in Section 2 the two arrays constitute the excited sector of an infinite structure.

very similar as expected, the differences lying on different peak gains and far out sidelobes slightly higher for the case of match off broadside, because of the lesser efficient filtering effect of the element pattern.

Figure 48 to 56 show the envelopes of the max array gain versus scan angle for linear polarization in the plane of scan and different match condition. In some of the figures the planar case is also indicated for reference. As expected the effect of the curvature is substantial only in the circumferential plane (Figure 48-49 and 51-52). The effect of match off broadside is shown in Figure 50 and 51 for the array with 37 elements, on the small cylinder. Figure 54 and 55 show analogous curves for the large array on the same cylinder. For match off broadside the gain drop off at 80 degrees is approximately 6 db for the circumferential plane and 7 db for the axial plane.

In Figure 56 to 67 curves of gain and axial ratio versus scan angle for nominally circularly polarized radiation are plotted. In this case the axial and circumferential polarization ports are excited with incident waves having equal magnitudes and a difference of phase such to yield for the axial and circumferential field components at broadside a phase difference equal to 90 degrees. Thus in general the "free" excitations of the two ports will not be in phase quadrature because of the different phase delays of the two field components through the matching networks and the element aperture. In Figure 56 to 58 different conical sections for broadside match are indicated for the array with 37 elements. In Figure 59 to 61 similar curves are plotted for the case of the two polarizations separately matched (according to the discussion of Section 4). The drop off of the gain is remarkably better than for broadside match. However at large scan angle these curves exhibit a gain decrease with respect to the peak approximately 3 db larger than that for nominal linear polarization (with the same match condition). This effect is clearly due to the polarization parallel to the surface which for radiation angles close to grazing incidence is almost completely rejected. It is thus confirmed the convenience of switching from nominal circular to linear polarization (belonging to the plane of scan) when extreme angles are approached. Because of the different gains for the two polarizations the axial ratio at broadside is different from unity.

Figure 62 to 67 depict gain versus scan angle and axial ratios for the array with 313 elements for the same match conditions considered for the small array. The general features of these curves are very similar to the ones for the small array. Interesting enough the axial ratio is slightly better for the large array.

6. CONCLUDING REMARKS

There are applications for which the gain of a scanned antenna is required not to fall below a certain level in a wide angle scan region. In these cases the average antenna gain in the scan sector is a parameter more relevant to system performance than the maximum gain in a particular direction. This typically occurs for a satellite to aircraft communication system for which a hemispherical scan coverage is ideally demanded by the variable attitude and aircraft to satellite geometry. The conventional use of terminals consisting of protruding mechanically scanned reflectors, or some other form of aperture radiators, mounted beneath a radome is severely limited by acrodynamic drag. A conformal array of flush mounted antennas presents itself as the complete solution of the problem.

In a conformal array the beam can be scanned generally through a combined phase and amplitude control of the array illumination. Considering a cylindrical surface (a reasonably good geometrical model for the center part of an aircraft fuselage) the amplitude control may serve the purpose of moving the illumination around the cylinder axis. In this way, however, the total array aperture is not optimally utilized and a complicated feed system is required. In order to save on the number of radiating elements and to simplify the feed system, it is advisable to rely as much as possible on conventional element phase control.

If no or limited amplitude control is used, in order to obtain a wide angle scan coverage it is necessary to make use of radiating elements having a realized gain pattern with a small gain drop-off with angle. In this report the results of a study have been presented having the objective of assessing the feasibility of an element having these desirable features and of establishing a practical approach to its design. It has been shown that element patterns with a gain variation of approximately 6 db in an angular sector of ±80 degrees around broadside can be obtained by using a technique consisting of inserting special "element pattern shaping networks" in the

Preceding page blank

waveguides feeding the radiators. Their purpose is to enhance the radiation off broadside via a control of the radiator mutual coupling mechanism.

To simplify the analysis the infinite array model has been used. Consequently no account has been taken of the end fire effect which for a finite array exists for radiation at or very close to grazing angles. This effect, related to interference and diffraction at the array edge, is particularly important for radiation in directions close to the cylinder axis, where the infinite array model always yields zero radiation, a physically improbable result. Although no substantial difficulties are anticipated in analyzing a finite array on an infinite cylinder, this model is not yet accurate enough because the fundamental role played by the diffraction at the edge of the structure, on which the array is mounted, is completely neglected. Little investigation has been performed in this area and very useful work can be done to study these effects, (possibly by using geometrical theory of diffraction) and to devise techniques to enhance the radiation in the direction of the axis of the structure.

TABLE 1

PARAMETERS OF ELEMENT PATTERN SHAPING NETWORK

R = 11, 61λ

TE_{11} Mode Normalized Waveguide Admittance

$$\eta Y_o = \sqrt{\epsilon_r - \left(\frac{x'_{11}}{2\pi a/\lambda}\right)^2} = 0.851 \text{ at } f_o$$

Circumferential Polarization Port	Axial Polarization Port
Match at $i/R = k \sin 80°$ ($w_o = 0$)	Match at $w = k \sin 80°$ ($i = 0$)
$G_o = 1.8967\ Y_o$	$G_o = 1.8402\ Y_o$
$-jB_o = -j\ 0.78749\ Y_o$	$-jB_o = j\ 0.56349\ Y_o$
$n_1/n_2 = 1.3772$	$n_1/n_2 = 1.3565$
Match at $i/R = k \sin 70°$ ($w_o = 0$)	Match at $w = k \sin 70°$ ($i = 0$)
$G_o = 1.1468\ Y_o$	$G_o = 0.97668\ Y_o$
$-jB_o = -j\ 0.4718\ Y_o$	$-jB_o = 0.52979\ Y_o$
$n_1/n_2 = 1.0708$	$n_1/n_2 = 0.9883$
Equiphase Match	Equiphase Match
$G_o = 0.51738\ Y_o$	$G_o = 0.51743\ Y_o$
$-jB_o = j\ 0.66859\ Y_o$	$-jB_o = j\ 0.67266\ Y_o$
$n_1/n_2 = 0.7193$	$n_1/n_2 = 0.7193$

TABLE 2

PARAMETERS OF ELEMENT PATTERN SHAPING NETWORK

R = 49.33λ

TE_{11} Mode Normalized Waveguide Admittance

$$\eta Y_o = \sqrt{\epsilon_r - \left(\frac{x'_{11}}{2\pi\ a/\lambda}\right)^2} = 0.851 \text{ at } f_o$$

Circumferential Polarization Port	Axial Polarization Port
Match at $i/R = k \sin 80°$ ($w_o = 0$)	Match at $w = k \sin 80°$ ($i = 0$)
$G_o = 2.2862\ Y_o$	$G_o = 1.8389\ Y_o$
$-jB_o = -j\ 1.6097\ Y_o$	$-jB_o = j\ 0.52134\ Y_o$
$n_1/n_2 = 1.5120$	$n_1/n_2 = 1.3560$
Match at $i/R = k \sin 70°$ ($w_o = 0$)	Match at $w = k \sin 70°$ ($i = 0$)
$G_o = 1.2354\ Y_o$	$G_o = 0.97649\ Y_o$
$-jB_o = -j\ 0.71224\ Y_o$	$-jB_o = j\ 0.52158\ Y_o$
$n_1/n_2 = 1.115$	$n_1/n_2 = 0.9882$
Equiphase Match	Equiphase Match
$G_o = 0.51741\ Y_o$	$G_o = 0.51742\ Y_o$
$-jB_o = j\ 0.67286\ Y_o$	$-jB_o = j\ 0.67169\ Y_o$
$n_1/n_2 = 0.7193$	$n_1/n_2 = 0.7193$

TABLE 3
ARRAY CHARACTERISTICS

ARRAY 1
Number of Elements: 37
Element Spacing: $h = 0.288\lambda$; $d = 1\lambda$
Array Maximum Diameter = 3.45λ
Gain at Broadside (Equiphase Match): 20.8 db at f_o
Gain at Broadside (Match for $i/R = k \sin 80°$) = 17.8 db at f_o
Gain at Broadside (Match for $w = k \sin 80°$) = 18.9 db at f_c
ARRAY 2
Number of Elements: 313
Element Spacing: $h = 0.288\lambda$; $d = 1\lambda$
Maximum Array Diameter: 10.6λ
Gain at Broadside (Equiphase Match) = 29.9 db at f_o
Gain at Broadside (Match for $i/R = k \sin 80°$) = 26.9 db at f_o
Gain at Broadside (Match for $w = k \sin 80°$) = 28 db at f_o

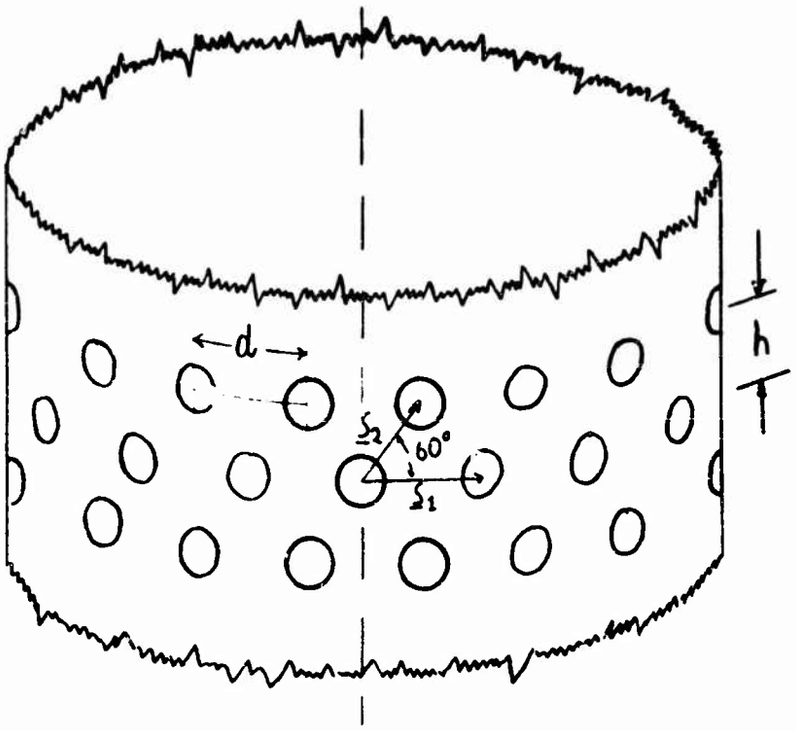
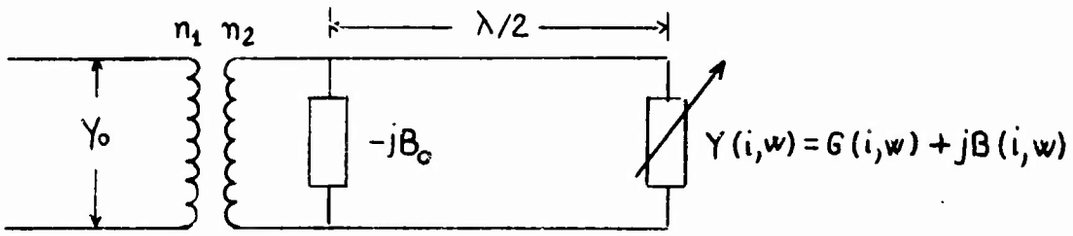


Figure 1 - Geometry of the Structure



$$\frac{n_1}{n_2} = \sqrt{\frac{G_o}{Y_o}}$$

$$G_o = G(i_o, w_o)$$

$$B_o = B(i_o, w_o)$$

Figure 2 - Element Pattern Shaping Network

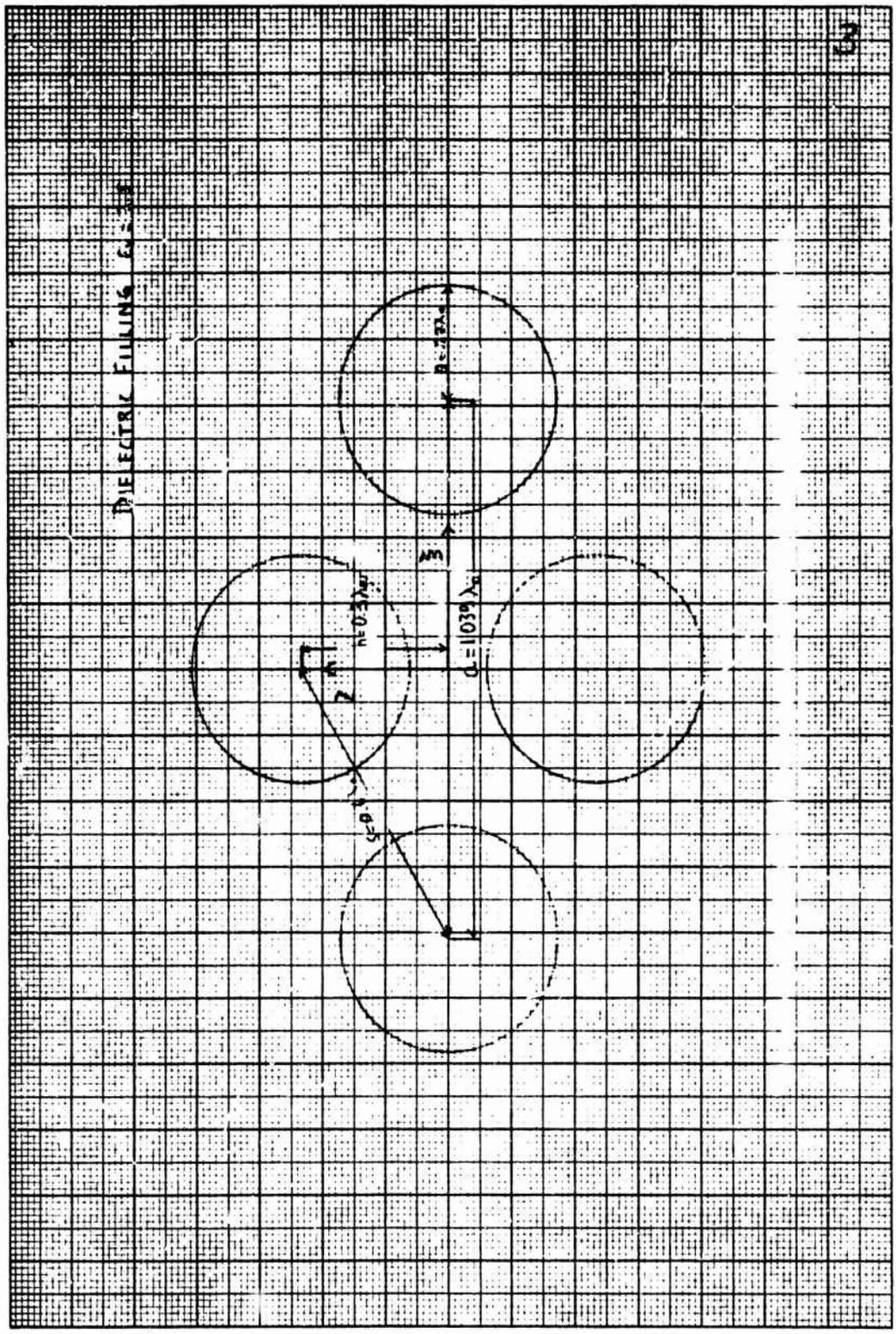


Figure 3 - Lattice 1

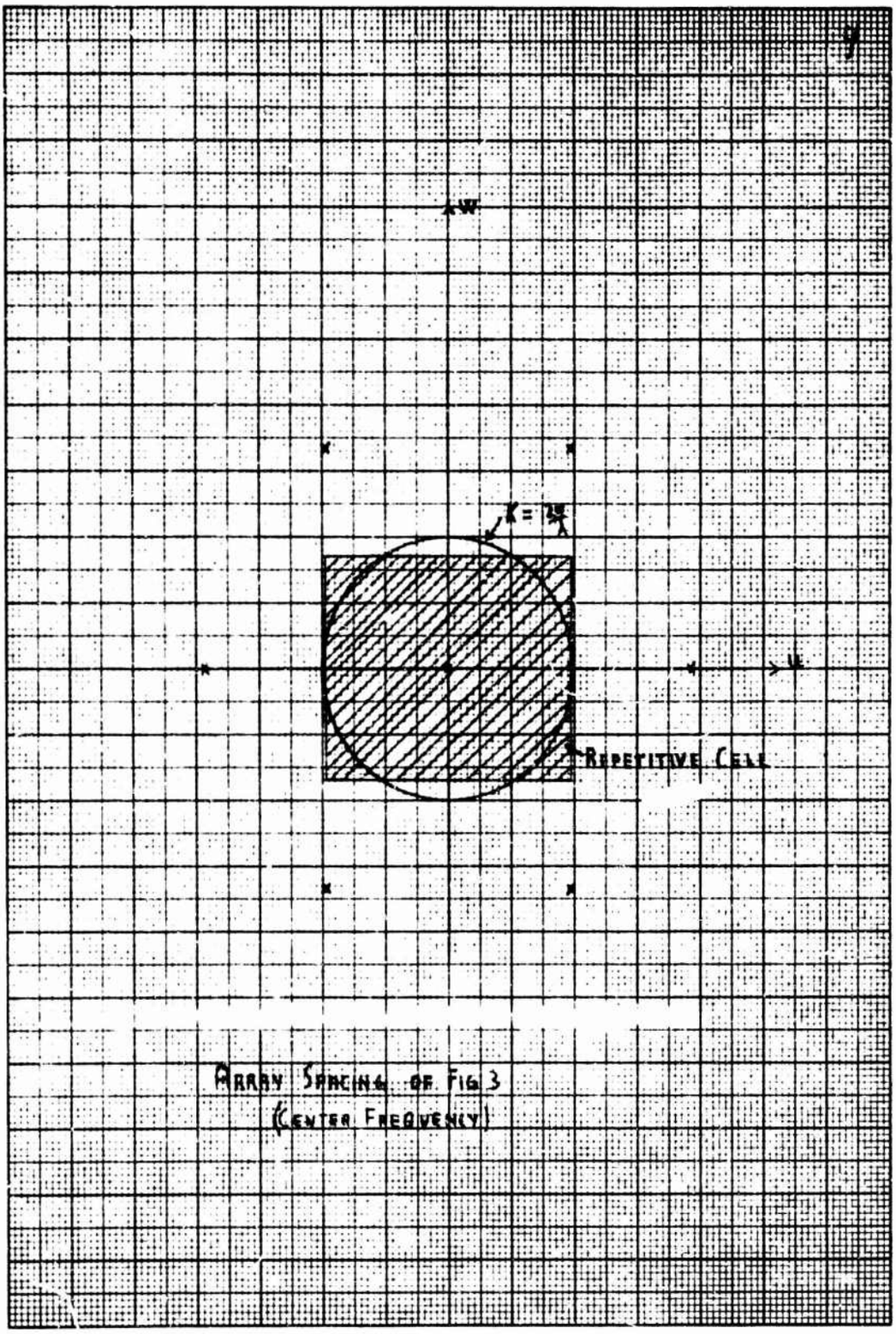


Figure 4 - Reciprocal Lattice of Cylindrical Array

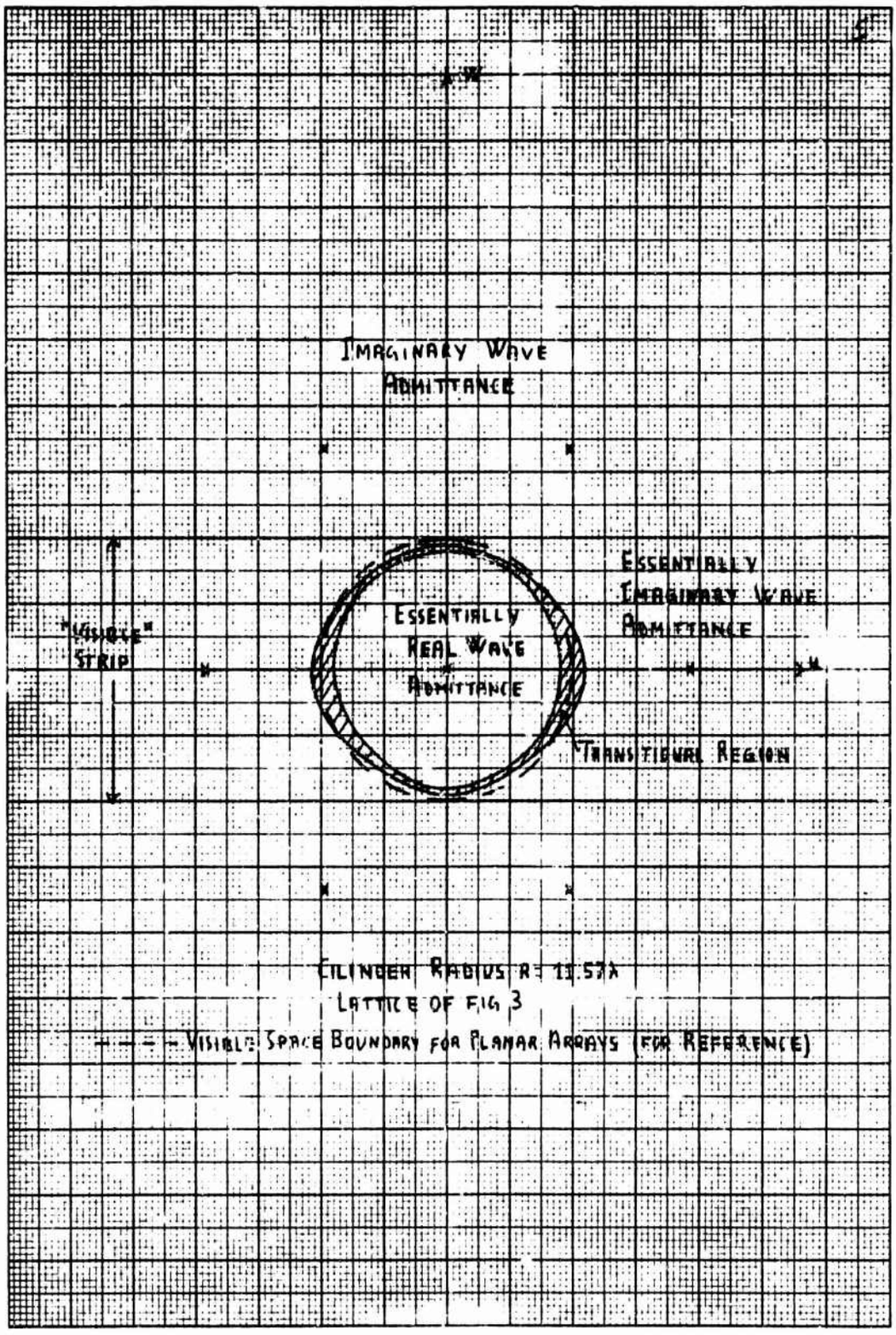


Figure 5 - "Continuous" Cut-off of Floquet-Bessel Harmonics

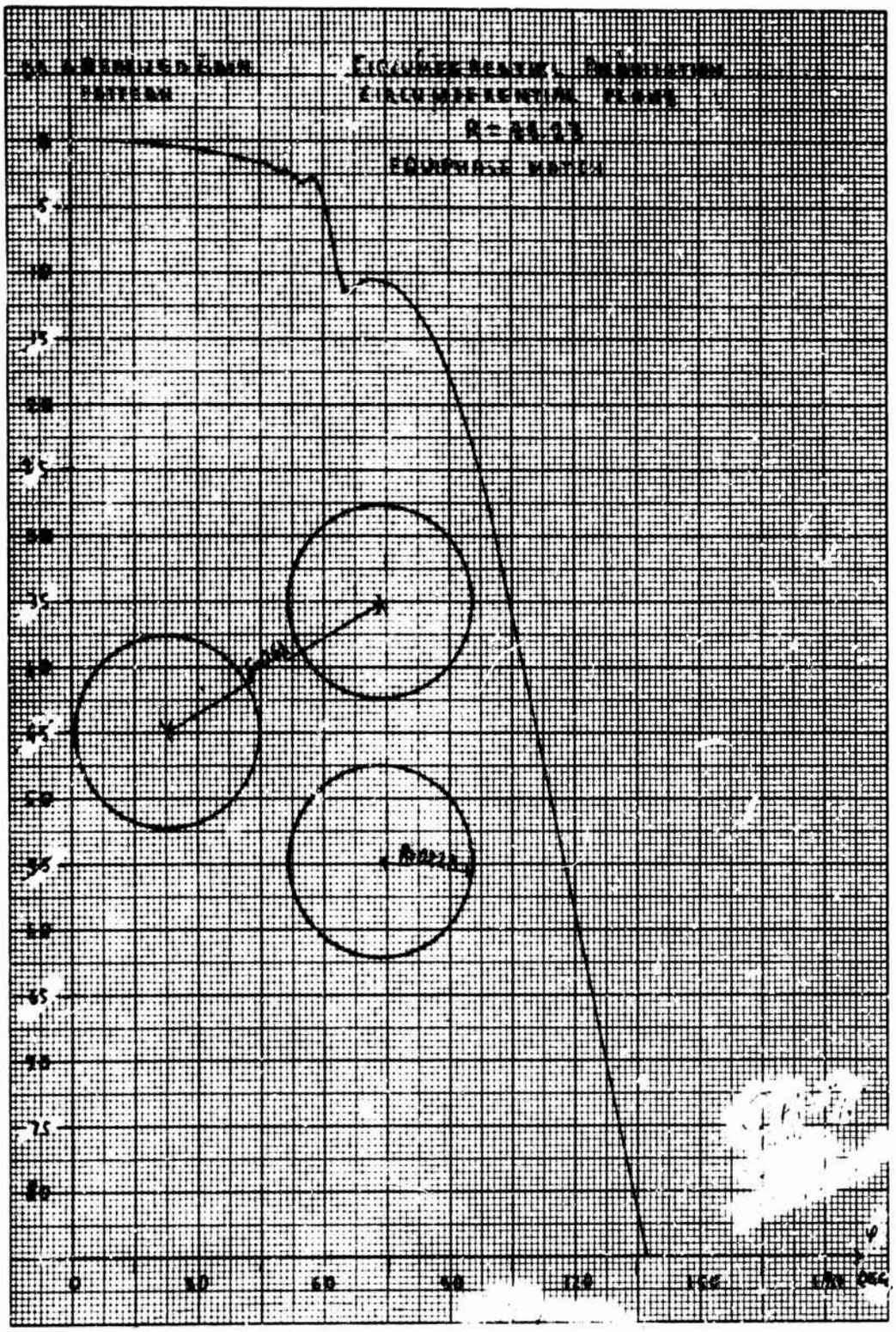


Figure 6 - Realized Gain Pattern. Circumferential Plane. Circumferential Polarization. Equiphase Match (R = 99.23λ)

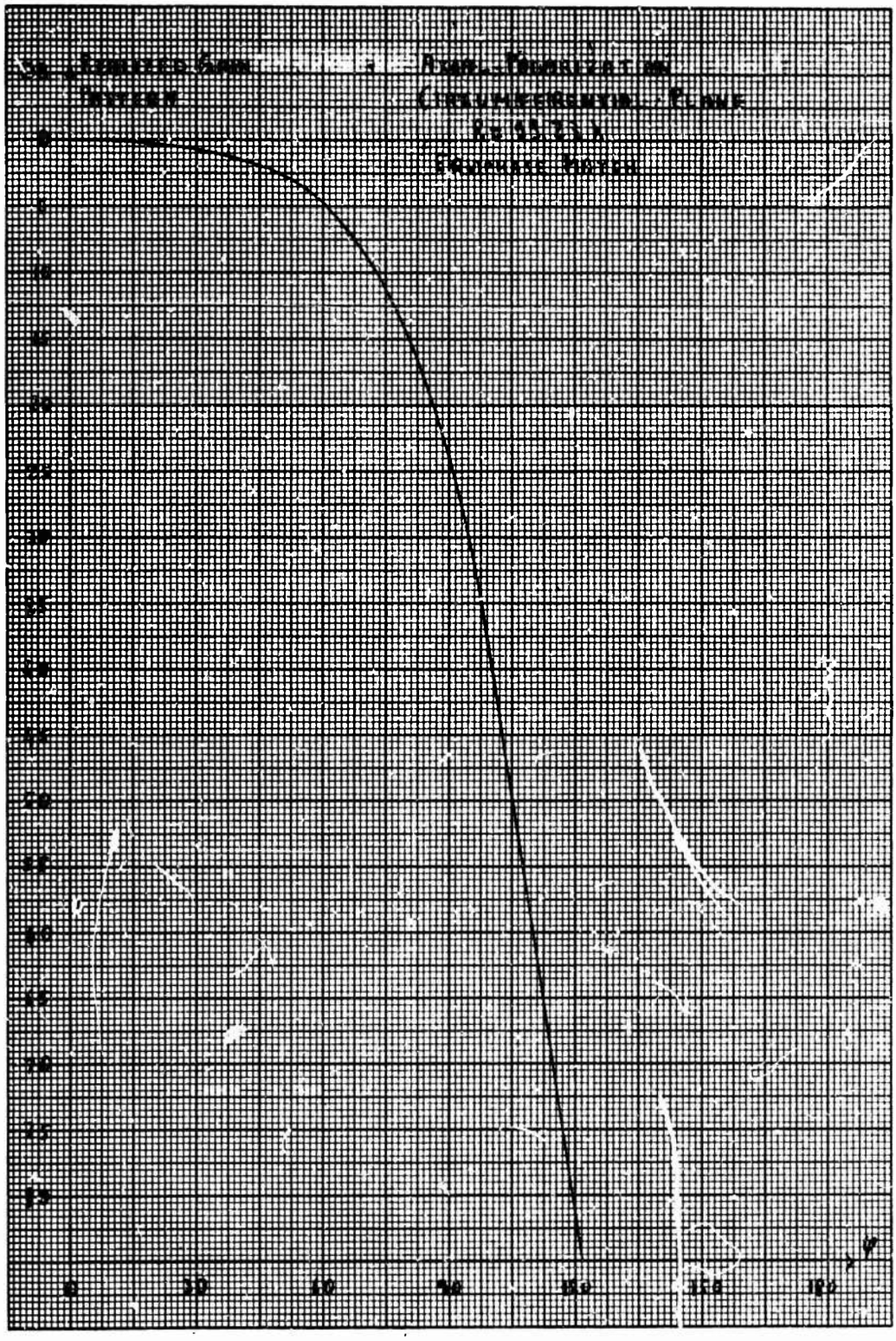


Figure 7 - Realized Gain Pattern. Circumferential Plane. Axial Polarization Equiphase Match (99.23λ)

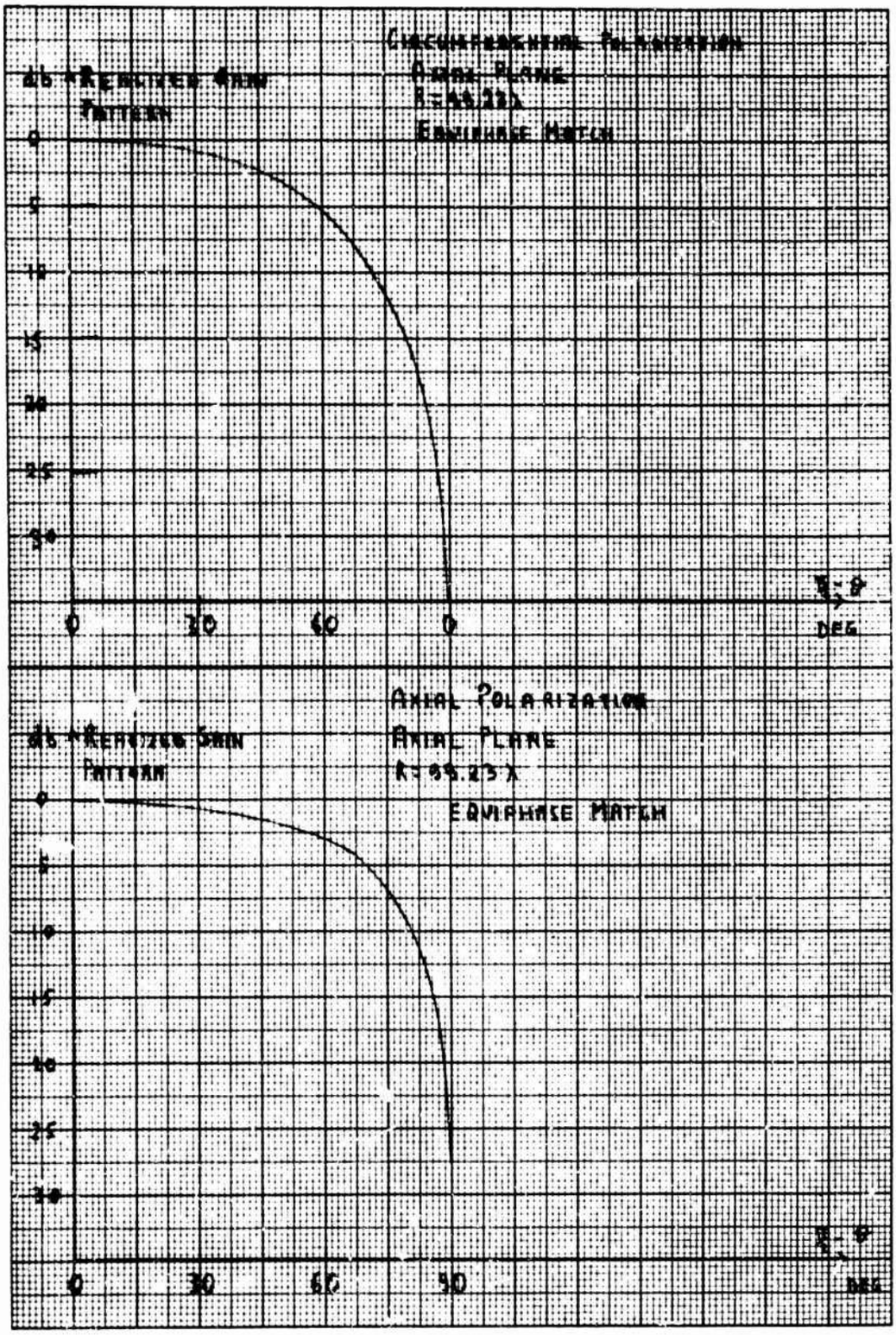


Figure 8 - Realized Gain Pattern. Axial Plane. Equiphase Match
(R = 99.23λ)

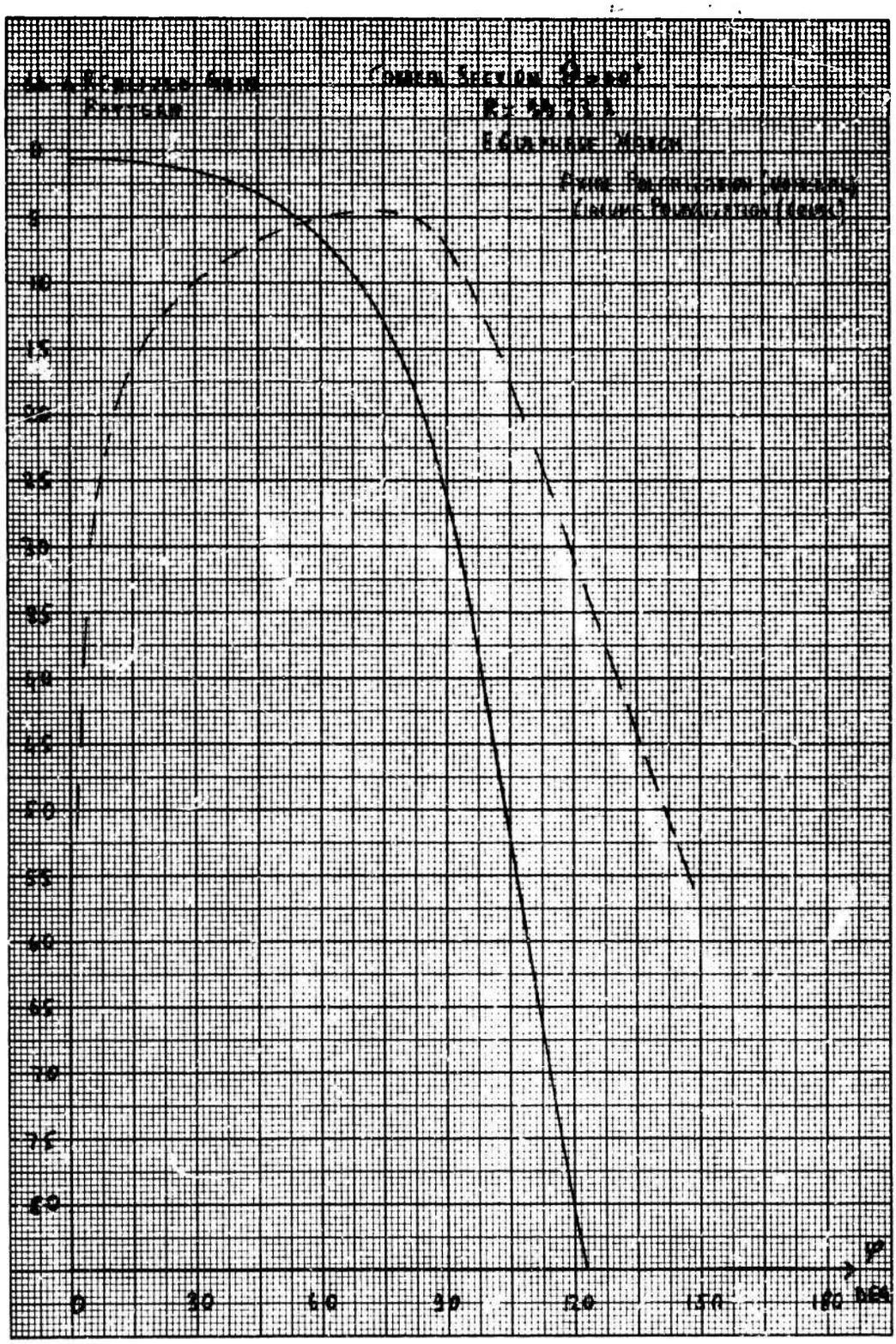


Figure 9 - Realized Gain Pattern. Conical Section $\theta = 60°$. Axial Polarization Excited. Equiphase Match ($R = 99.23\lambda$)

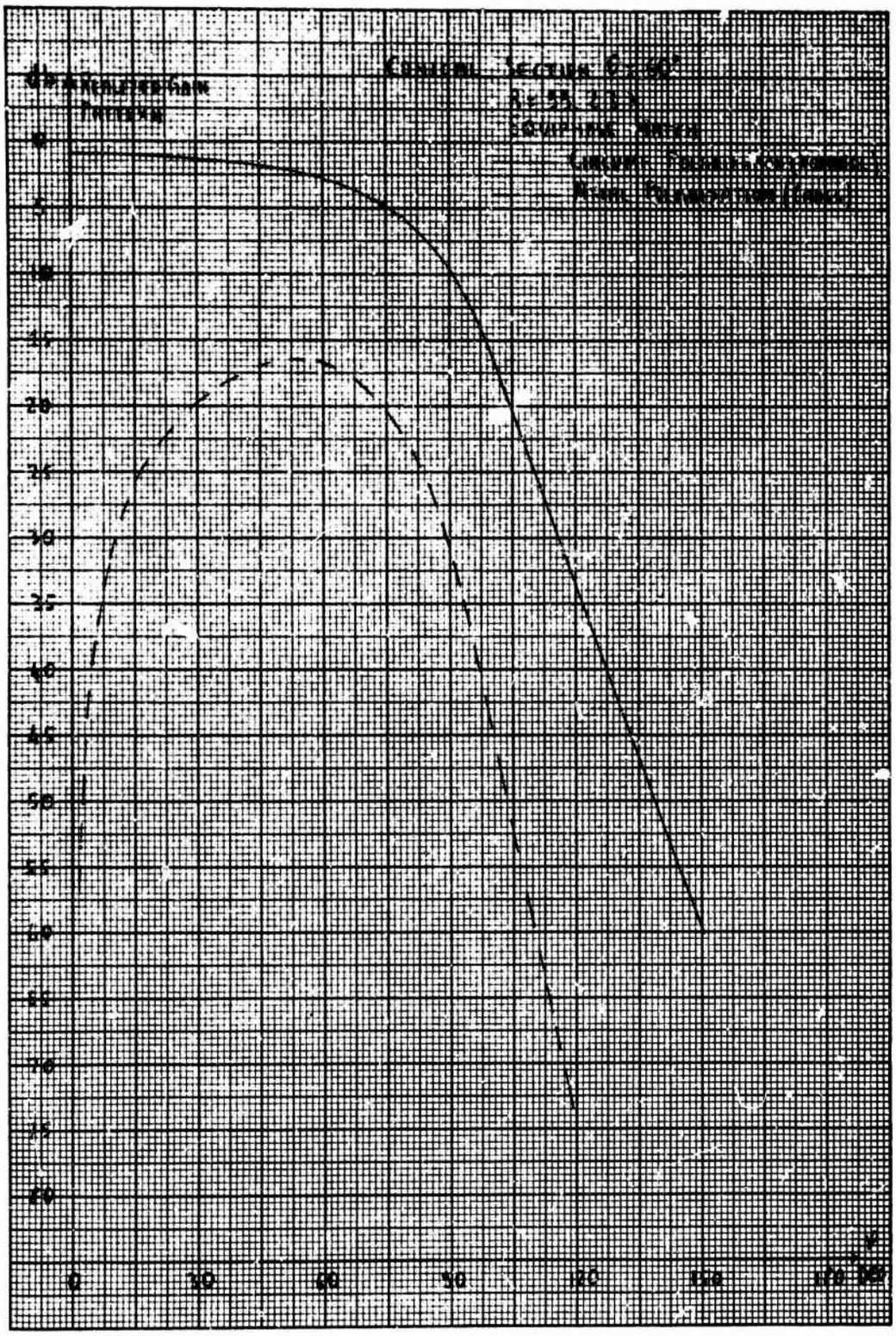


Figure 10 - Realized Gain Pattern. Conical Section θ = 60°. Circumferential Polarization Excited. Equiphase Match (R = 99.23λ)

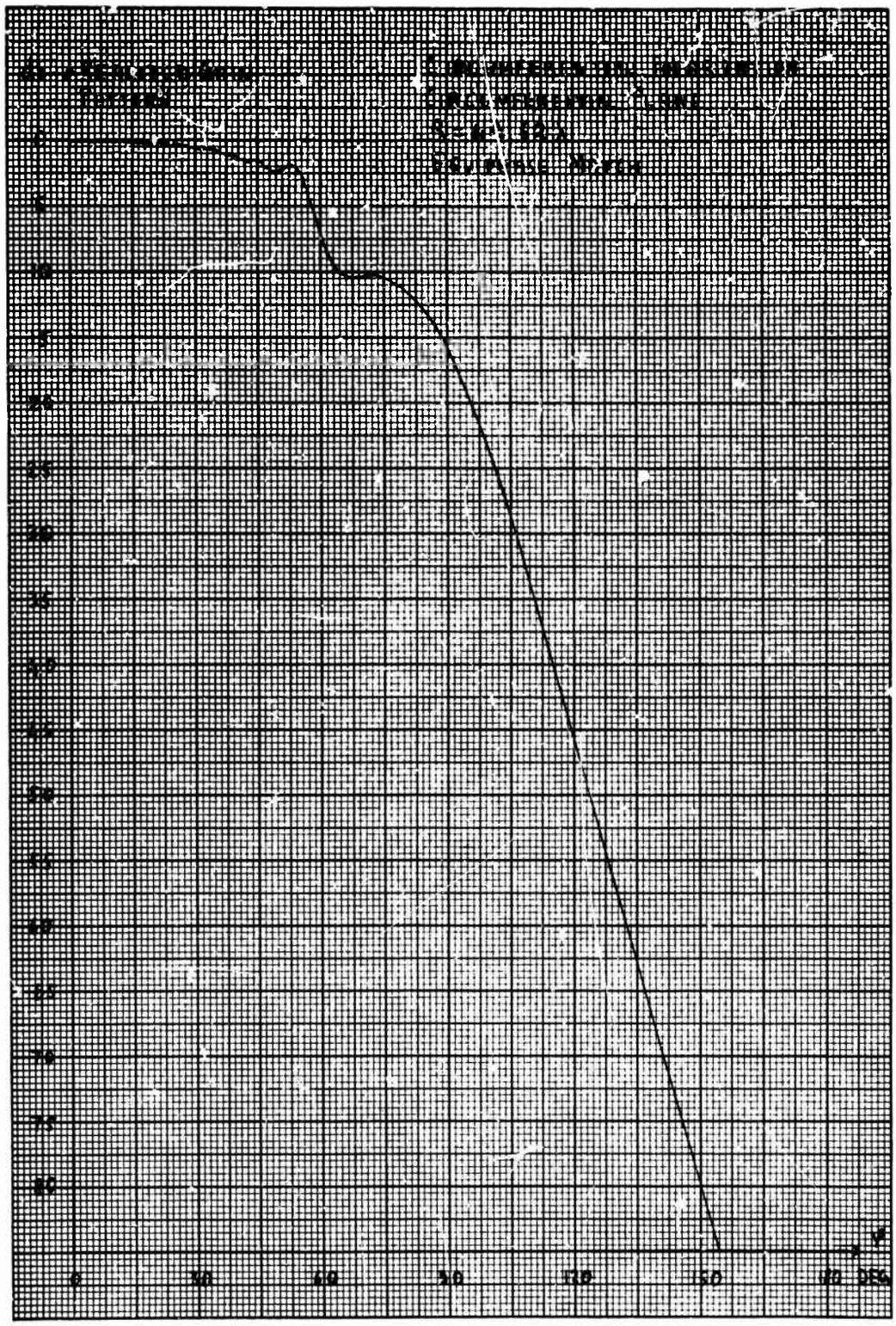


Figure 11 - Realized Gain Pattern. Circumferential Plane. Circumferential Polarization. Equiphase Match (R = 49.62λ)

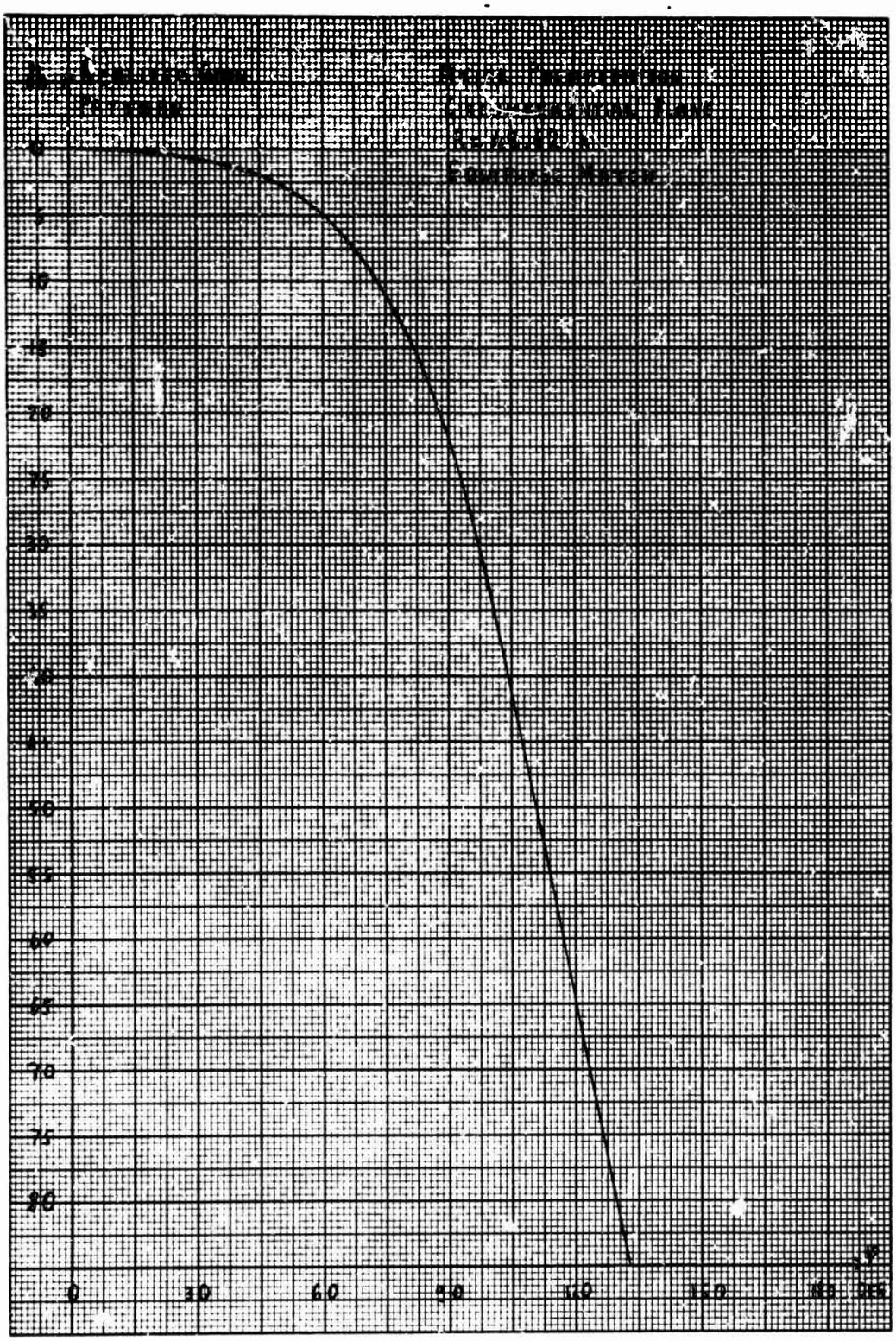


Figure 12 - Realized Gain Pattern. Circumferential Plane. Axial Polarization. Equiphase Match (R = 49.62λ)

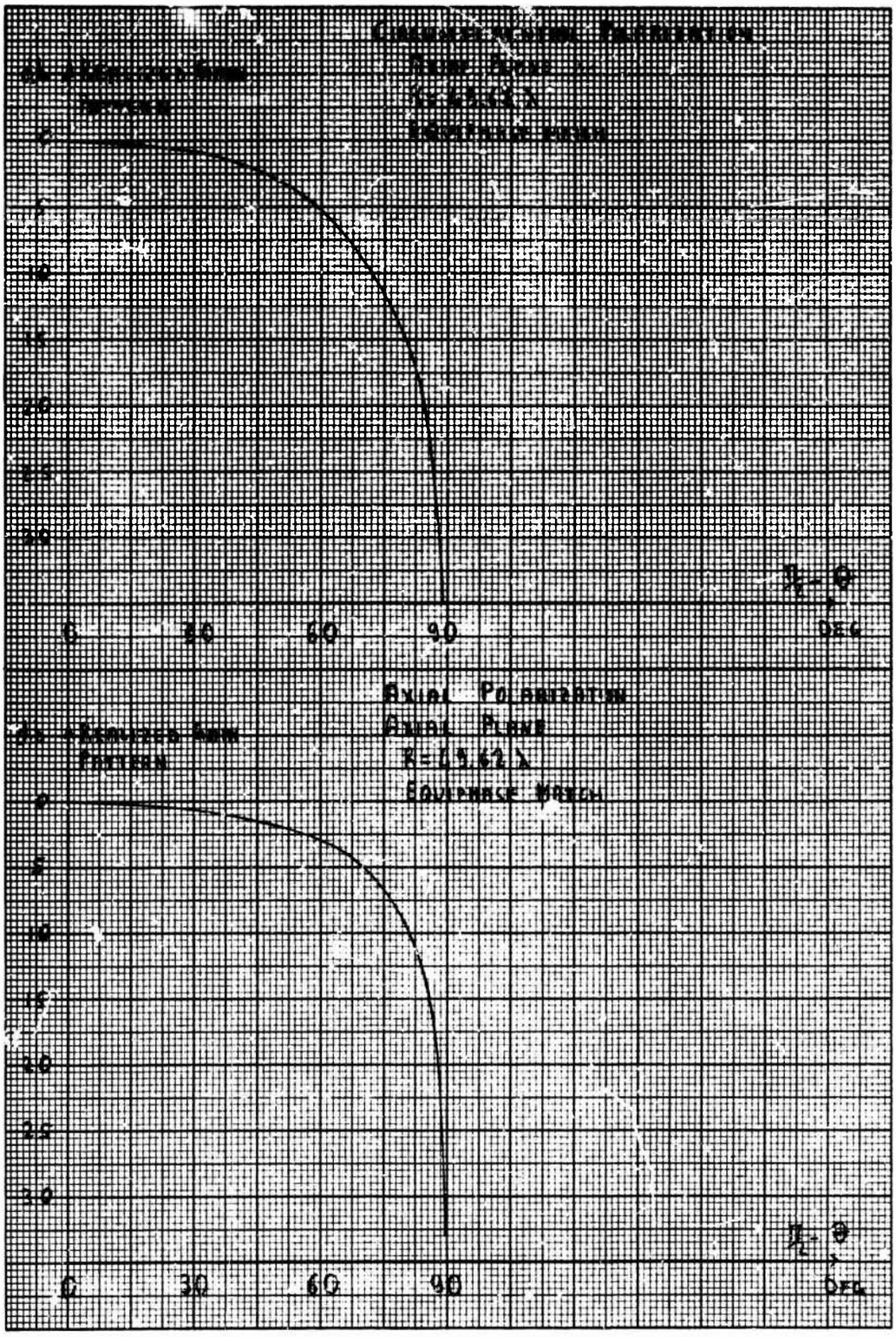


Figure 13 - Realized Gain Pattern. Axial Plane. Equiphase Ma..ch (R = 49.62λ)

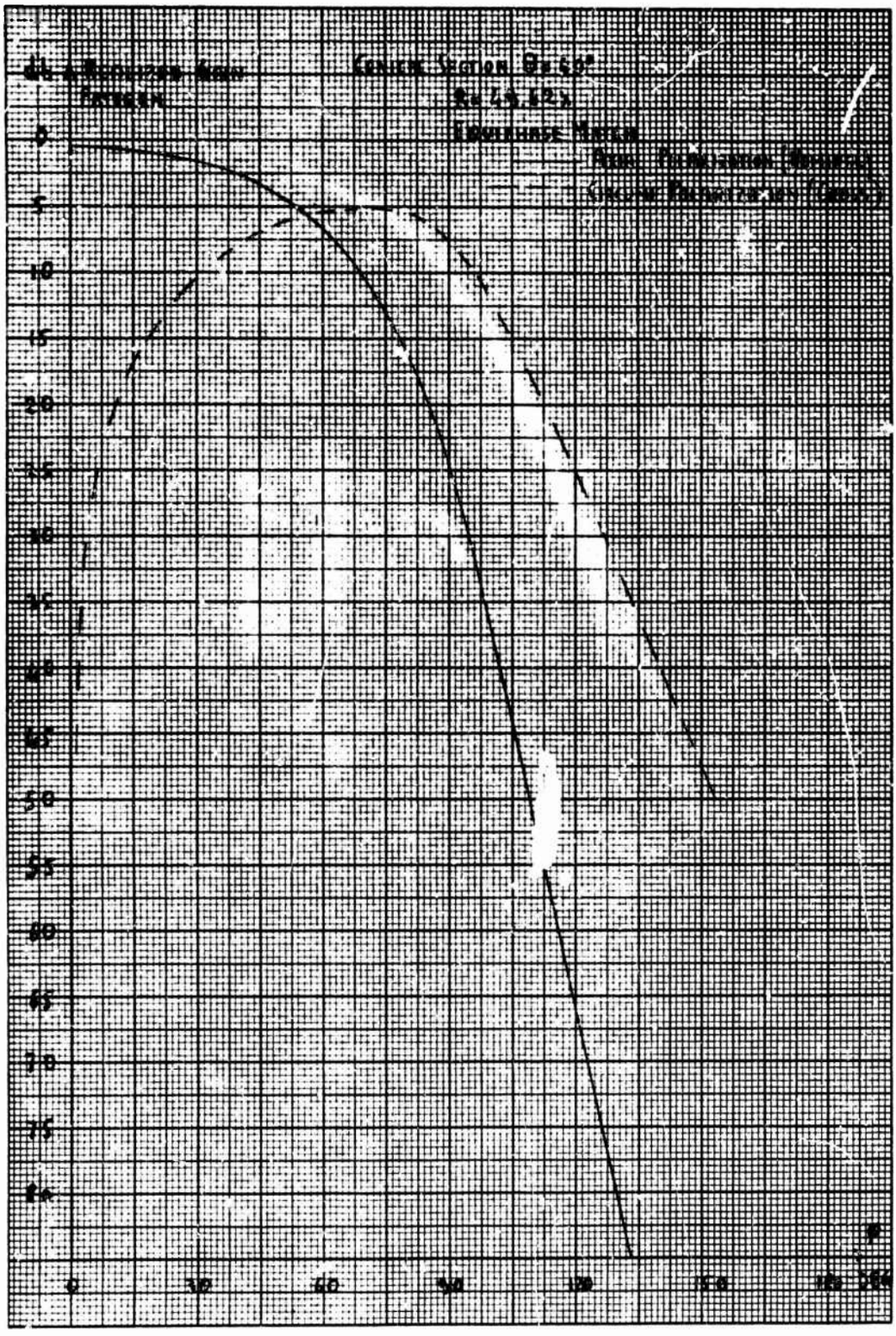


Figure 14 - Realized Gain Pattern. Conical Section θ = 60°. Axial Polarization Excited. Equiphase Match (R = 49.62λ)

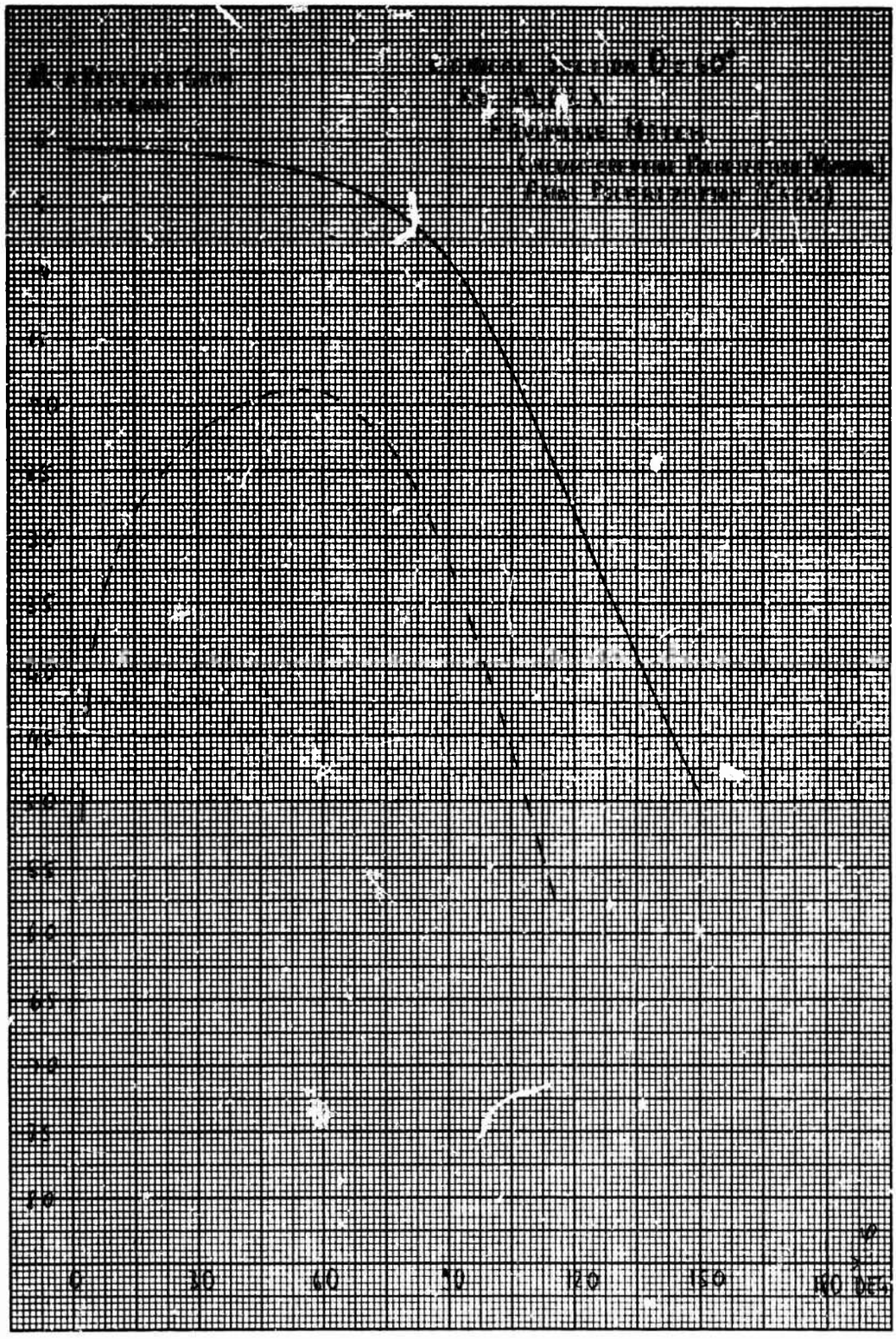


Figure 15 - Realized Gain Pattern. Conical Section $\theta = 60°$. Circumferential Polarization Excited. Equiphase Match ($R = 49.62\lambda$)

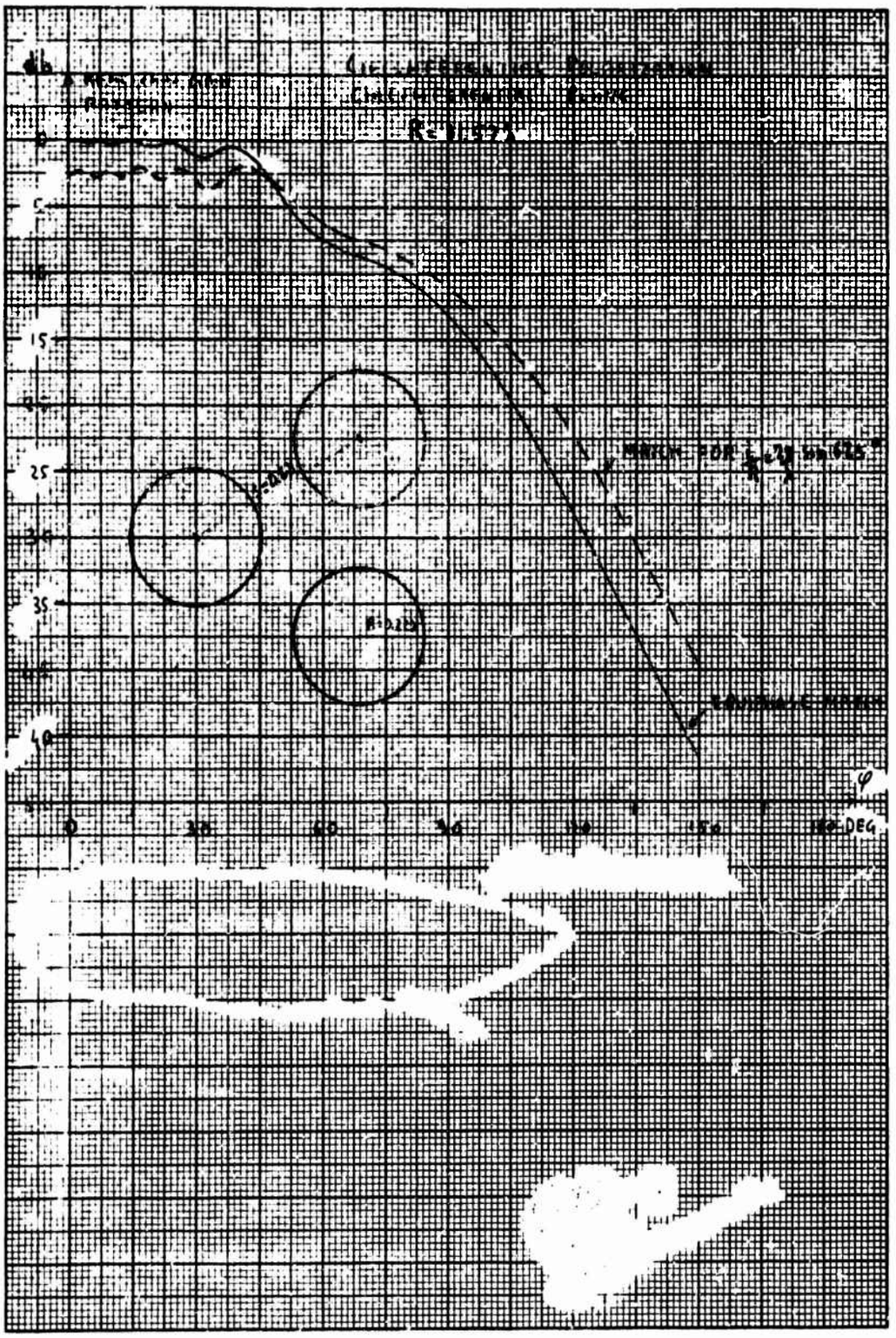


Figure 16 - Realized Gain Pattern, Circumferential Plane, Circumferential Polarization (R = 11.57 λ)

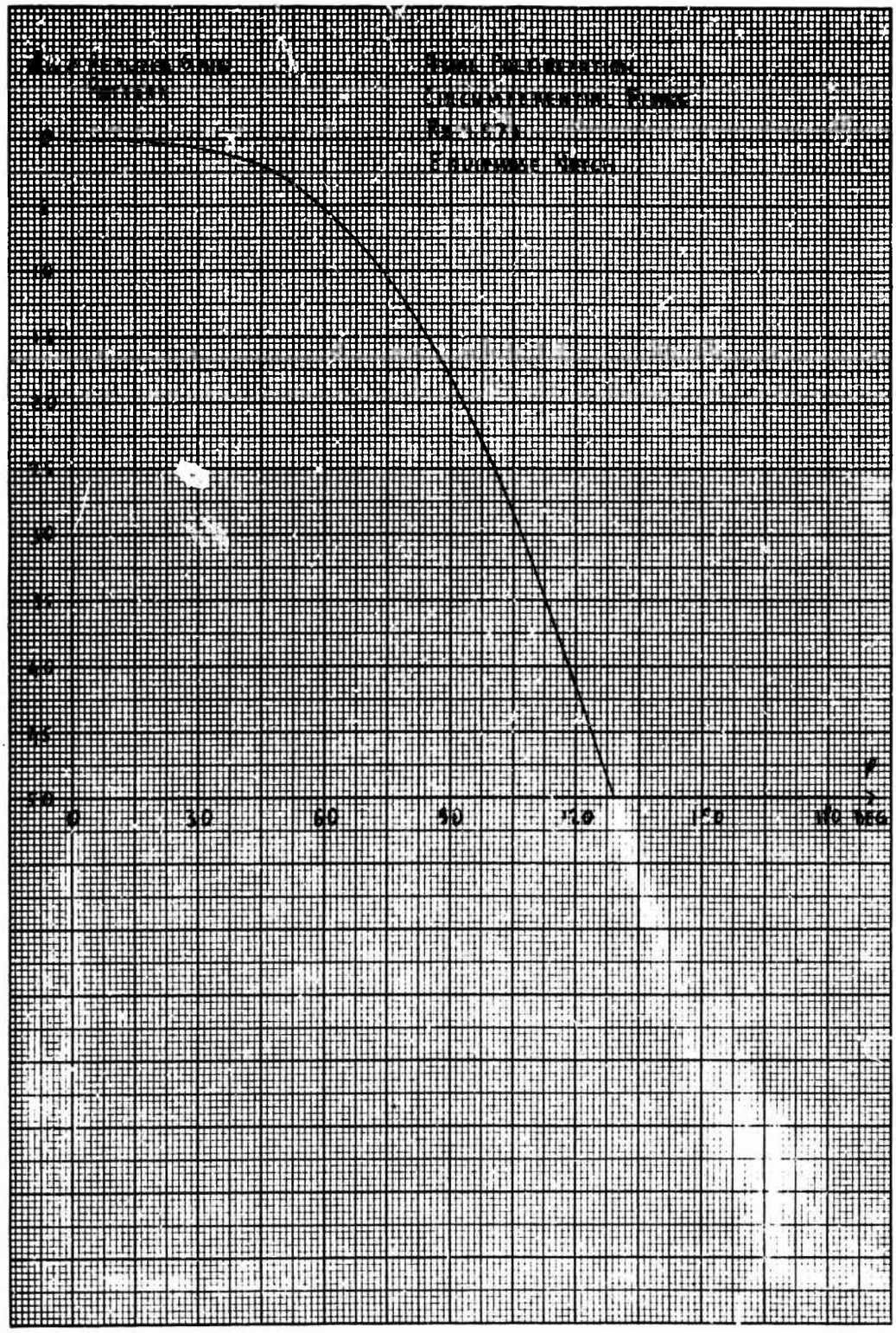


Figure 17 - Realized Gain Pattern. Circumferential Plane. Axial Polarization. Equiphase Match (R = 11.57λ)

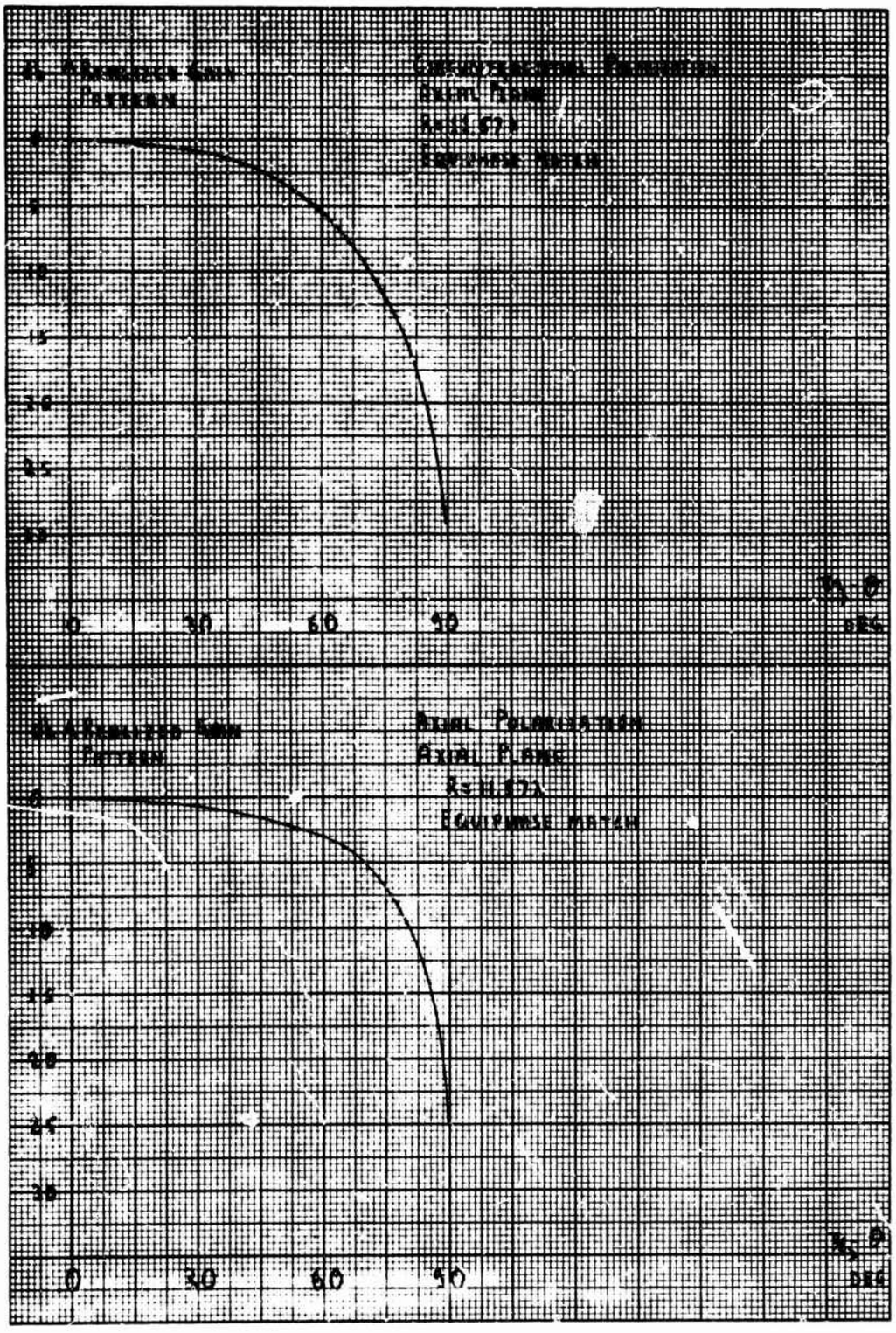


Figure 18 - Realized Gain Pattern. Axial Plane. Equiphase Match
(R = 11.57λ)

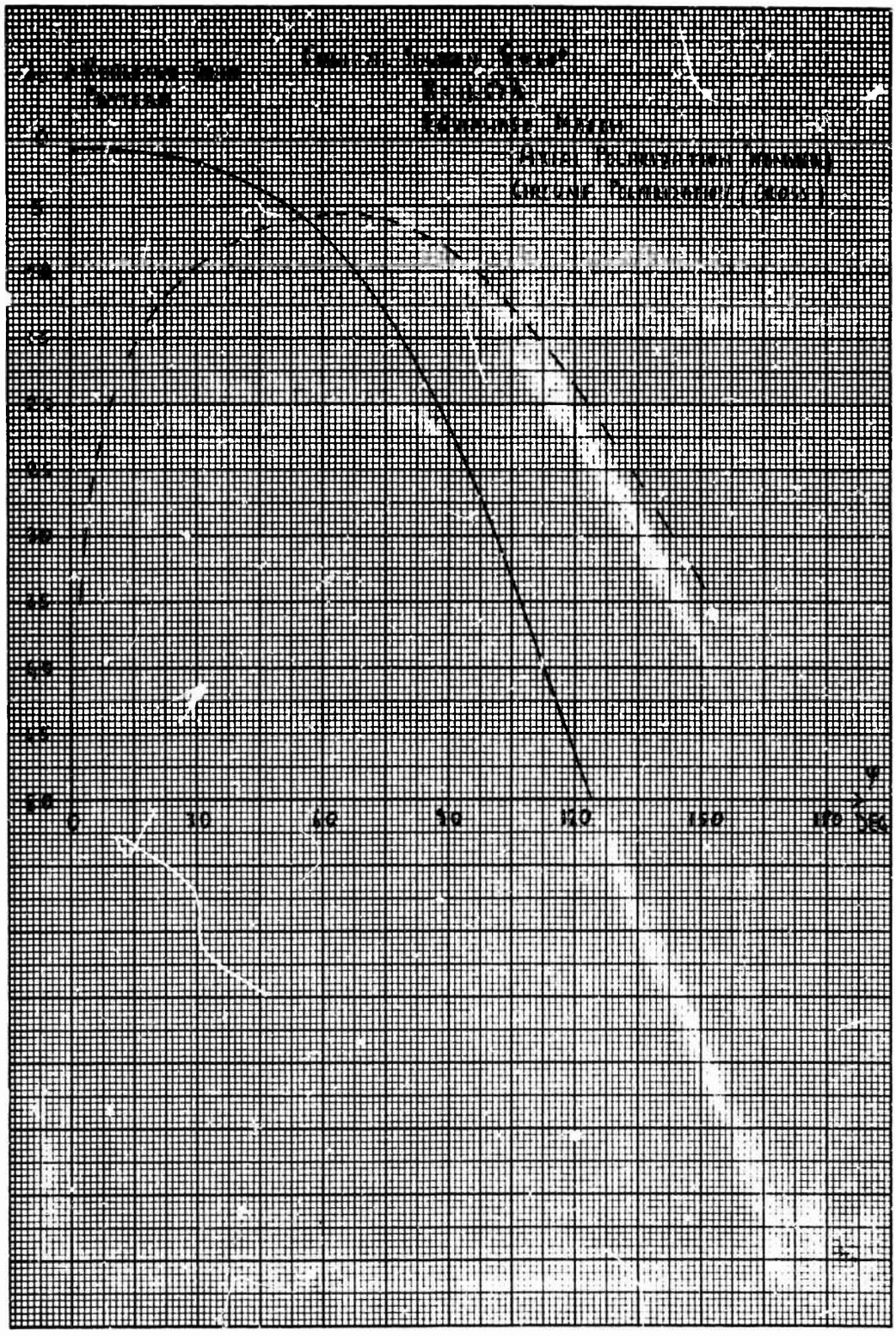


Figure 19 - Realized Gain Pattern. Conical Section θ = 60°. Axial Polarization Excited. Equiphase Match (R = 11.57λ)

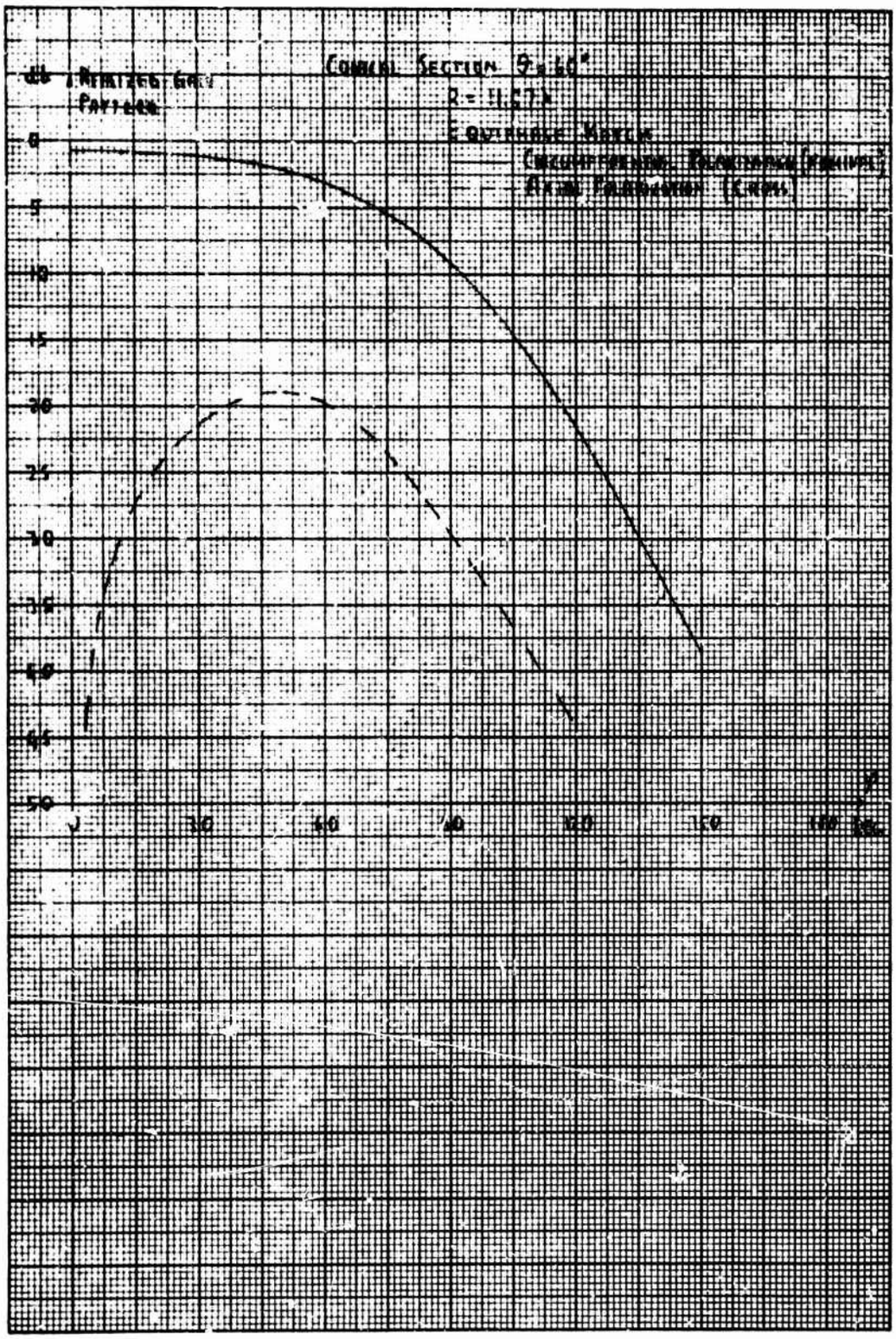


Figure 20 - Realized Gain Pattern. Conical Section θ = 60°. Circumferential Polarization Excited. Equiphase Match (R = 11.57λ)

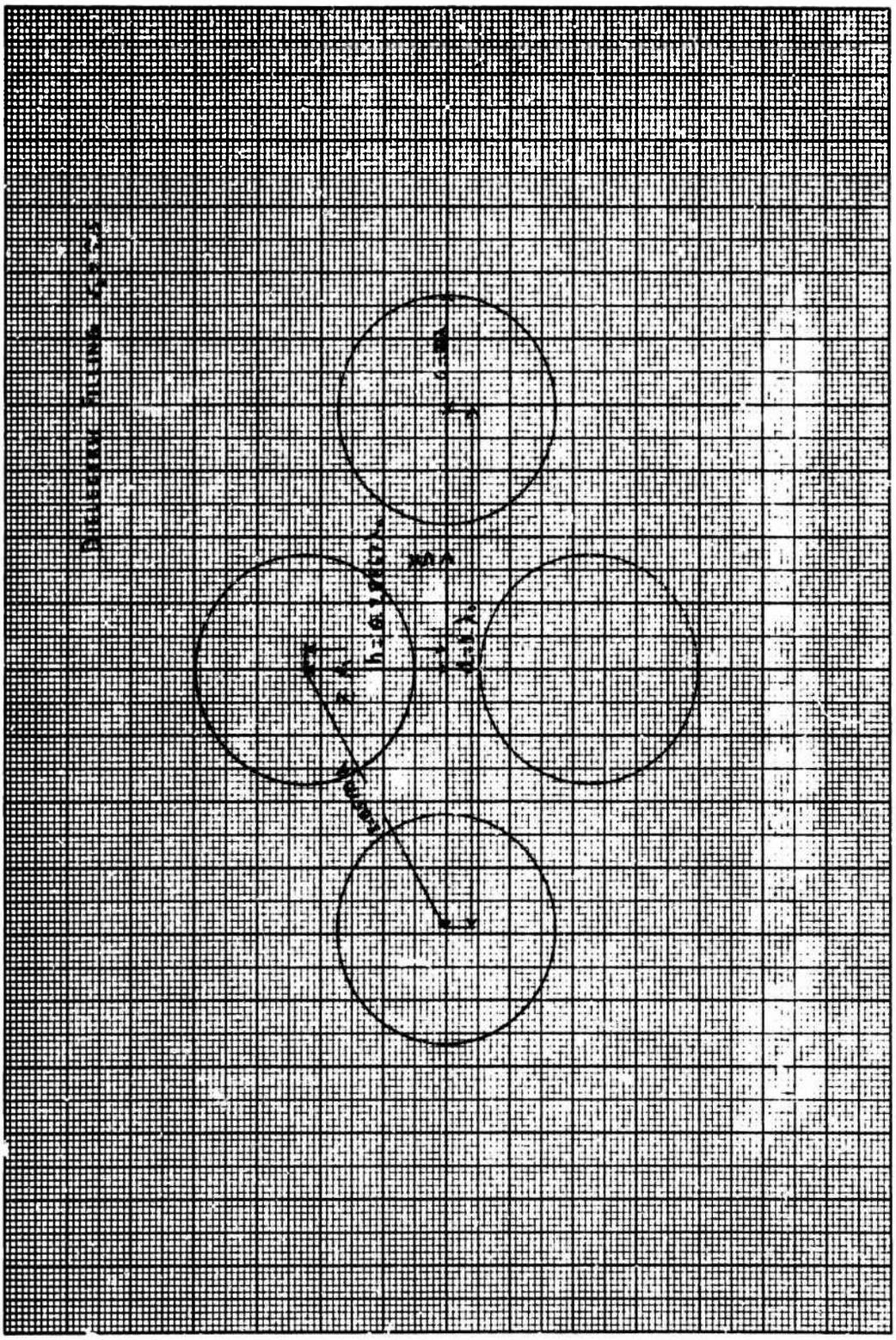


Figure 21 - Lattice 2

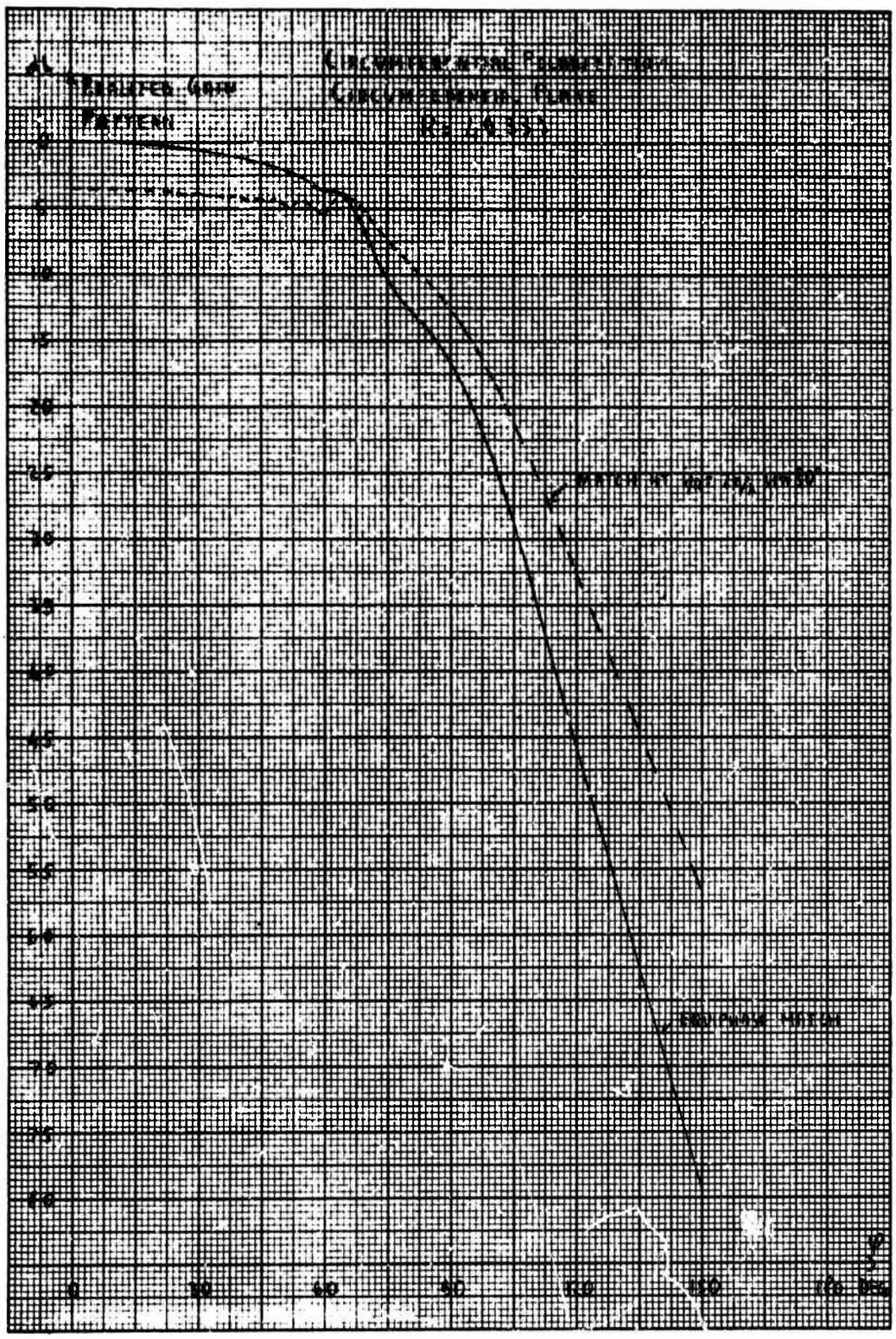


Figure 22 - Realized Gain Pattern, Circumferential Plane, Circumferential Polarization (R = 49.33λ)

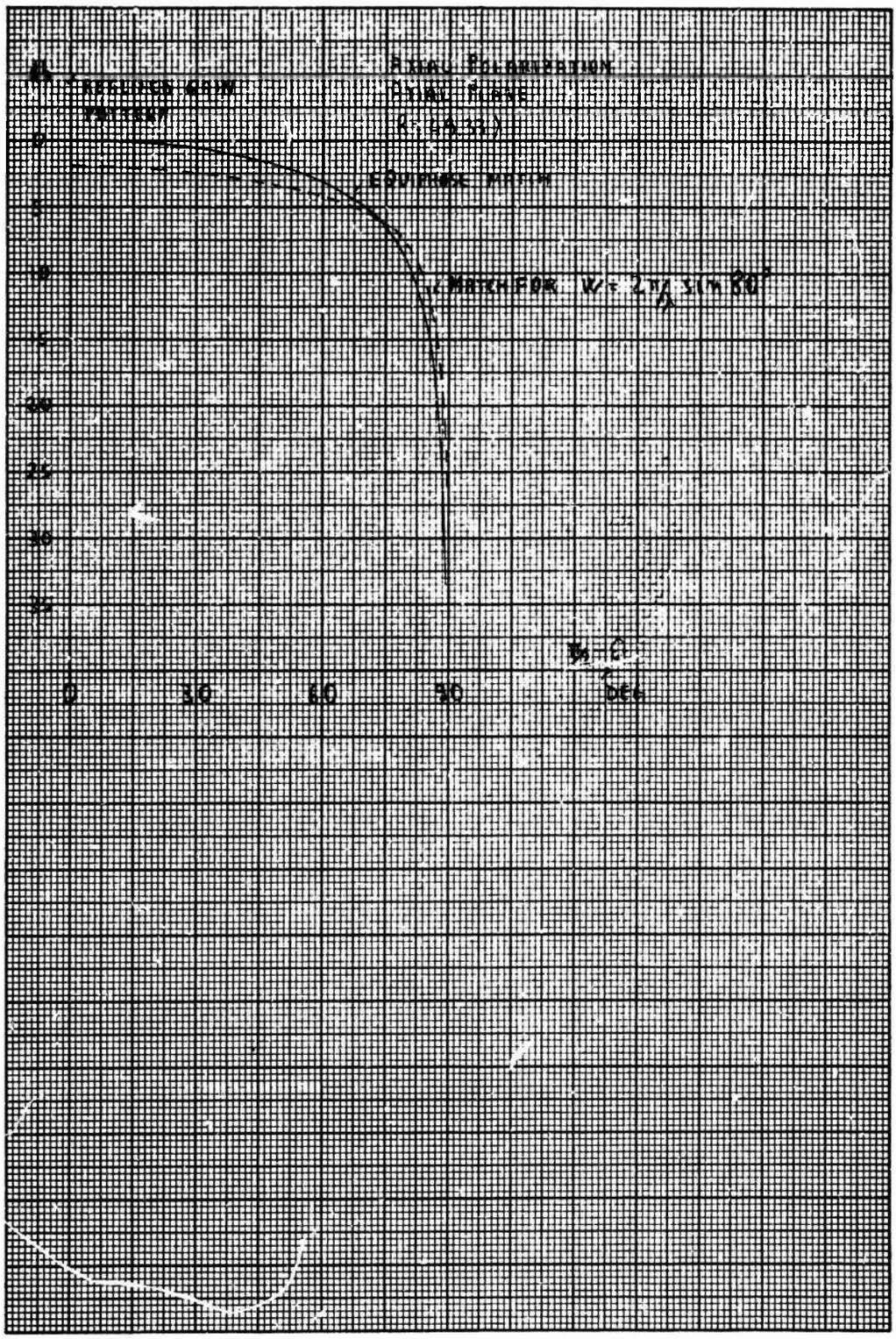


Figure 23 - Realized Gain Pattern. Axial Plane. Axial Polarization. (R = 49. 33λ)

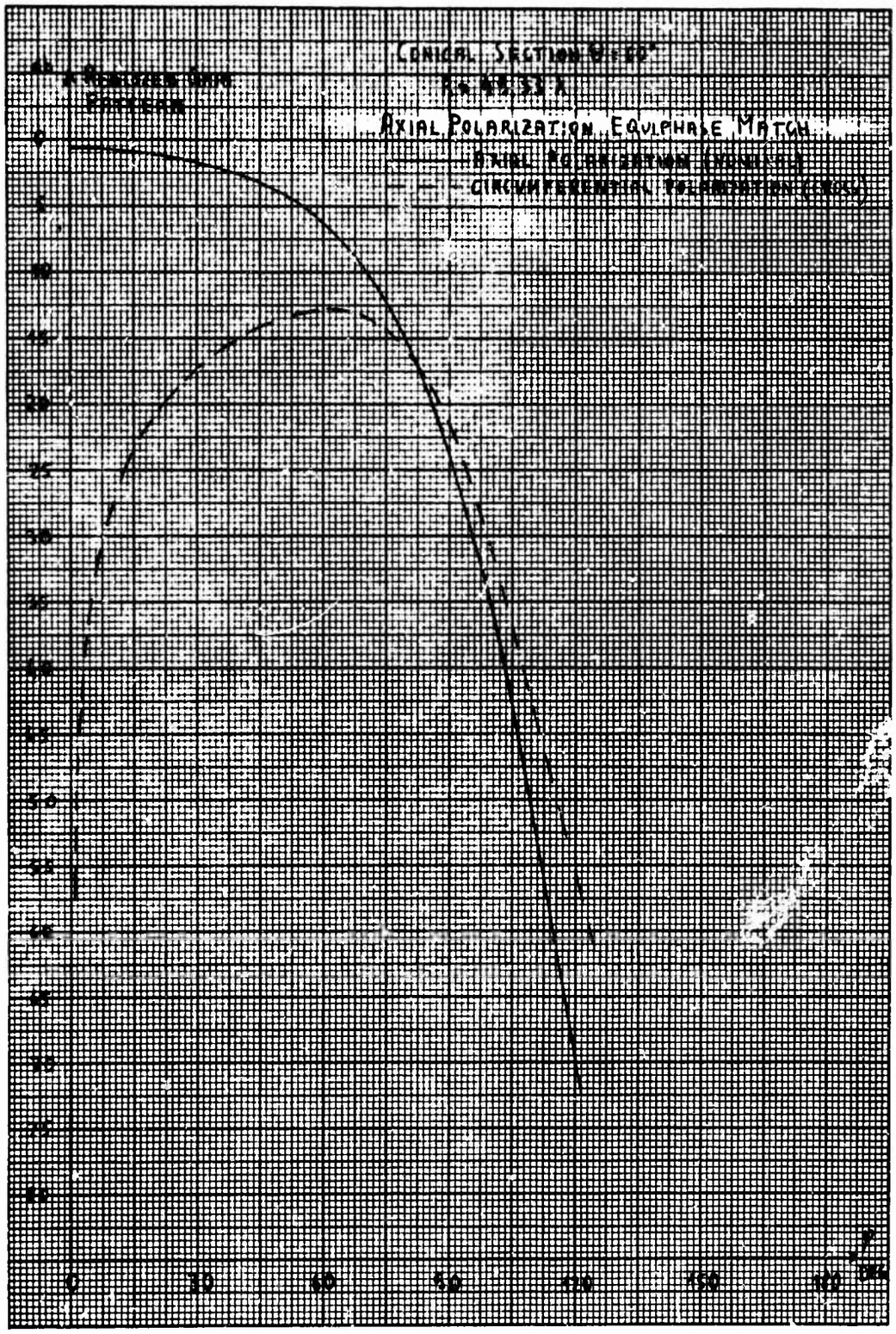


Figure 24 - Realized Gain Pattern, Conical Section θ= 60°. Axial Polarization Excited, Equiphase Match (R = 49.33λ)

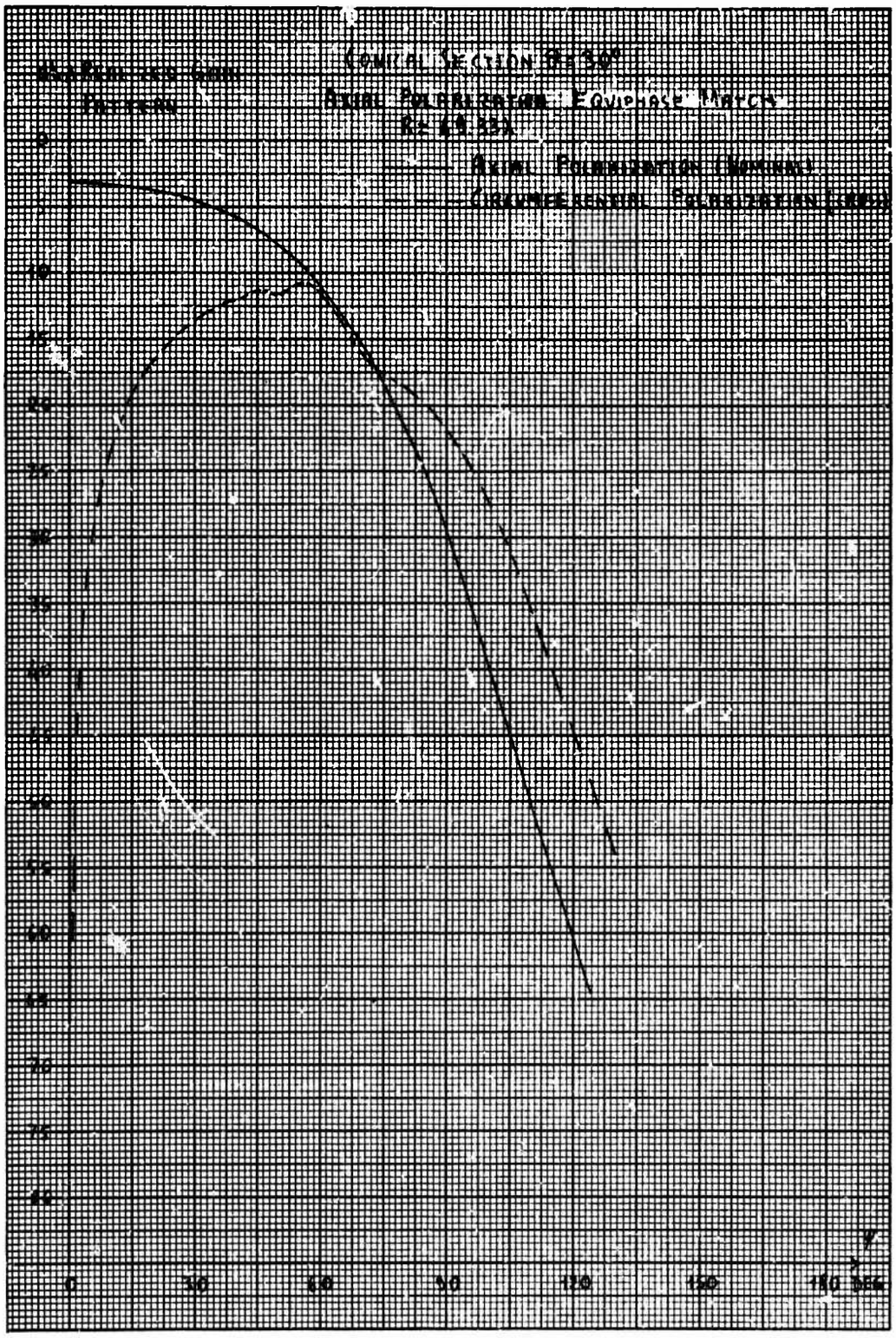


Figure 25 - Realized Gain Pattern. Conical Section θ= 30°. Axial Polarization Excited. Equiphase Match (R = 49. 33λ)

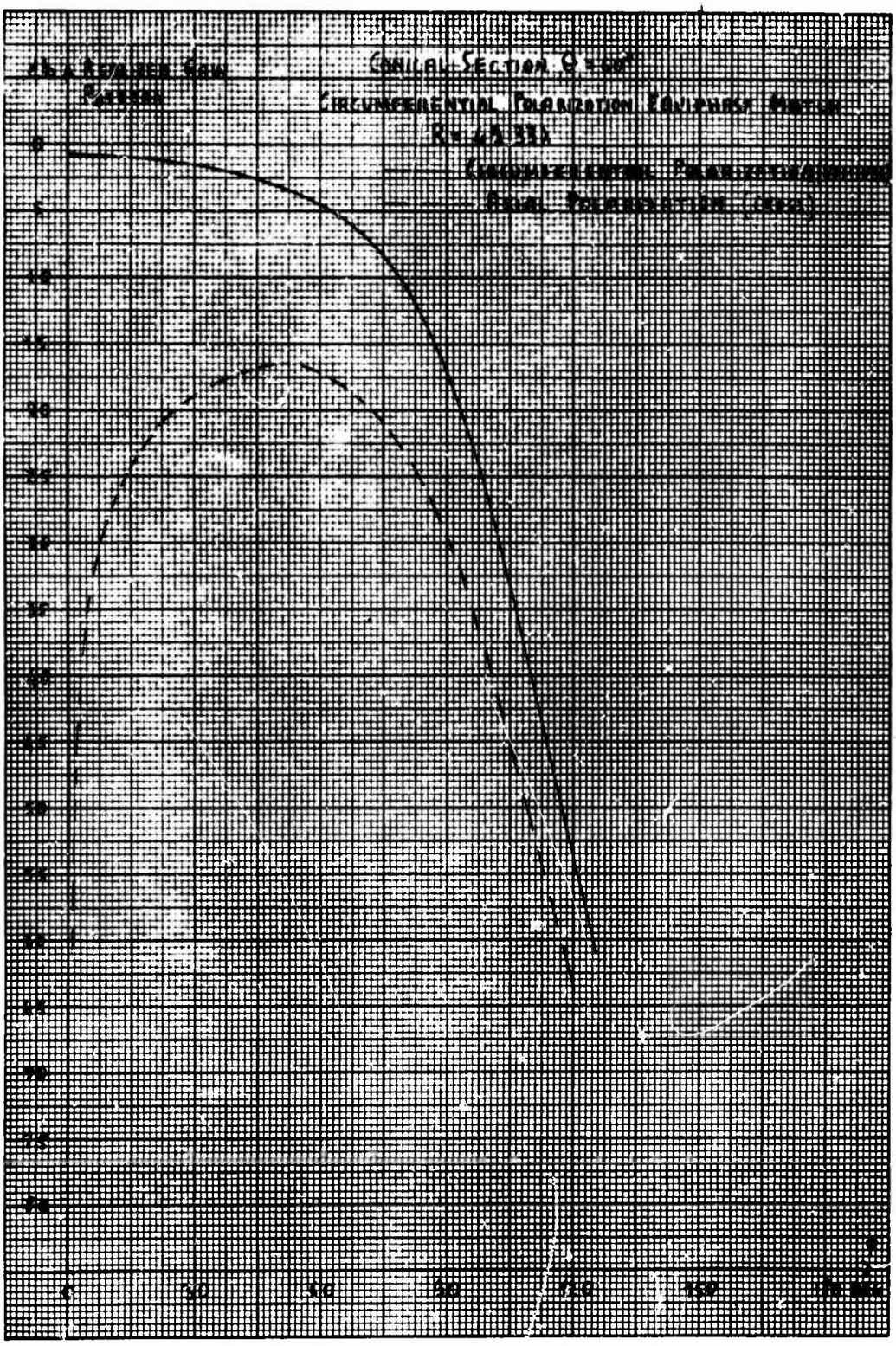


Figure 26 - Realized Gain Pattern, Conical Section $\theta = 60°$, Circumferential Polarization Excited, Equiphase Match (R = 49.33λ)

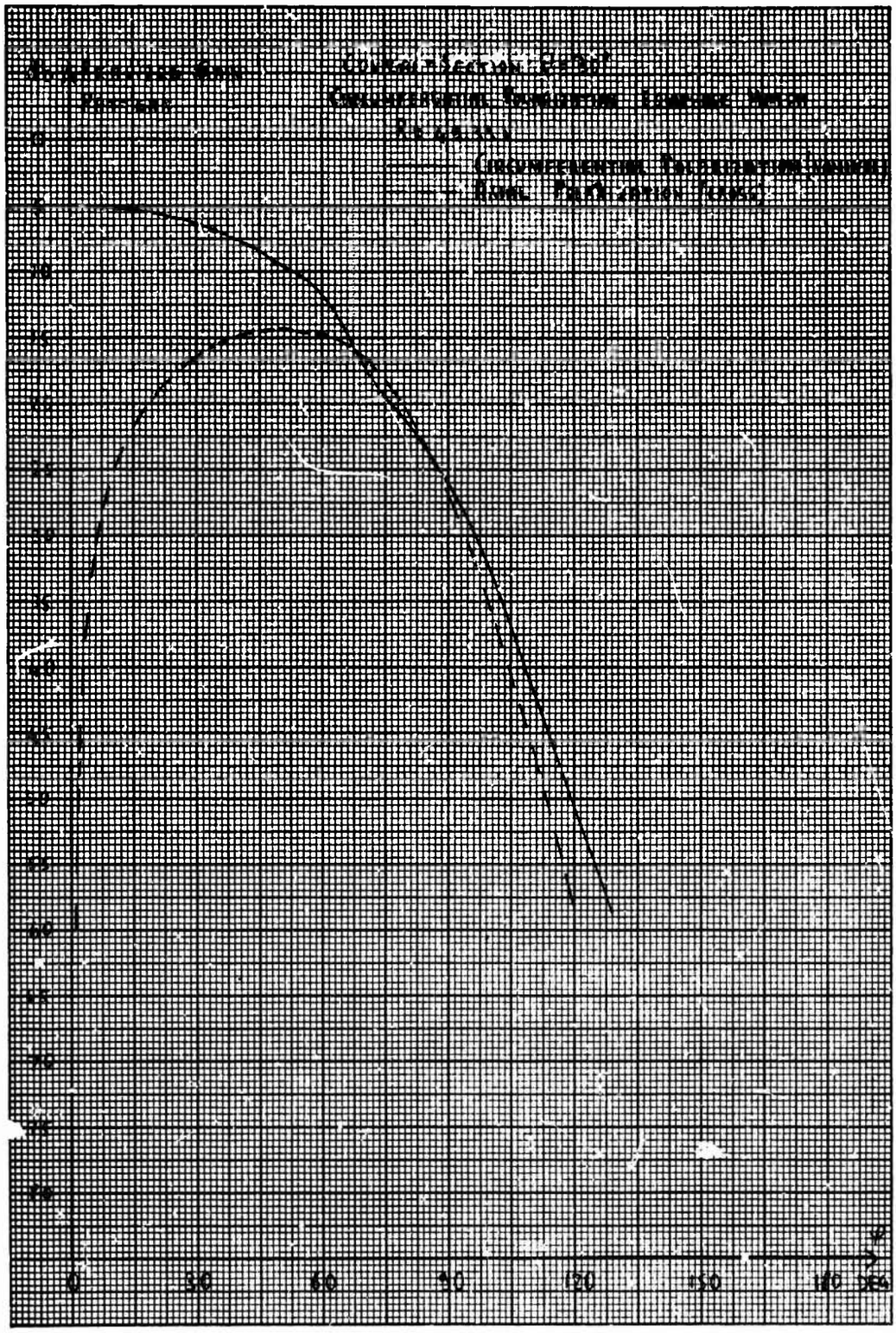


Figure 27 - Realized Gain Pattern, Conical Section $\theta = 30^\circ$, Circumferential Polarization Excited, Equiphase Match (R = 49.33λ)

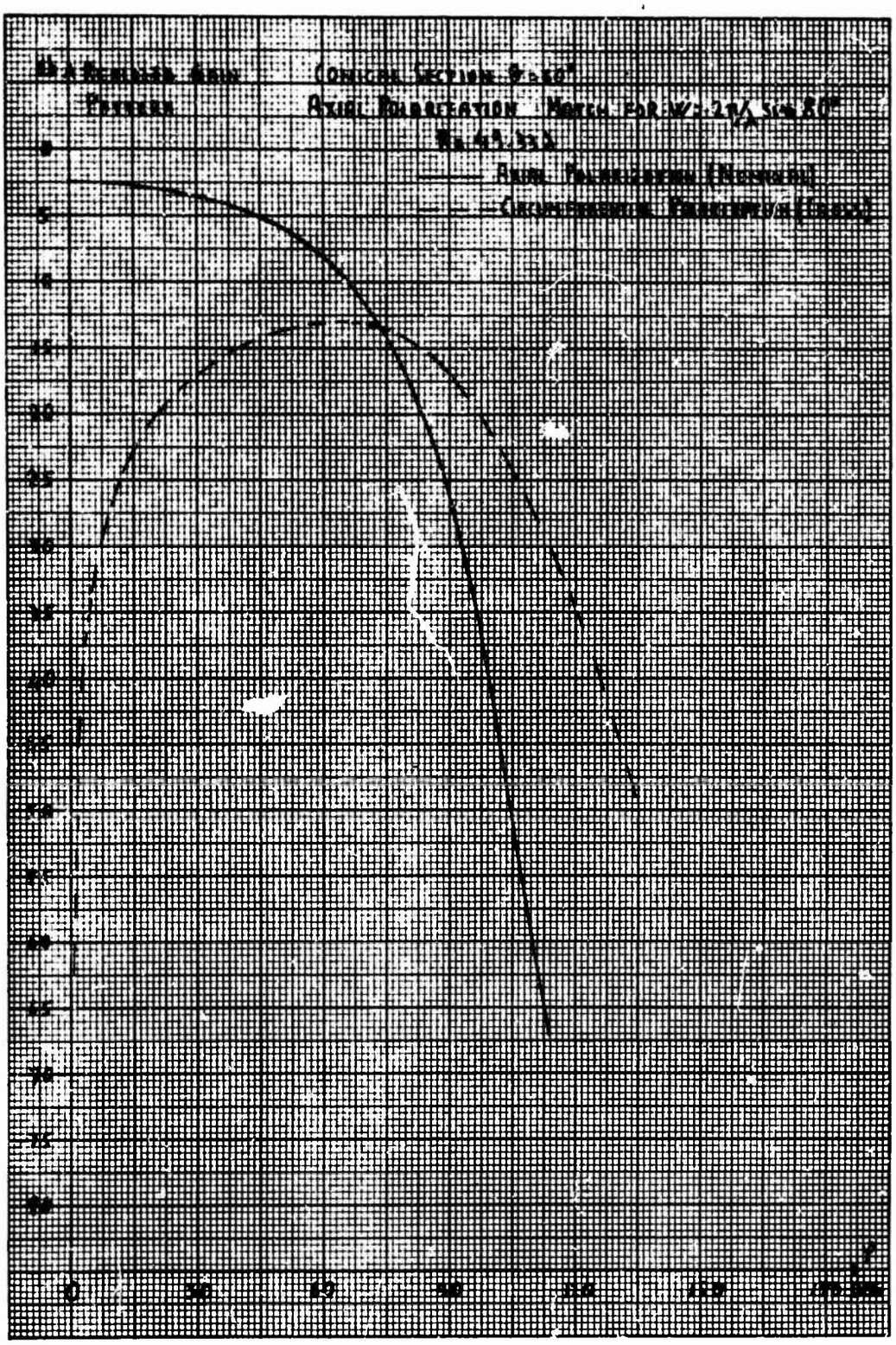


Figure 28 - Realized Gain Pattern, Conical Section $\theta = 60°$, Axial Polarization Excited, Match for $w = k \sin 80°$ ($R = 49.33\lambda$)

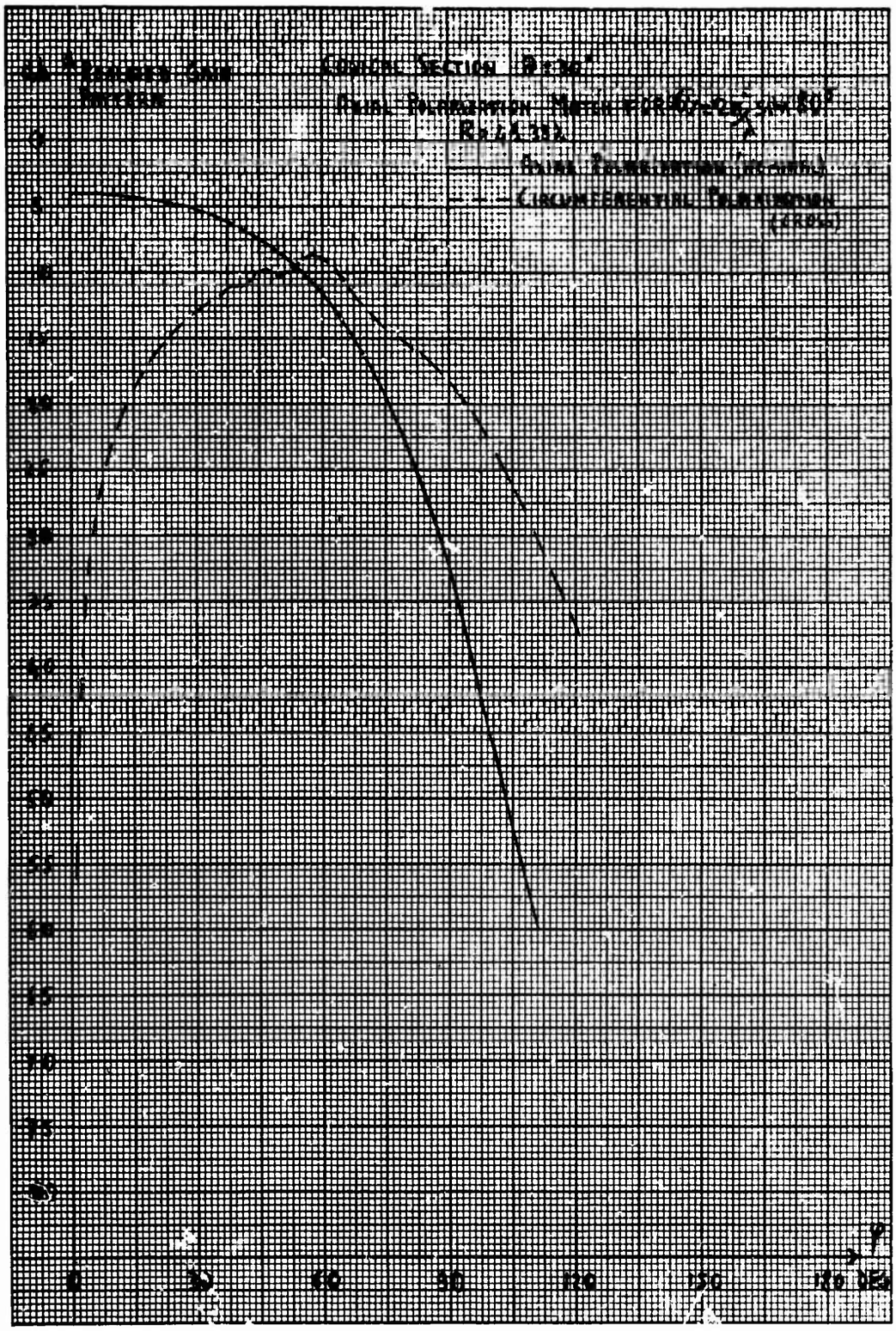


Figure 29 - Realized Gain Pattern. Conical Sectio_ $\theta = 30^\circ$. Axial Polarization Excited. Match for $w = k \sin 80^\circ$ ($R = 49.33\lambda$)

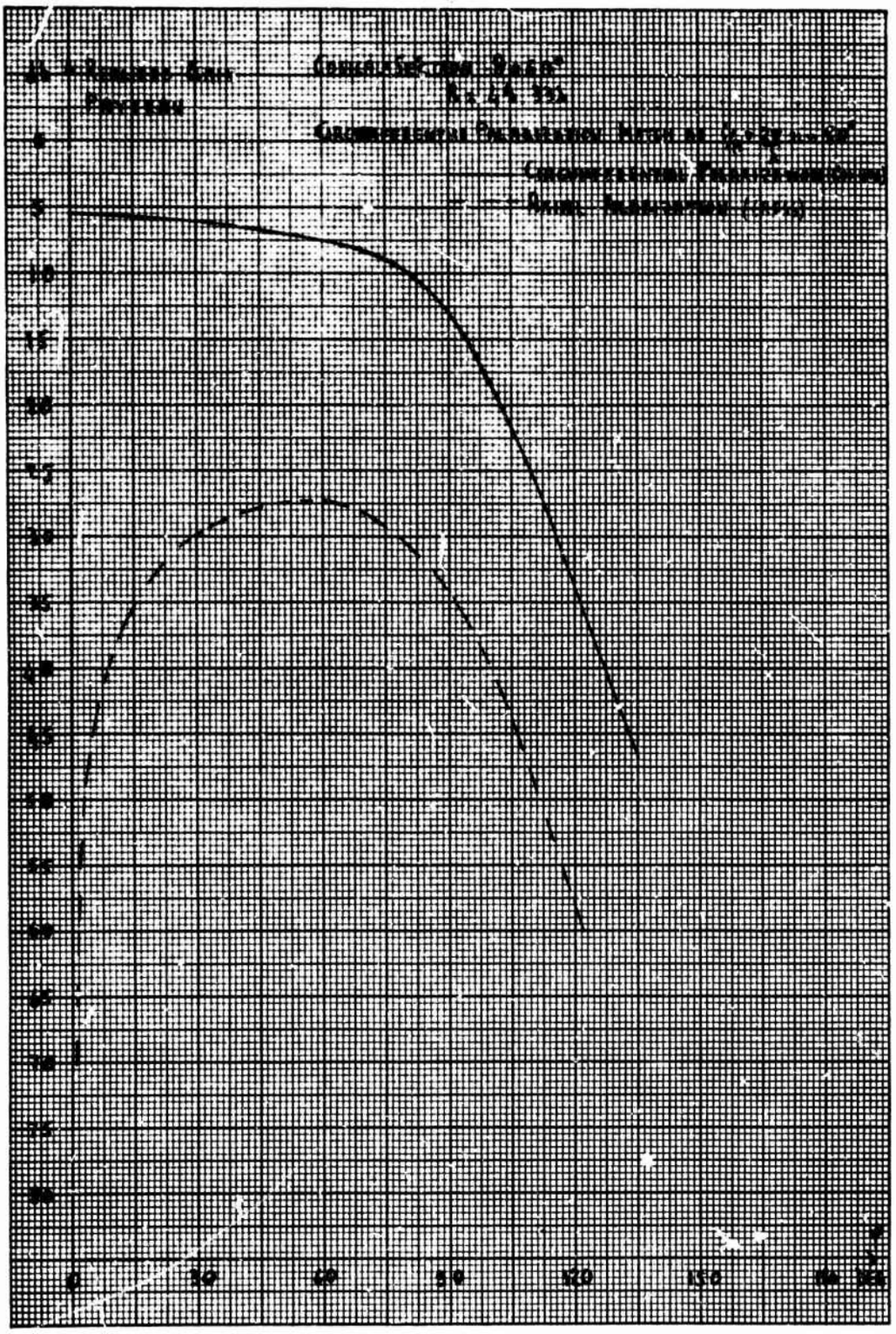


Figure 30 - Realized Gain Pattern. Conical Section $\theta = 60°$. Circumferential Polarization Excited. Match for $i/R = k \sin 80°$. ($R = 49.33\lambda$)

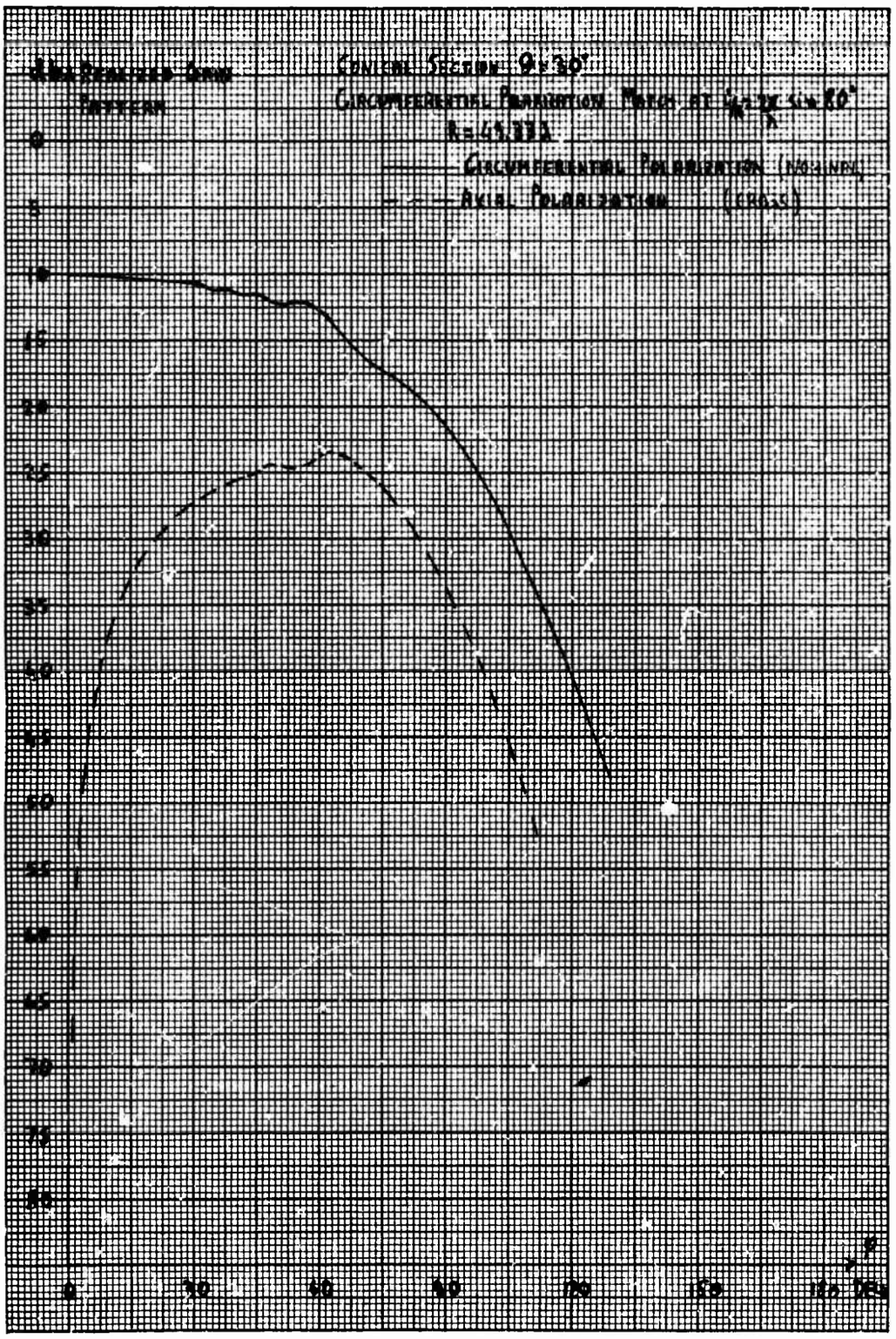


Figure 31 - Realized Gain Pattern. Conical Section $\theta = 30°$. Circumferential Polarization Excited. Match for $i/R = k \sin 80°$. ($R = 49.33\lambda$)

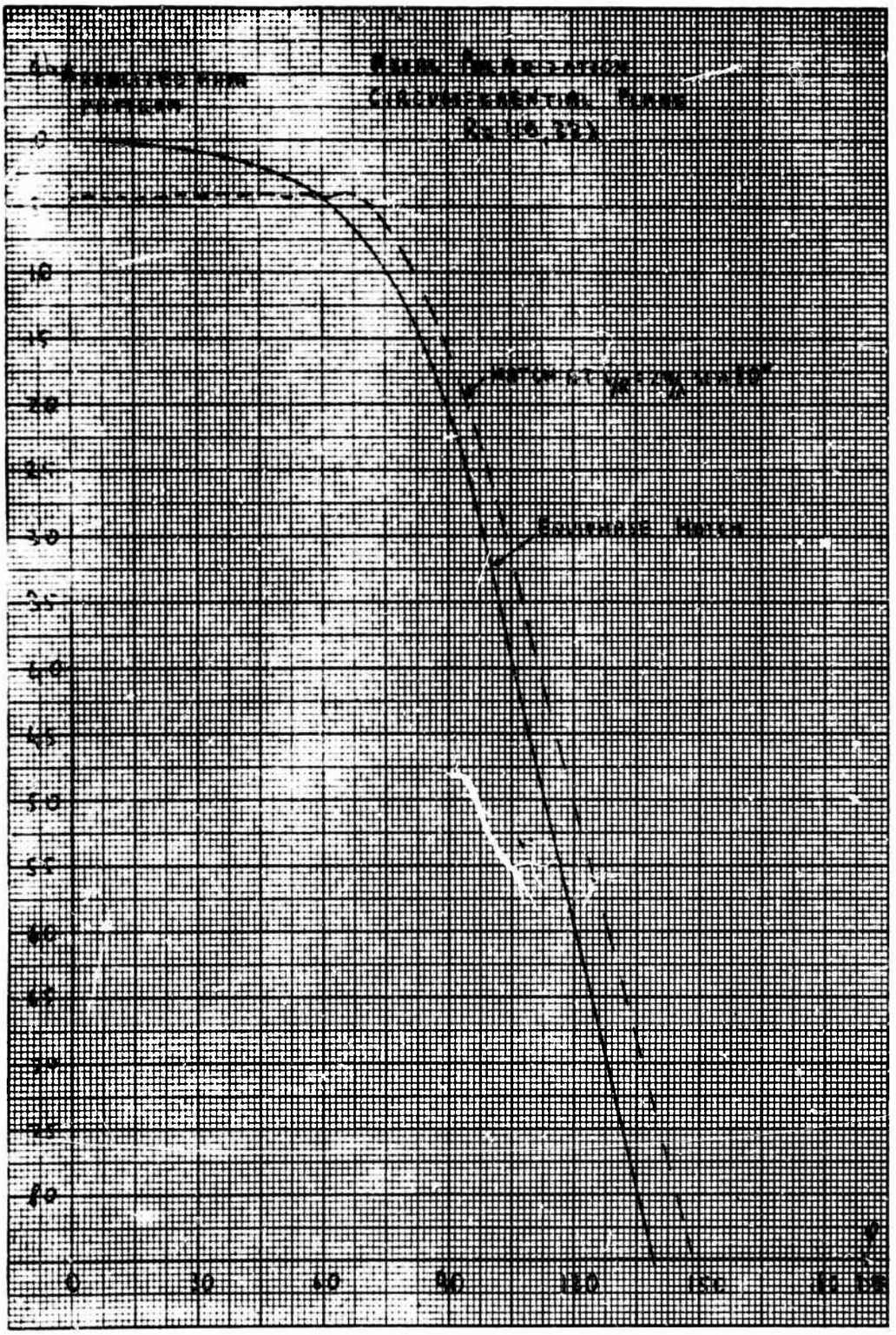


Figure 32 - Realized Gain Pattern, Circumferential Plane, Axial Polarization (R = 49.33λ)

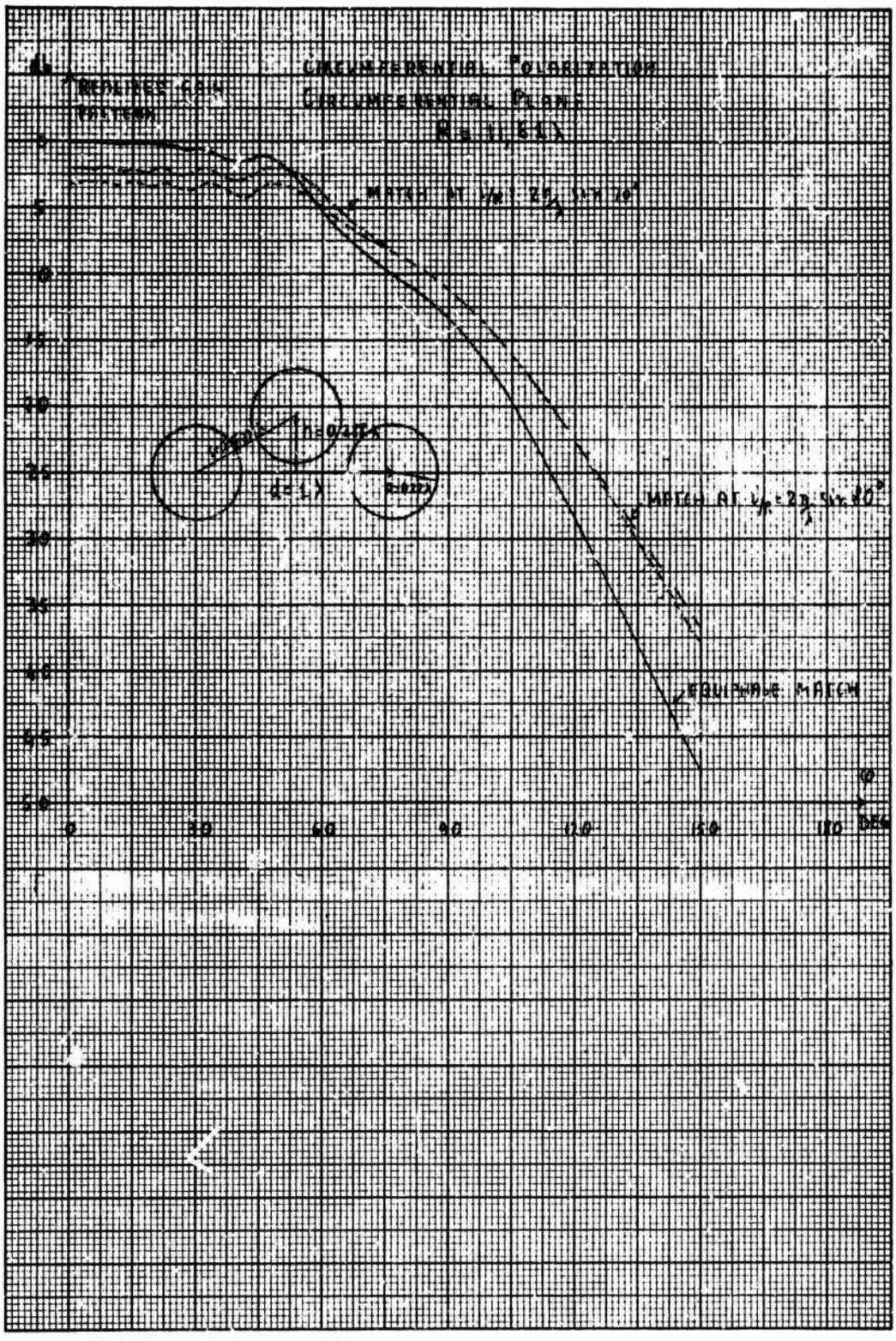


Figure 33 - Realized Gain Pattern, Circumferential Plane, Circumferential Polarization (R = 11.61λ)

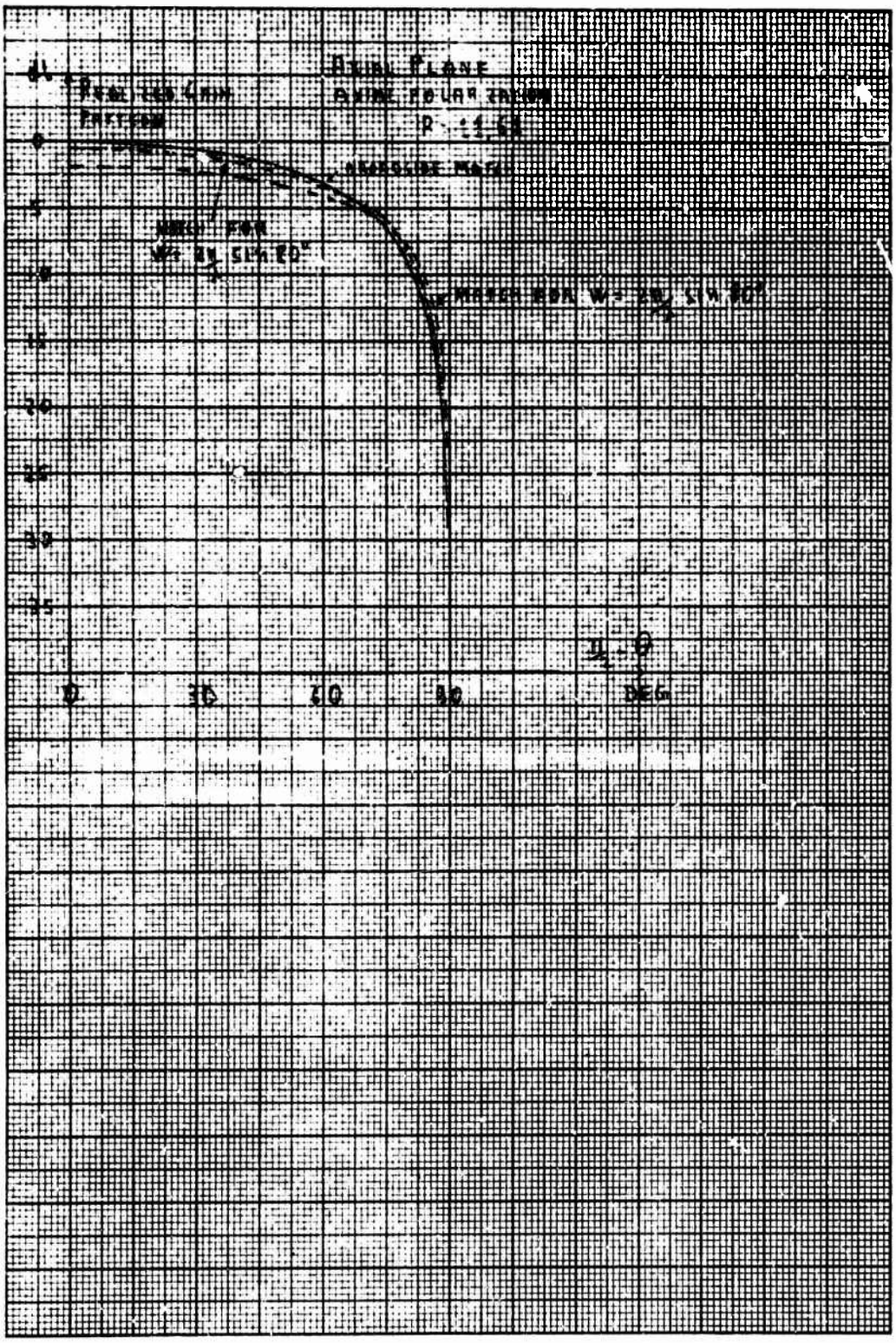


Figure 34 - Realized Gain Pattern, Axial Plane, Axial Polarization, (R = 11.61 λ)

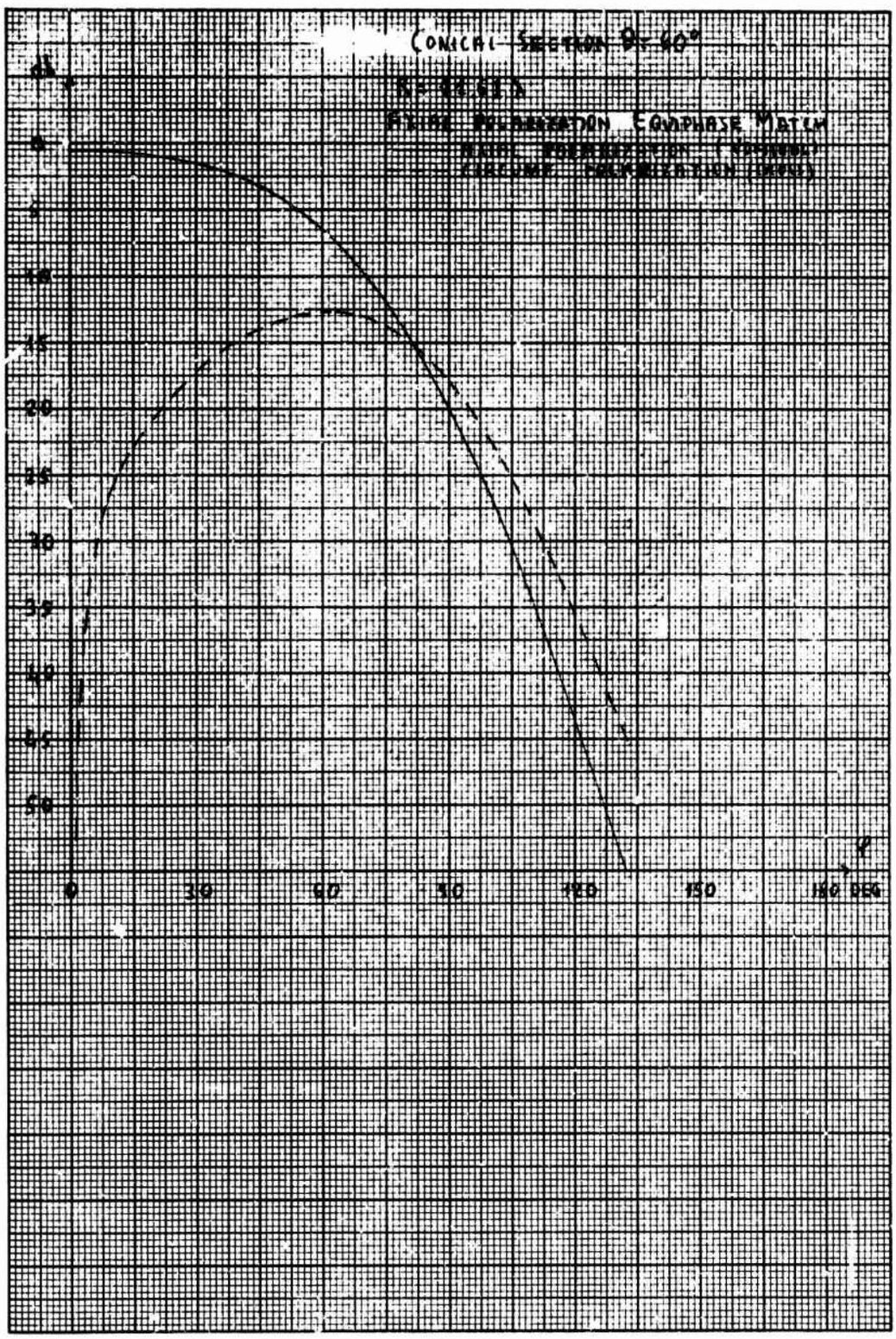


Figure 35 - Realized Gain Pattern. Conical Section $\theta = 60°$. Axial Polarization Excited. Equiphase Match ($R = 11.61\lambda$)

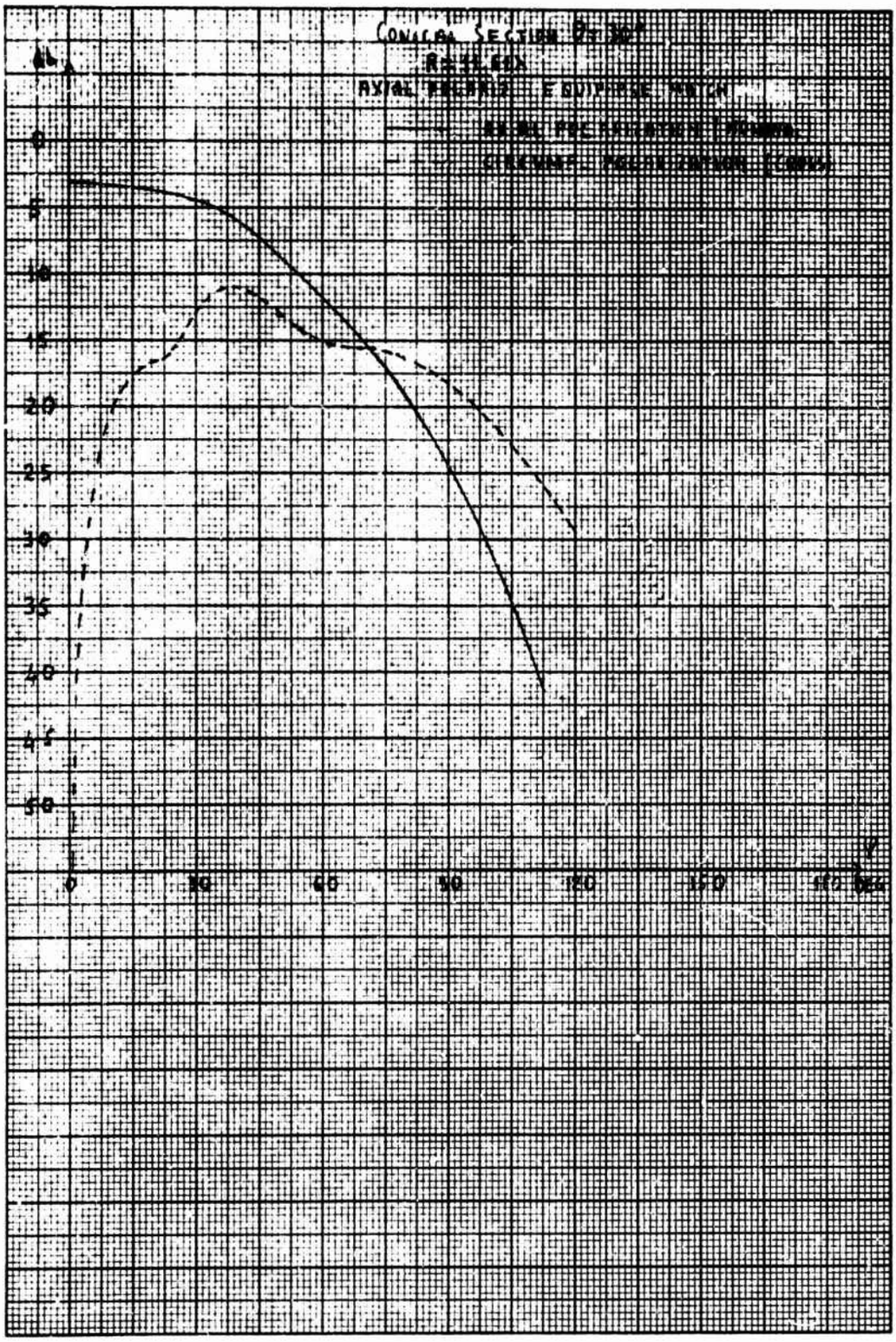


Figure 36 - Realized Gain Pattern, Conical Section $\theta = 30°$, Axial Polarization Excited, Equiphase Match ($R = 11.61\lambda$)

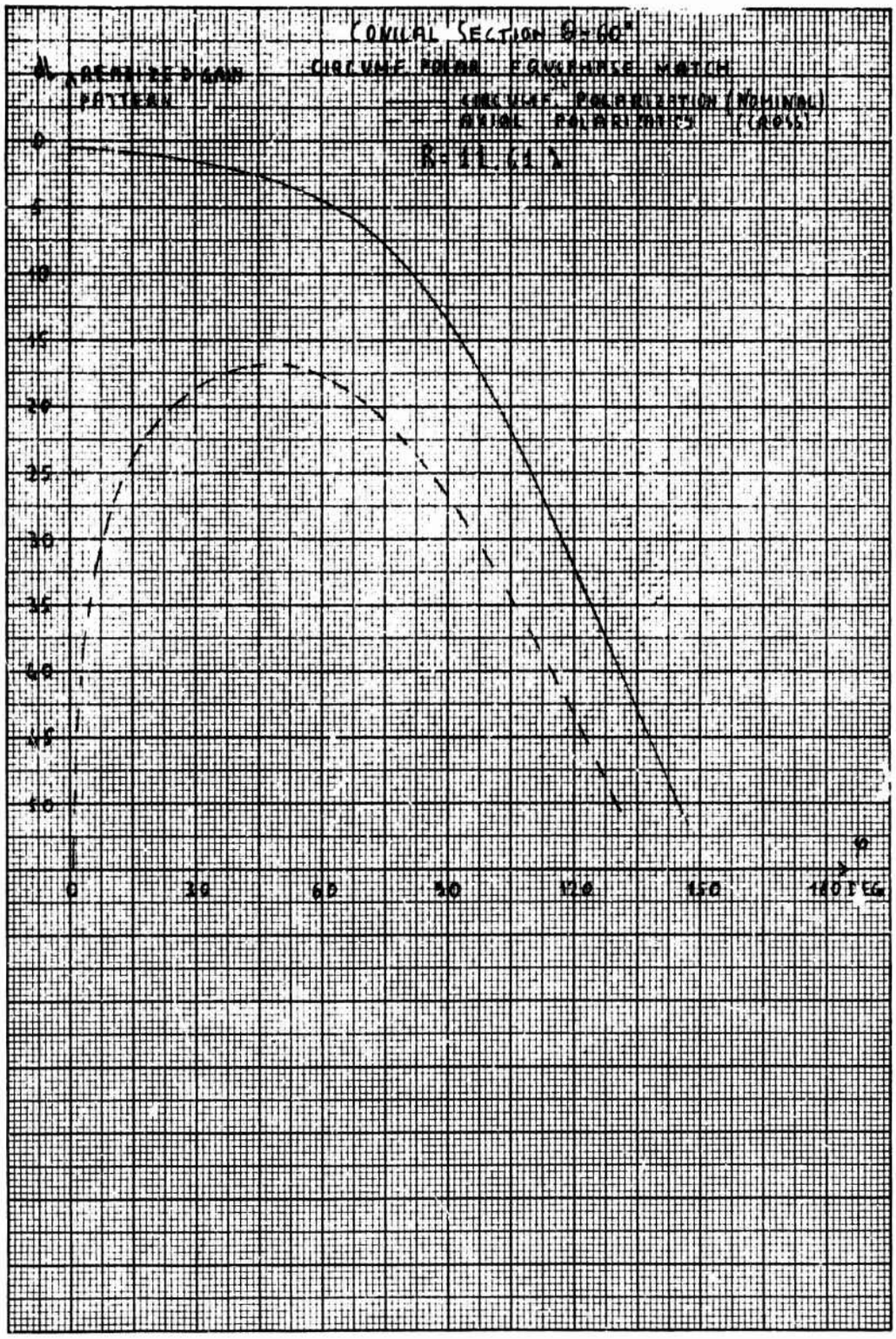


Figure 37 - Realized Gain Pattern. Conical Section $\theta = 60°$. Circumferential Polarization Excited. Equiphase Match ($R = 11.61\lambda$)

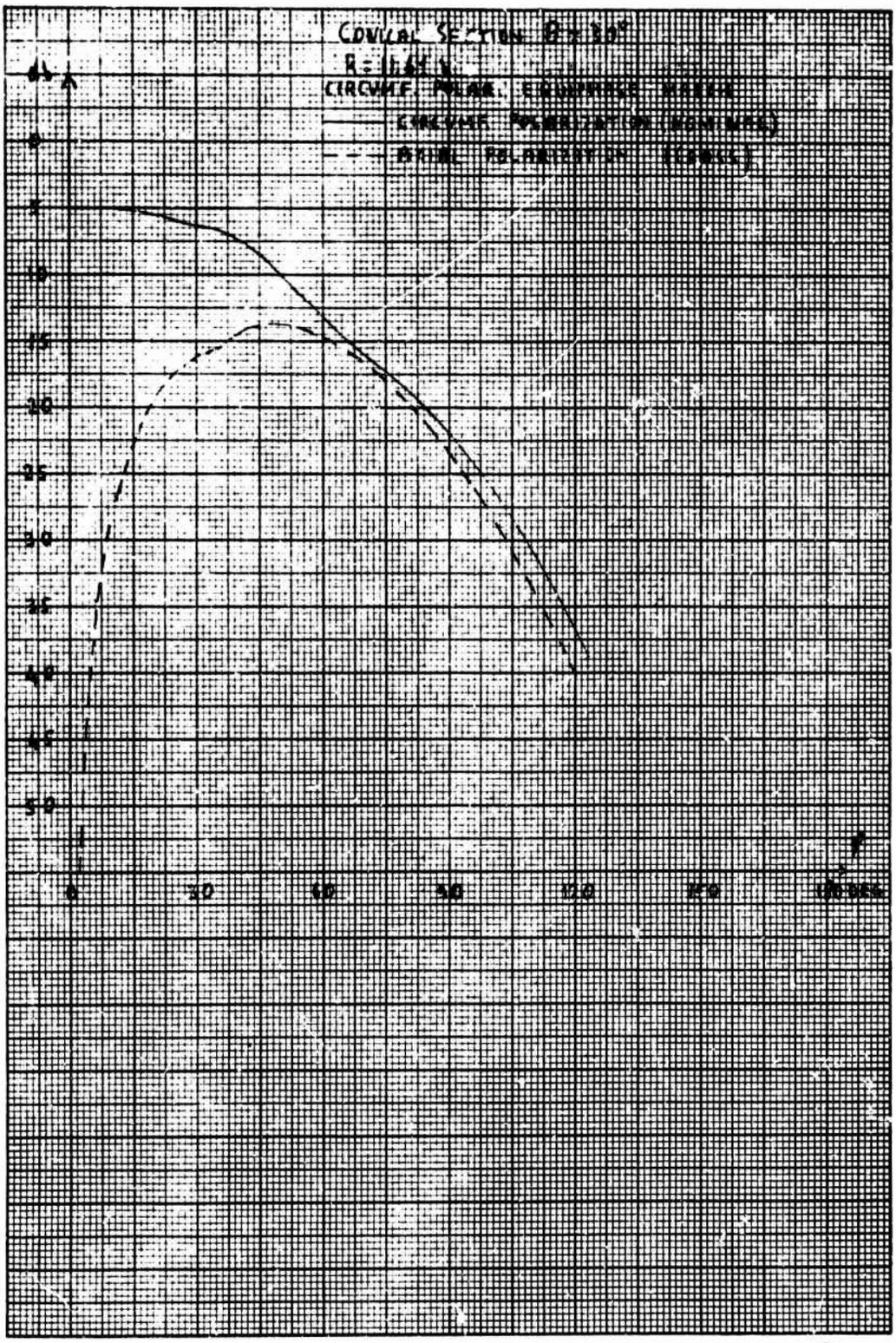


Figure 38 - Realized Gain Pattern. Conical Section $\theta = 30^{\circ}$. Circumferential Polarization Excited. Equiphase Match ($R = 11.61\lambda$)

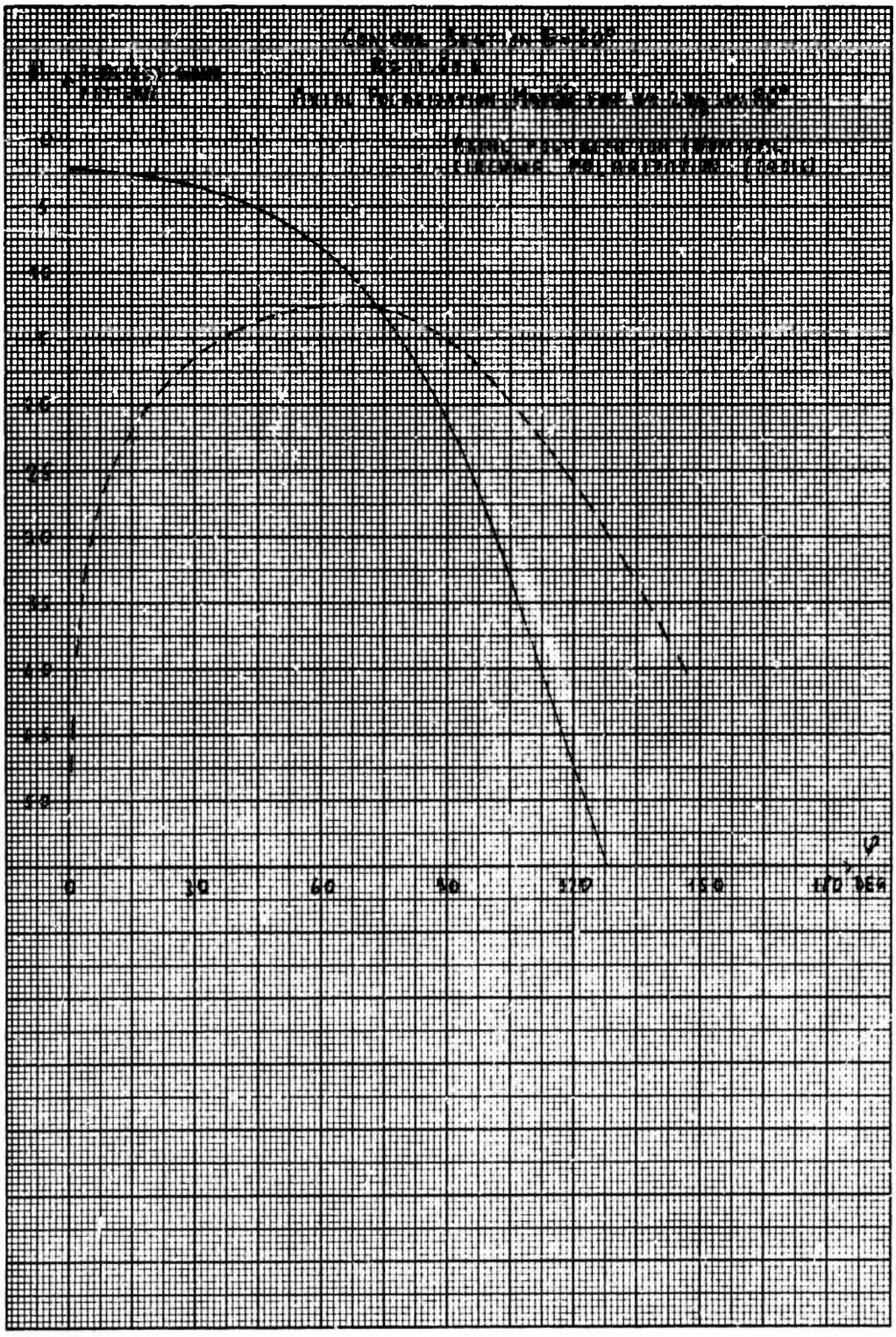


Figure 39 - Realized Gain Pattern. Conical Section $\theta = 60^{\circ}$. Axial Polarization Excited. Match for $w = k \sin 80^{\circ}$ ($R = 11.61\lambda$)

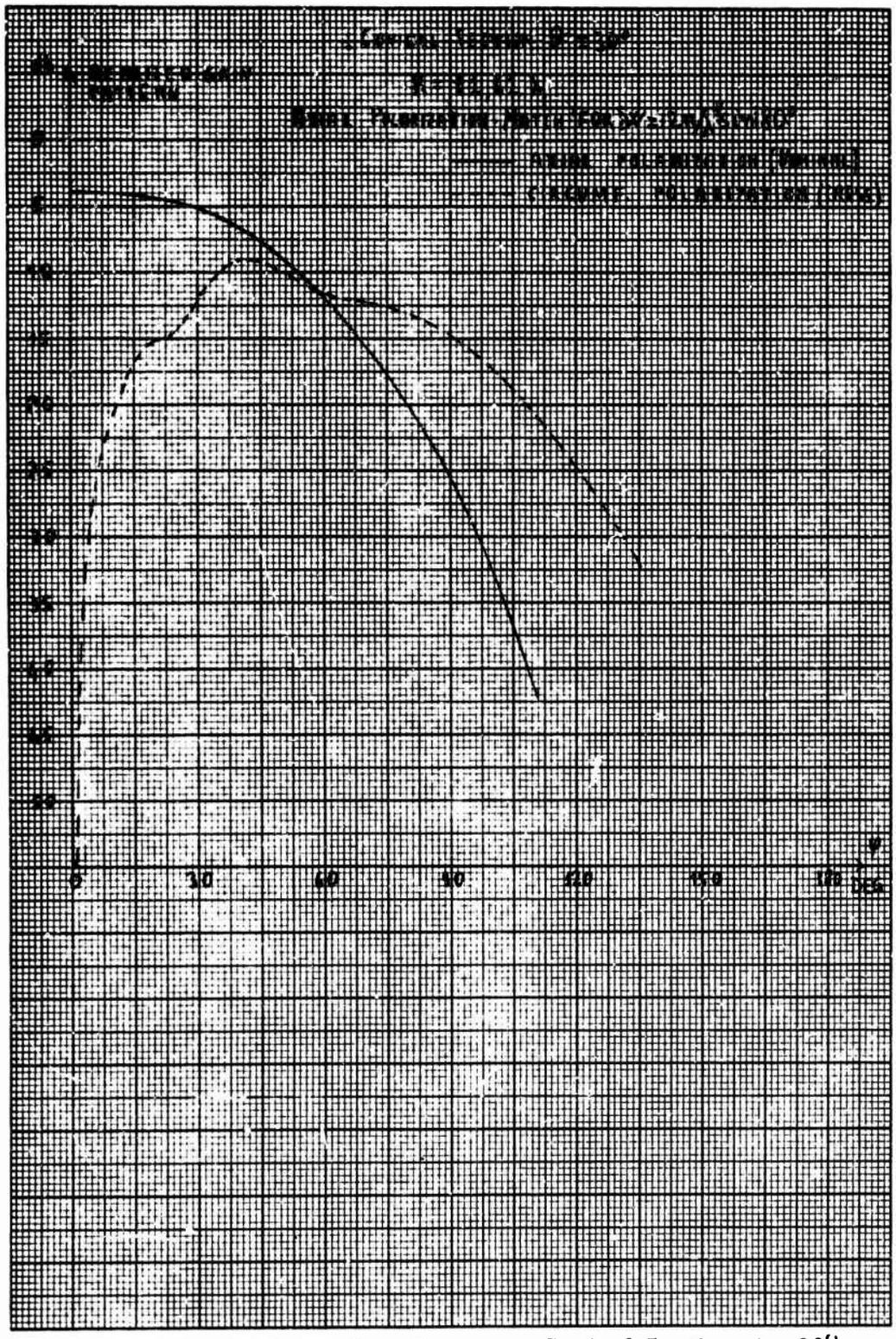


Figure 40 - Realized Gain Pattern. Conical Section $\theta = 30^{\circ}$. Axial Polarization Excited. Match for $w = k \sin 80^{\circ}$ ($R = 11.61\lambda$)

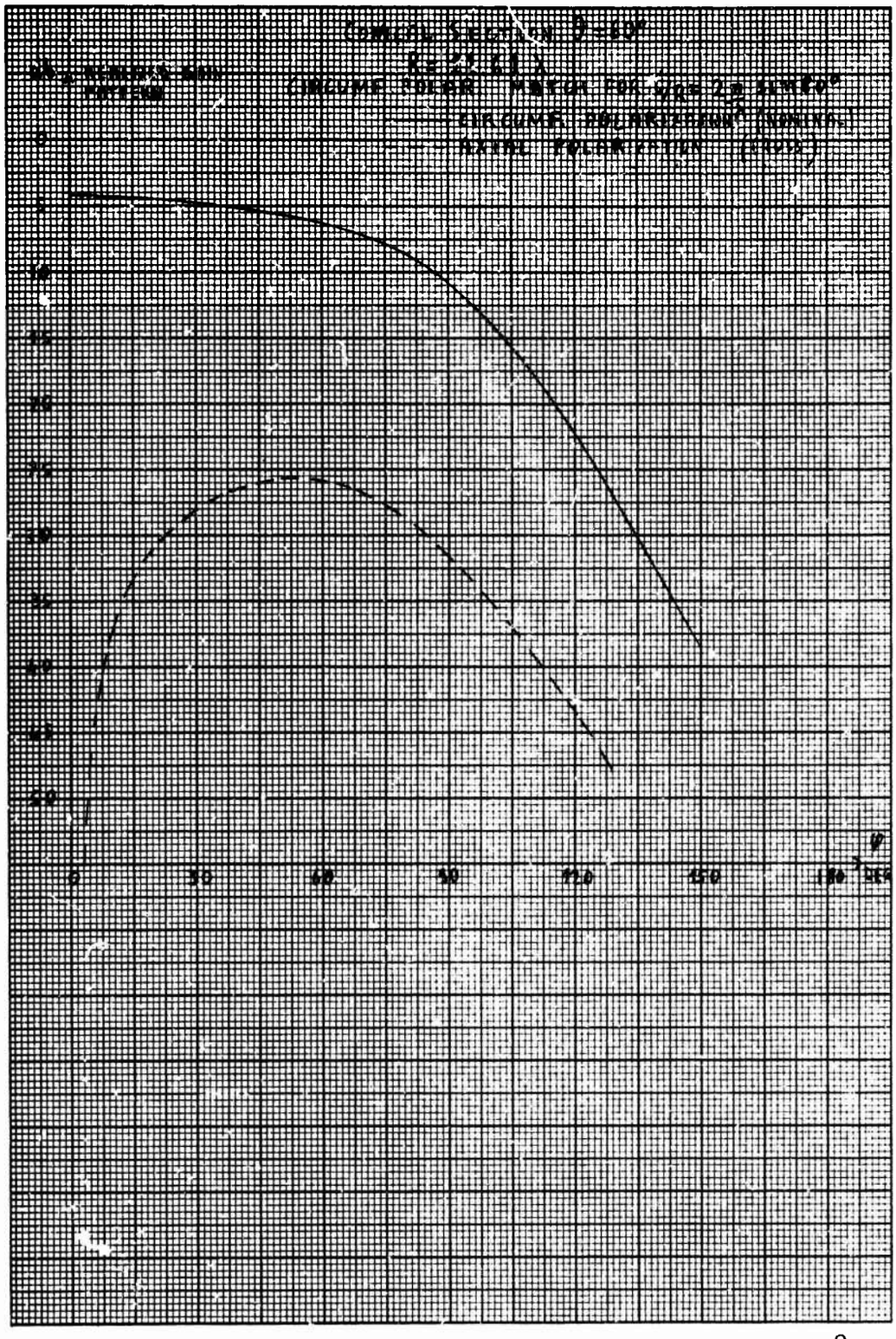


Figure 41 - Realized Gain Pattern. Conical Section $\theta = 60^{\circ}$. Circumferential Polarization Excited. Match for $i/R = k \sin 80^{\circ}$ (R = 11.61λ)

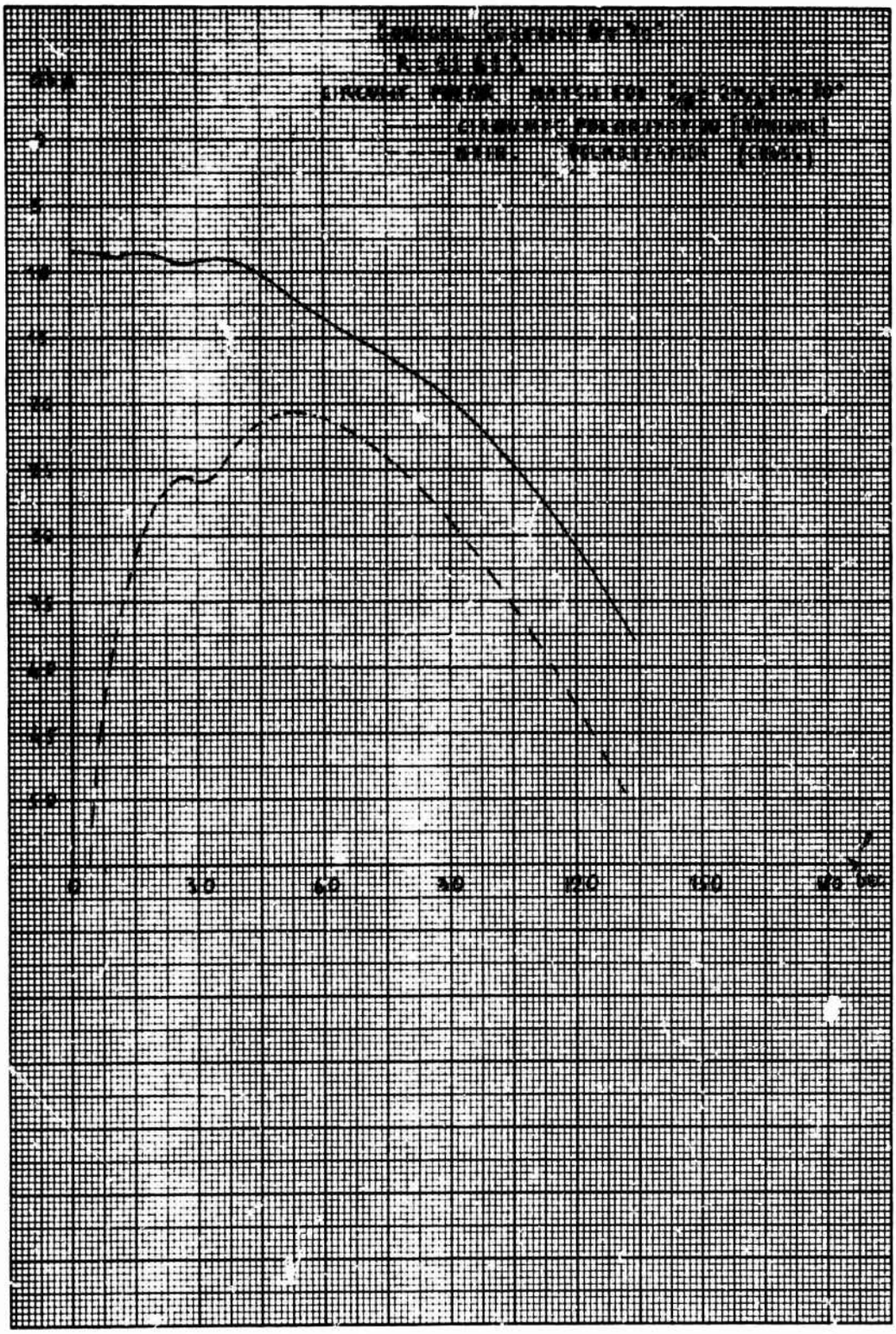


Figure 42 - Realized Gain Pattern. Conical Section $\theta = 30^{\circ}$. Circumferential Polarization Excited. Match for $i/R = k \sin 80^{\circ}$. (R = 11.61λ)

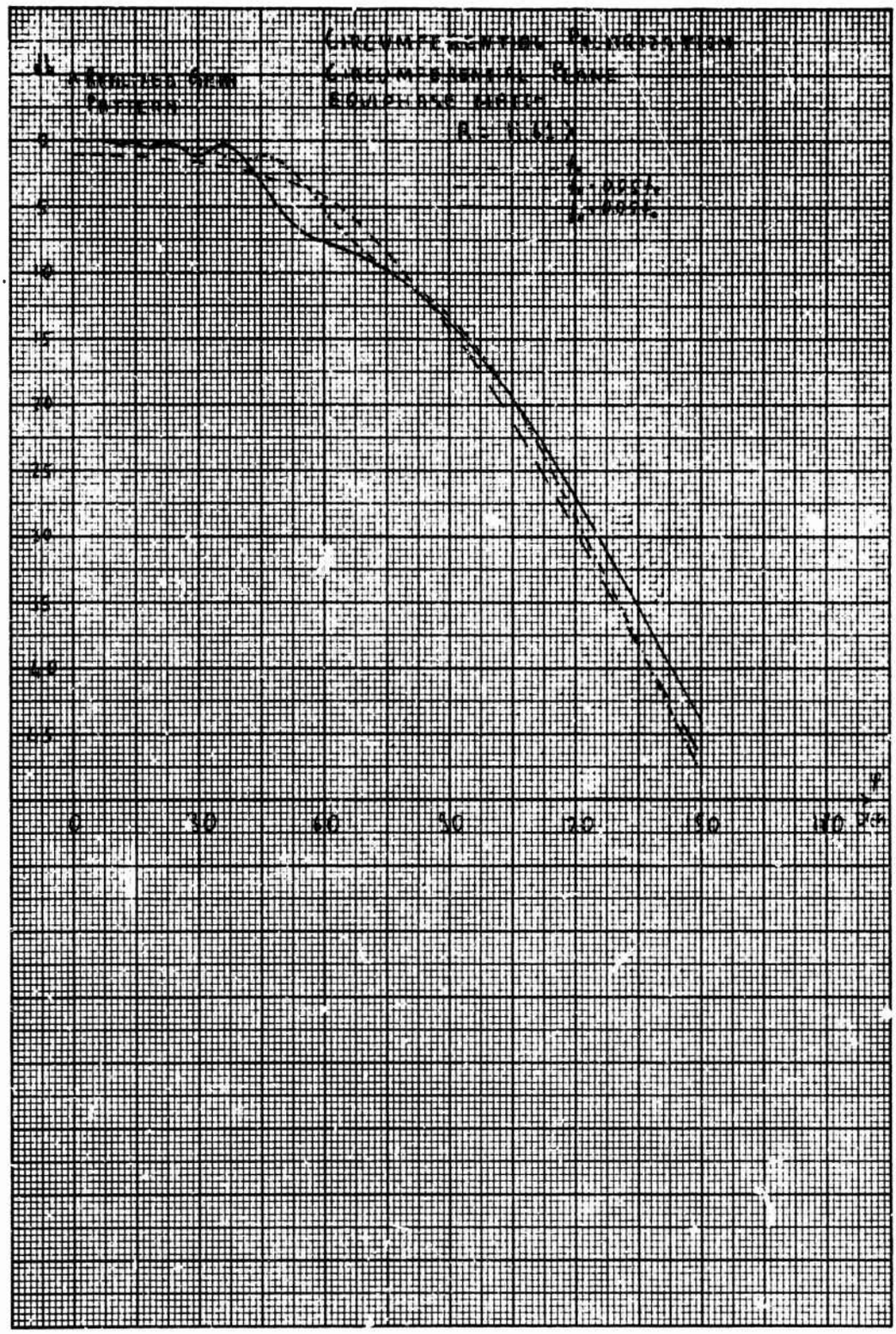


Figure 43 - Realized Gain Pattern. Frequency Sensitivity

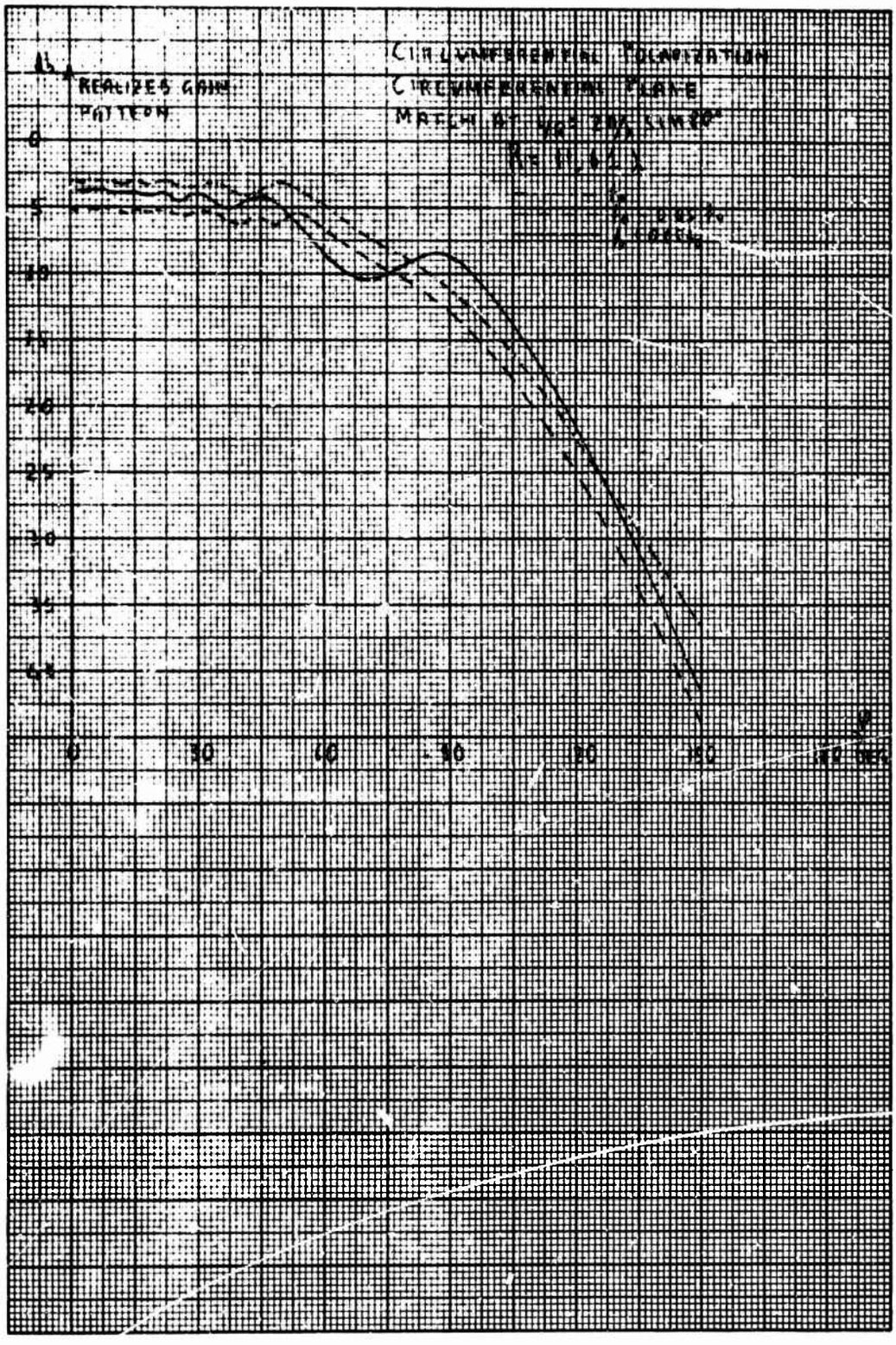


Figure 44 - Realized Gain Pattern. Frequency Sensitivity

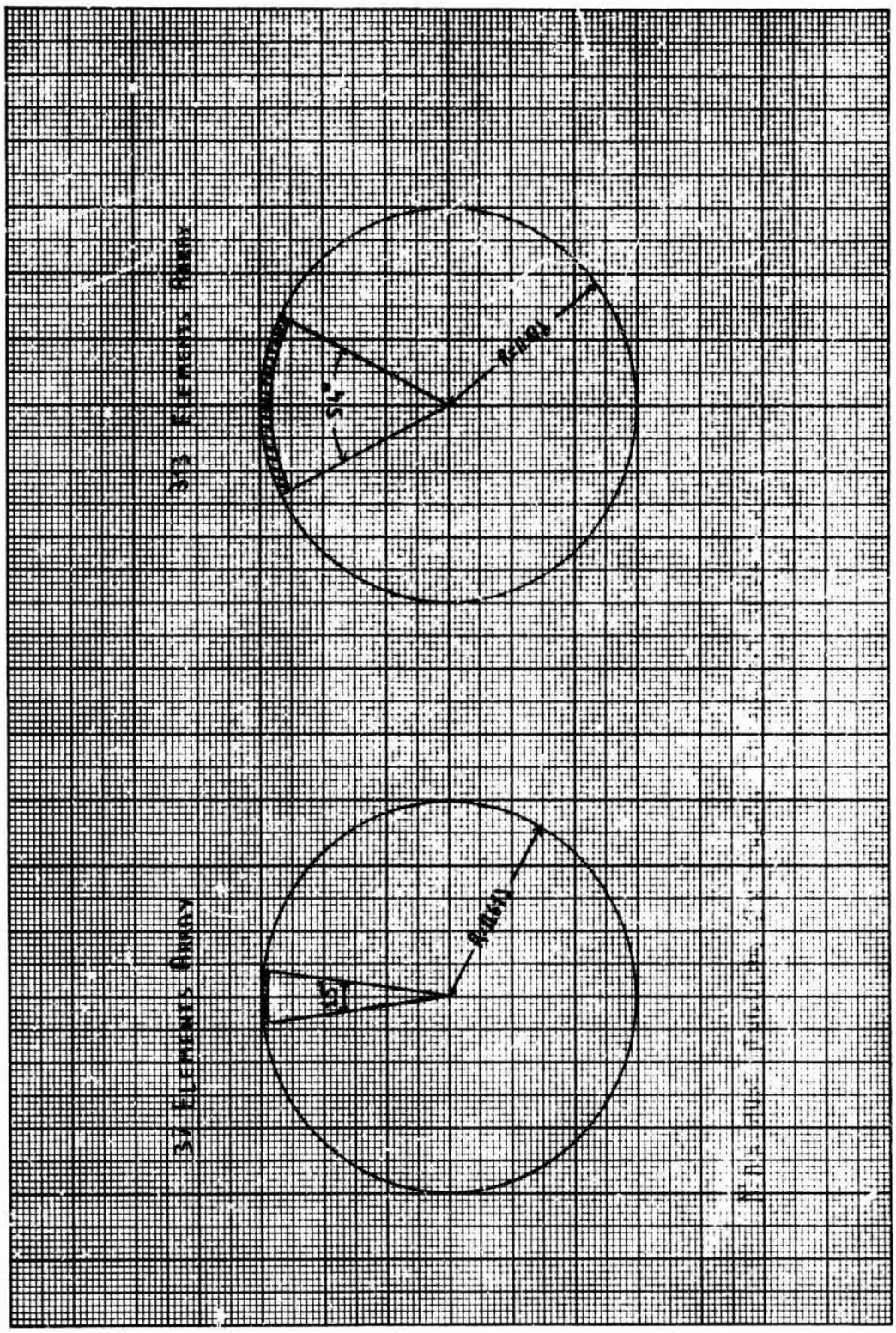


Figure 45 - Maximum Angular Extension of Array Aperture

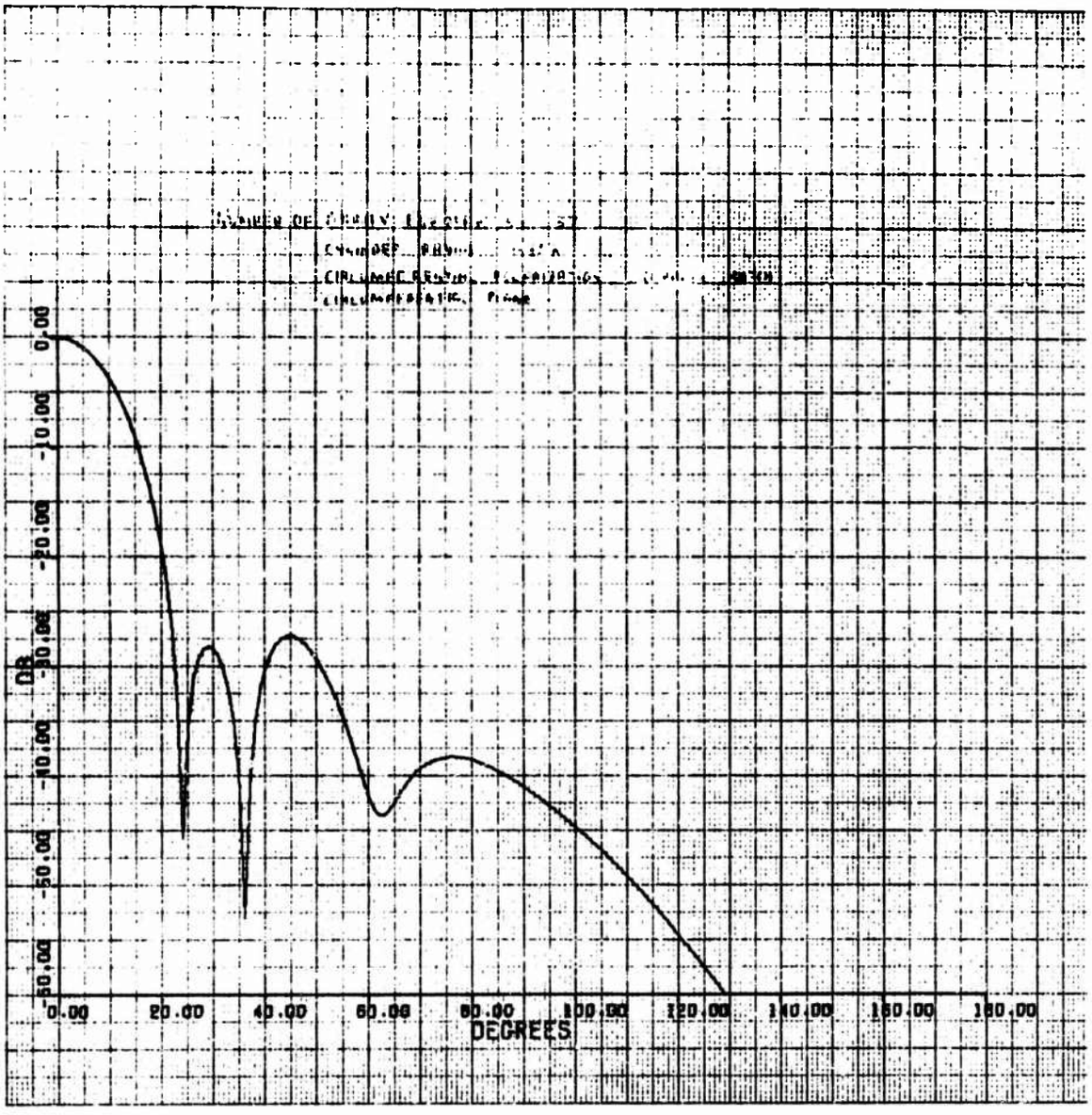


Figure 46 - Array Pattern. Circumferential Plane. Circumferential Polarization. Number of Array Elements 37

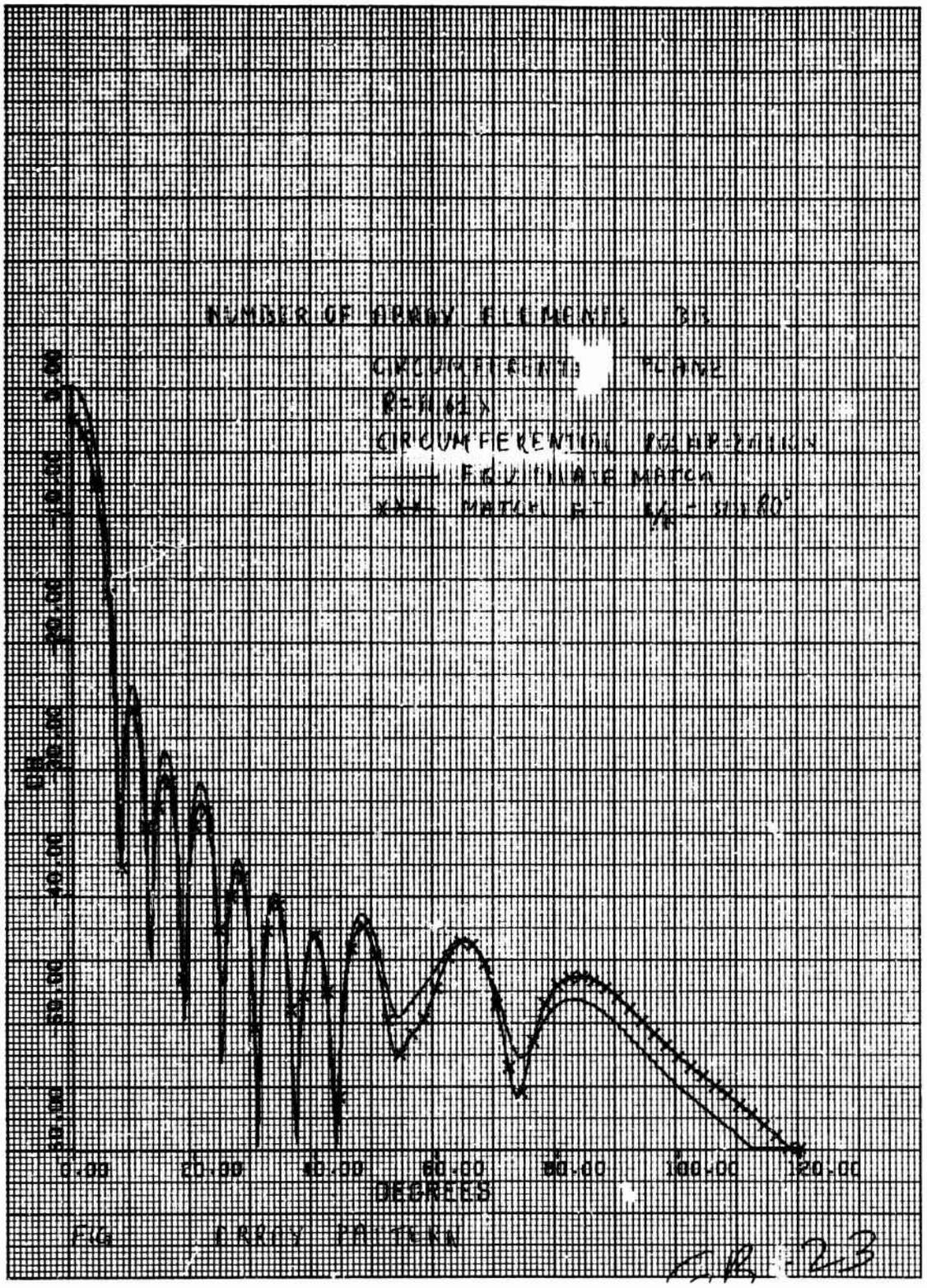


Figure 47 - Array Pattern. Circumferential Plane. Circumferential Polarization. Number of Array Elements 313

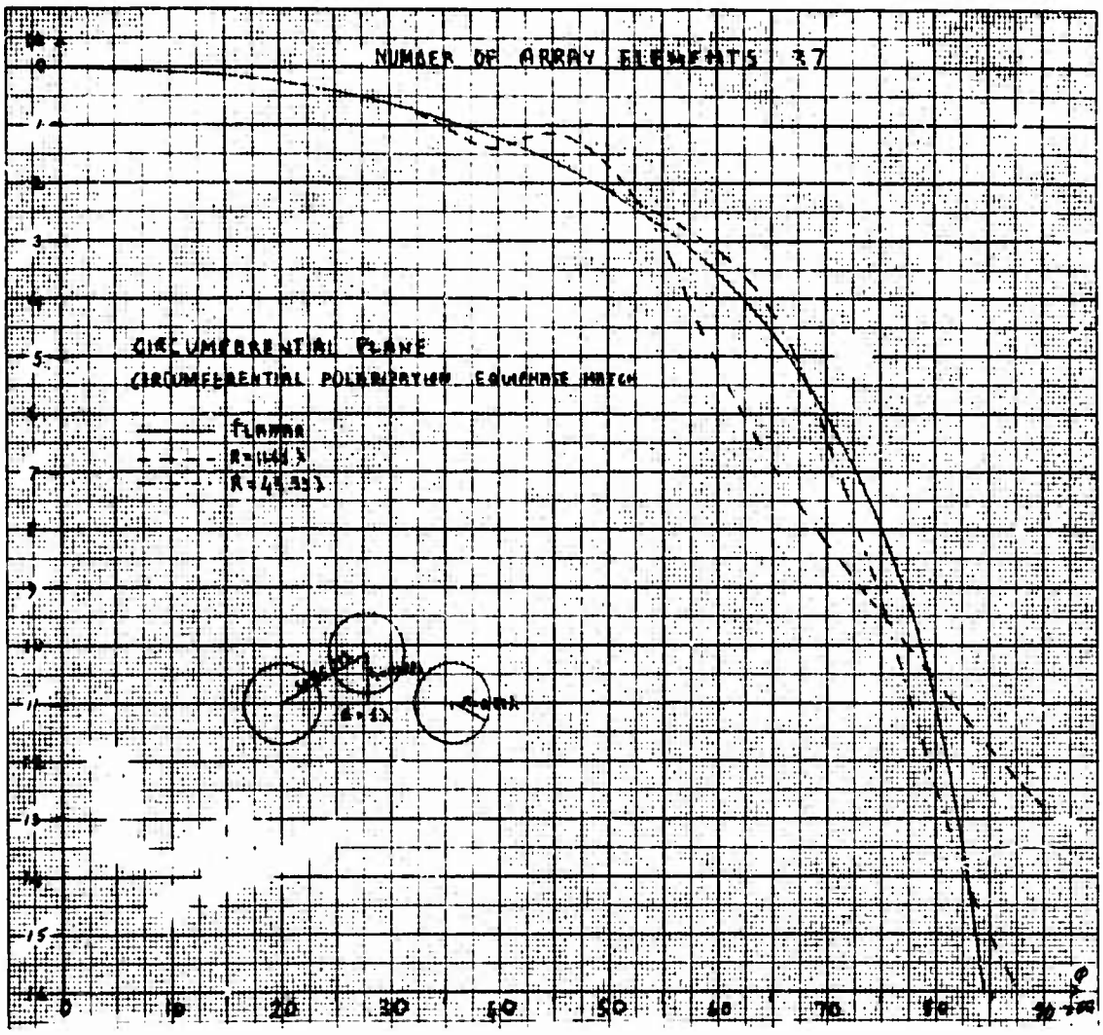


Figure 48 - Array Scan Coverage. Circumferential Plane. Circumferential Polarization. Equiphase Match. Number of Array Elements 37

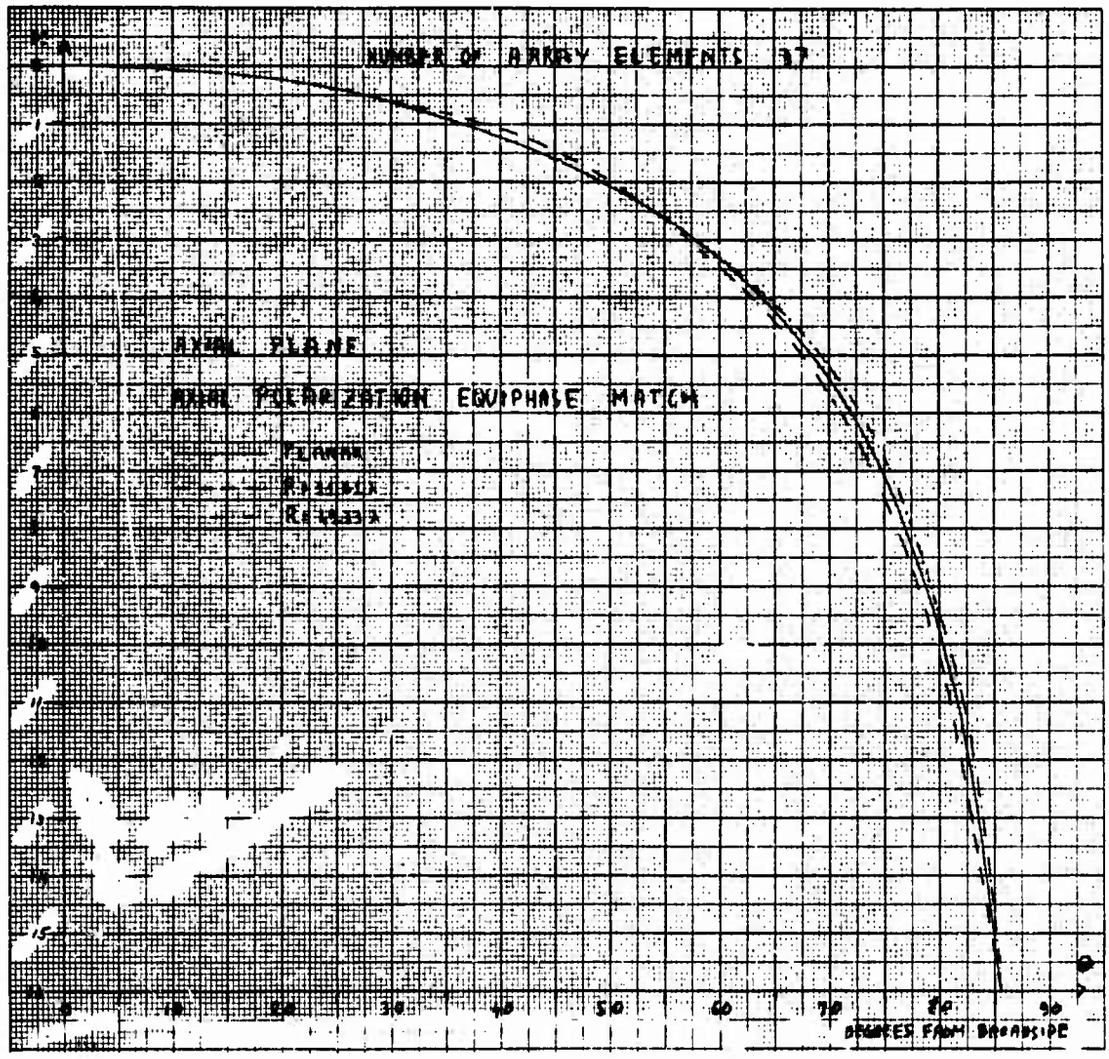


Figure 49 - Array Scan Coverage. Axial Plane. Axial Polarization. Equiphase Match. Number of Array Elements 37

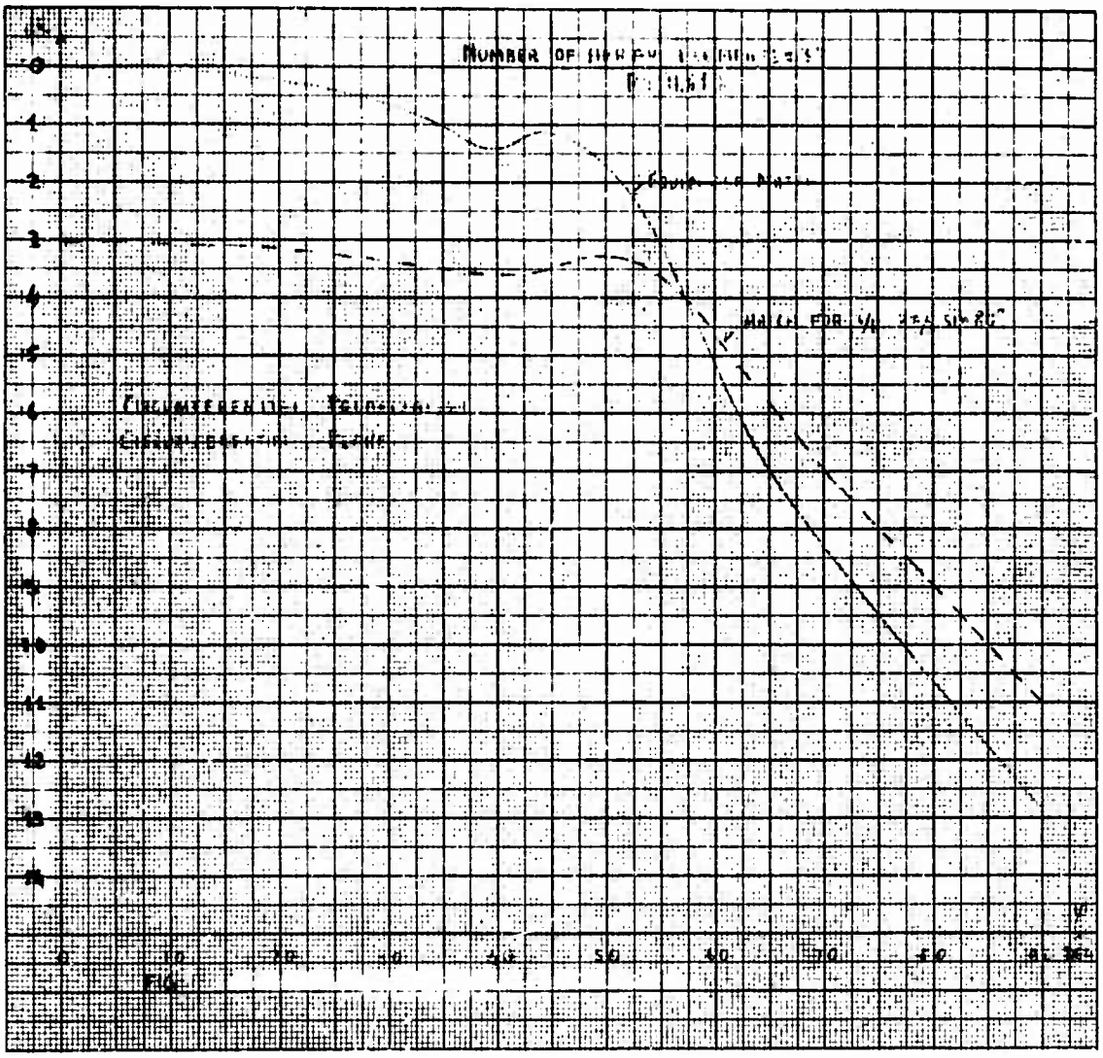


Figure 50 - Array Scan Coverage. Circumferential Plane. Circumferential Polarization Match for i/R = k sin 80°. Number of Array Elements 37

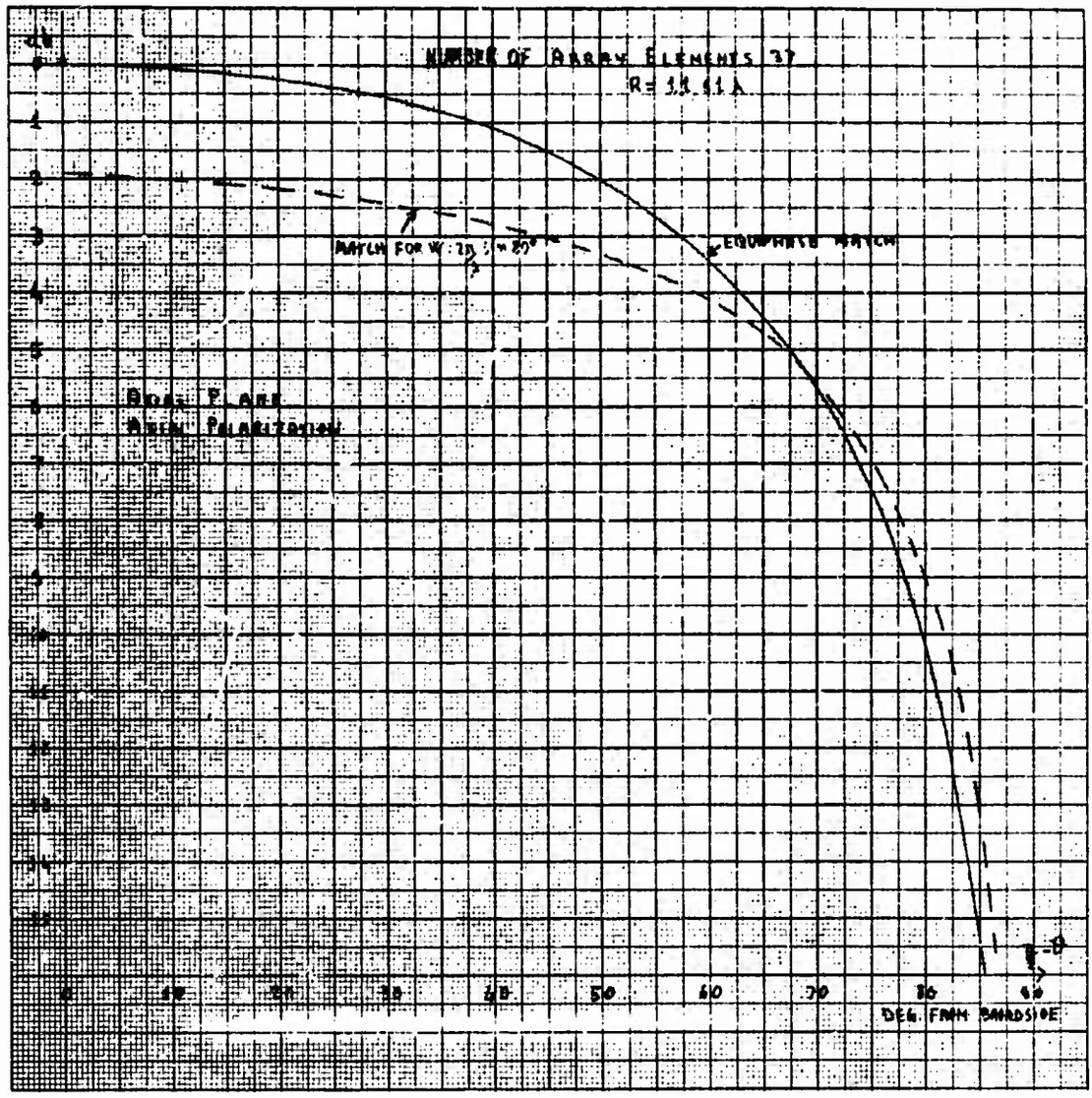


Figure 51 - Array Scan Coverage. Axial Plane. Axial Plane Match for w = k sin 80°. Number of Array Elements 37

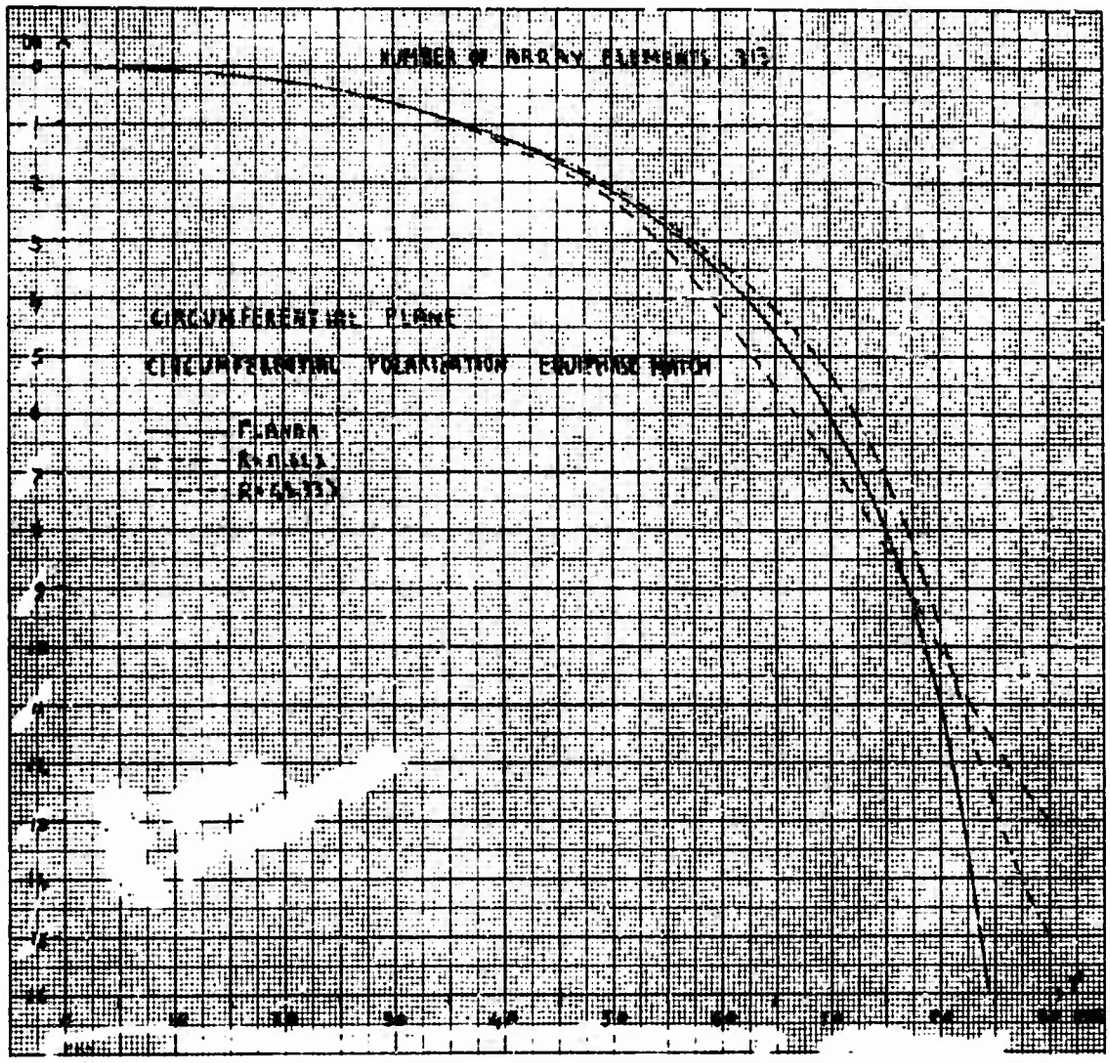


Figure 52 - Array Scan Coverage. Circumferential Plane. Circumferential Polarization Equiphase Match. Number of Array Elements 313

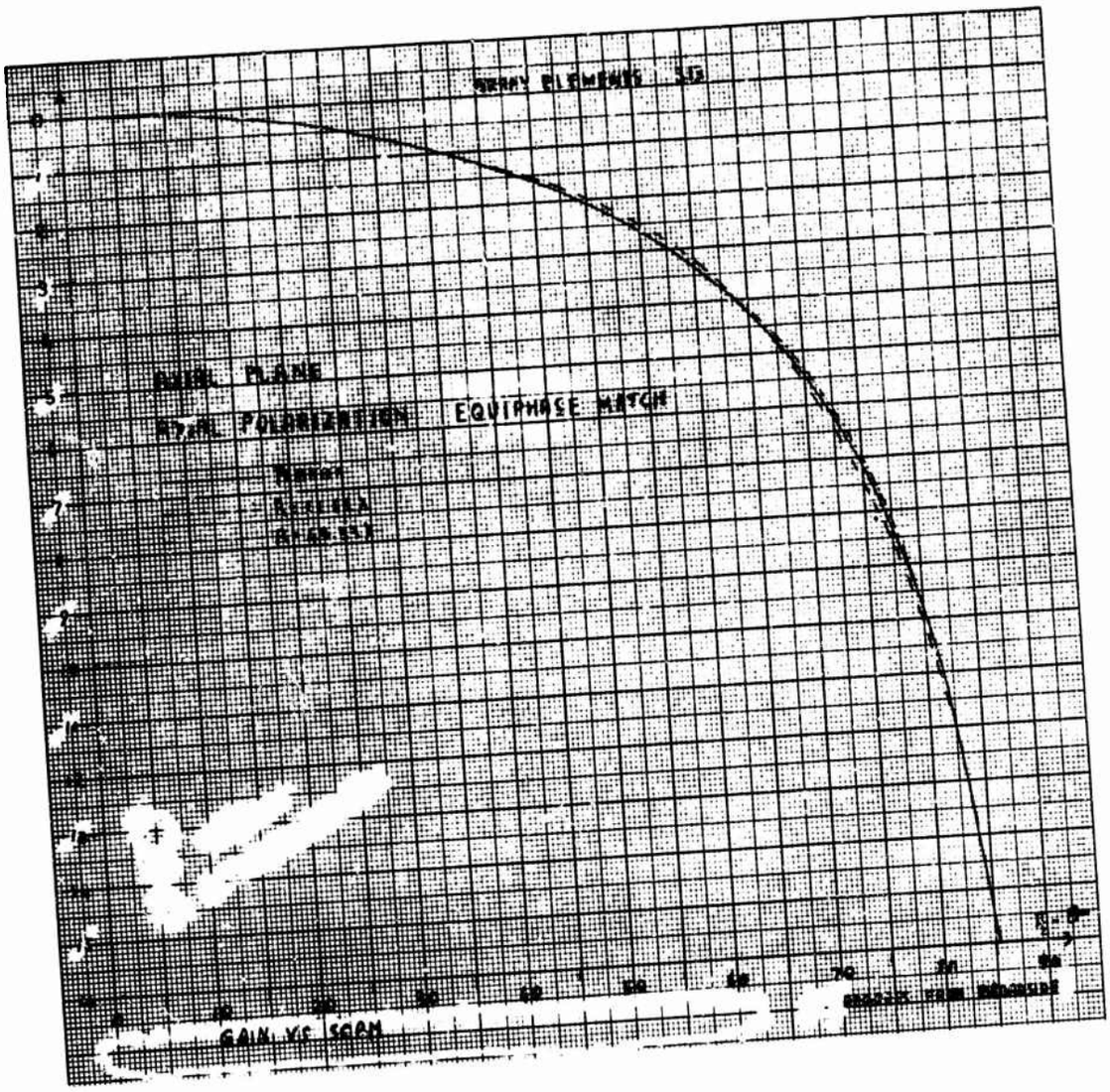


Figure 53 - Array Scan Coverage. Axial Plane. Axial Polarization. Equiphase Match. Number of Array Elements 313

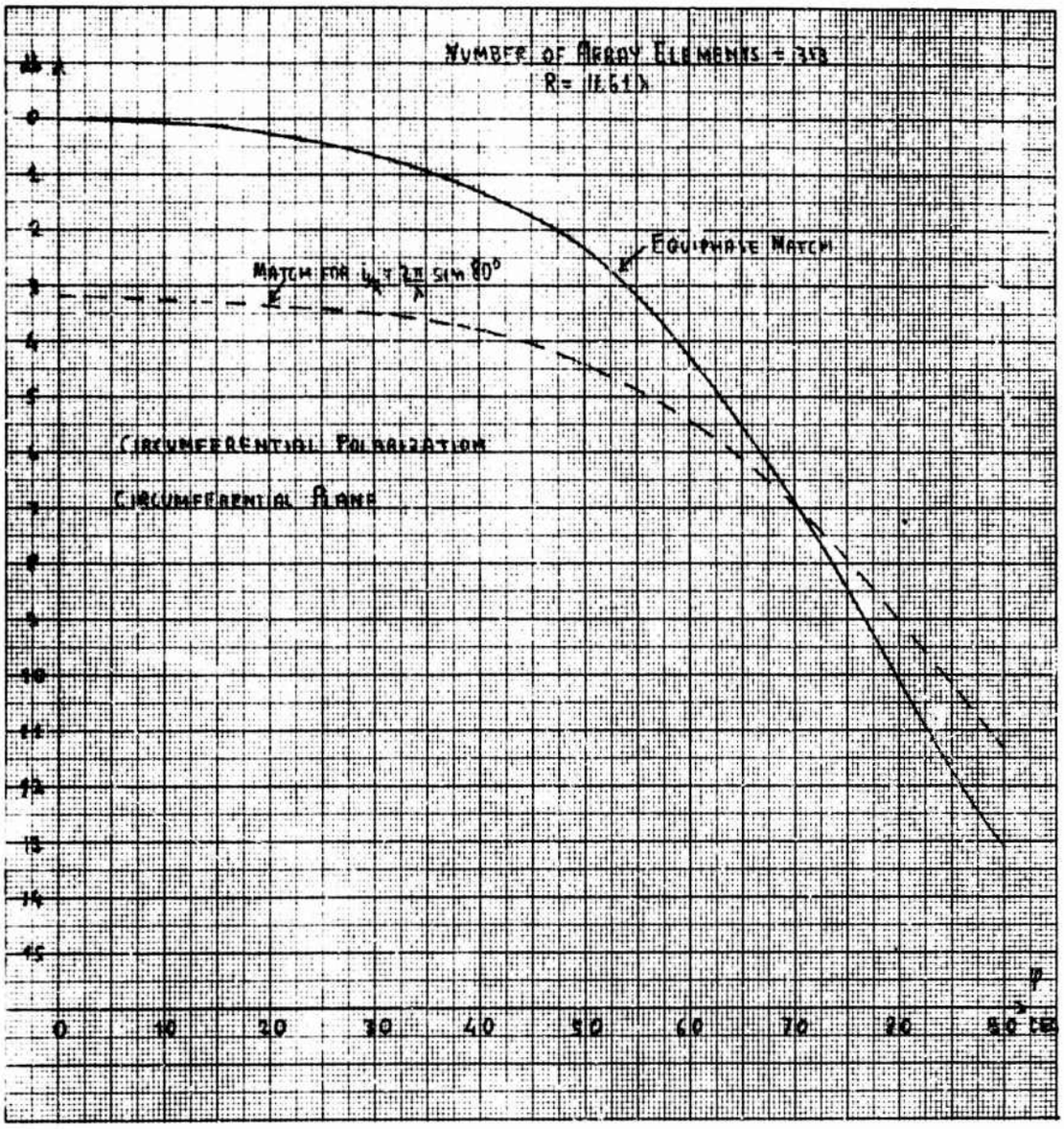


Figure 54 - Array Scan Coverage. Circumferential Plane. Circumferential Polarization Match for i/R = k sin 80°. Number of Array Elements 313

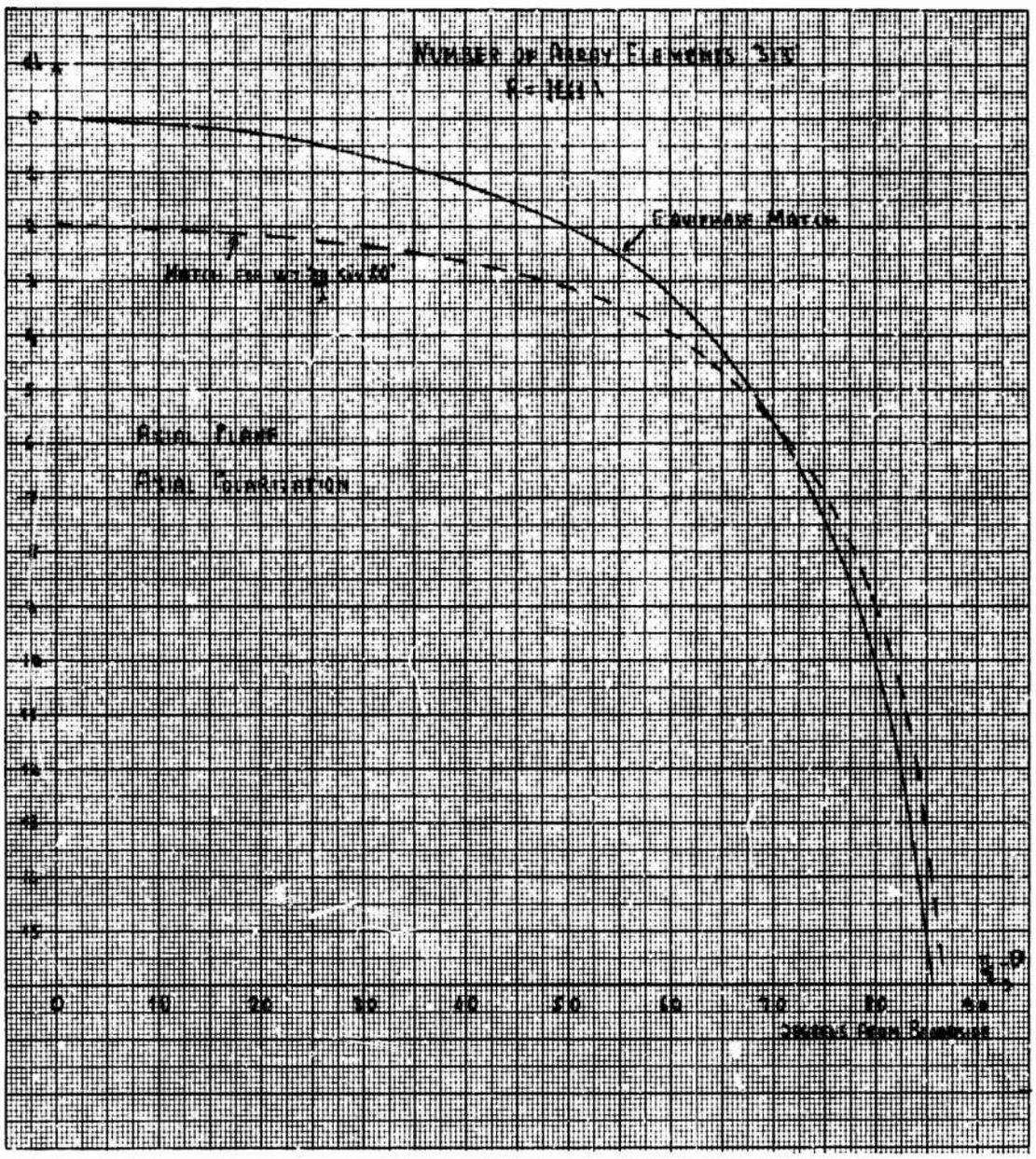


Figure 55 - Array Scan Coverage. Axial Plane. Axial Polarization Match for w = k sin 80°. Number of Array Elements 313

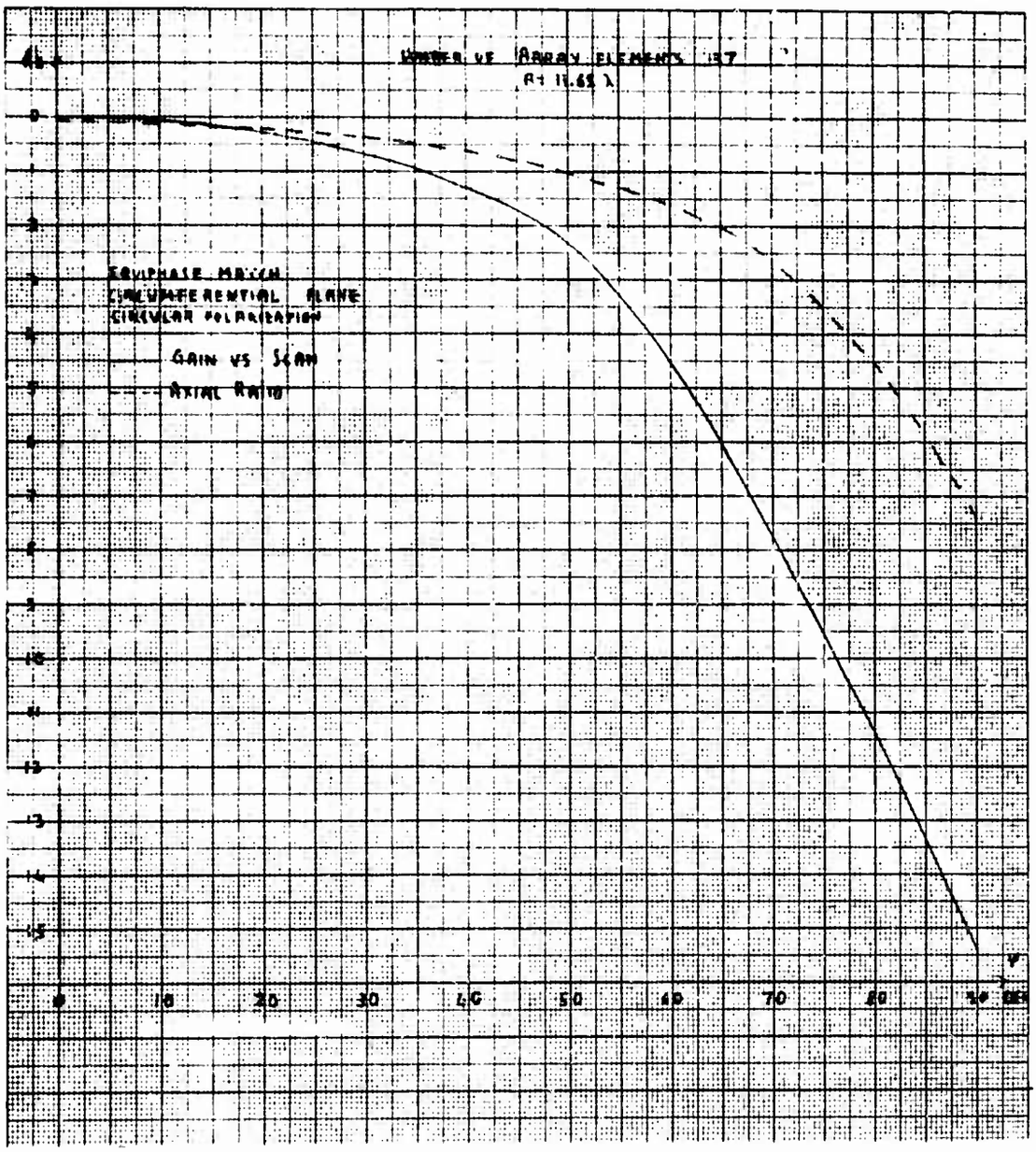


Figure 56 - Array Scan Coverage. Circumferential Plane. Circular Polarization. Equiphase Match. Number of Array Elements 37

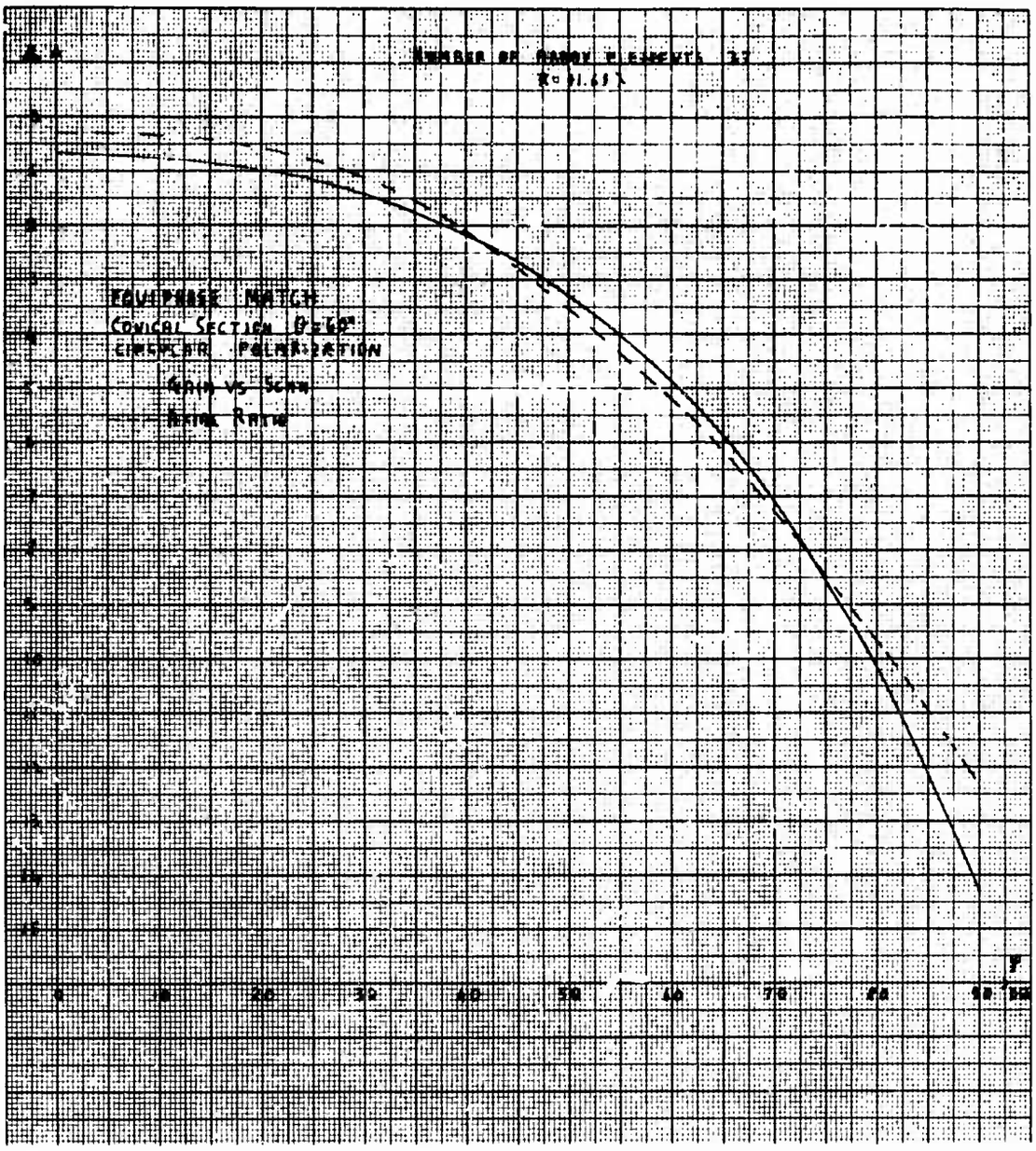


Figure 57 - Array Scan Coverage. Conical Section θ = 60°. Circular Polarization. Equiphase Match. Number of Array Elements 37

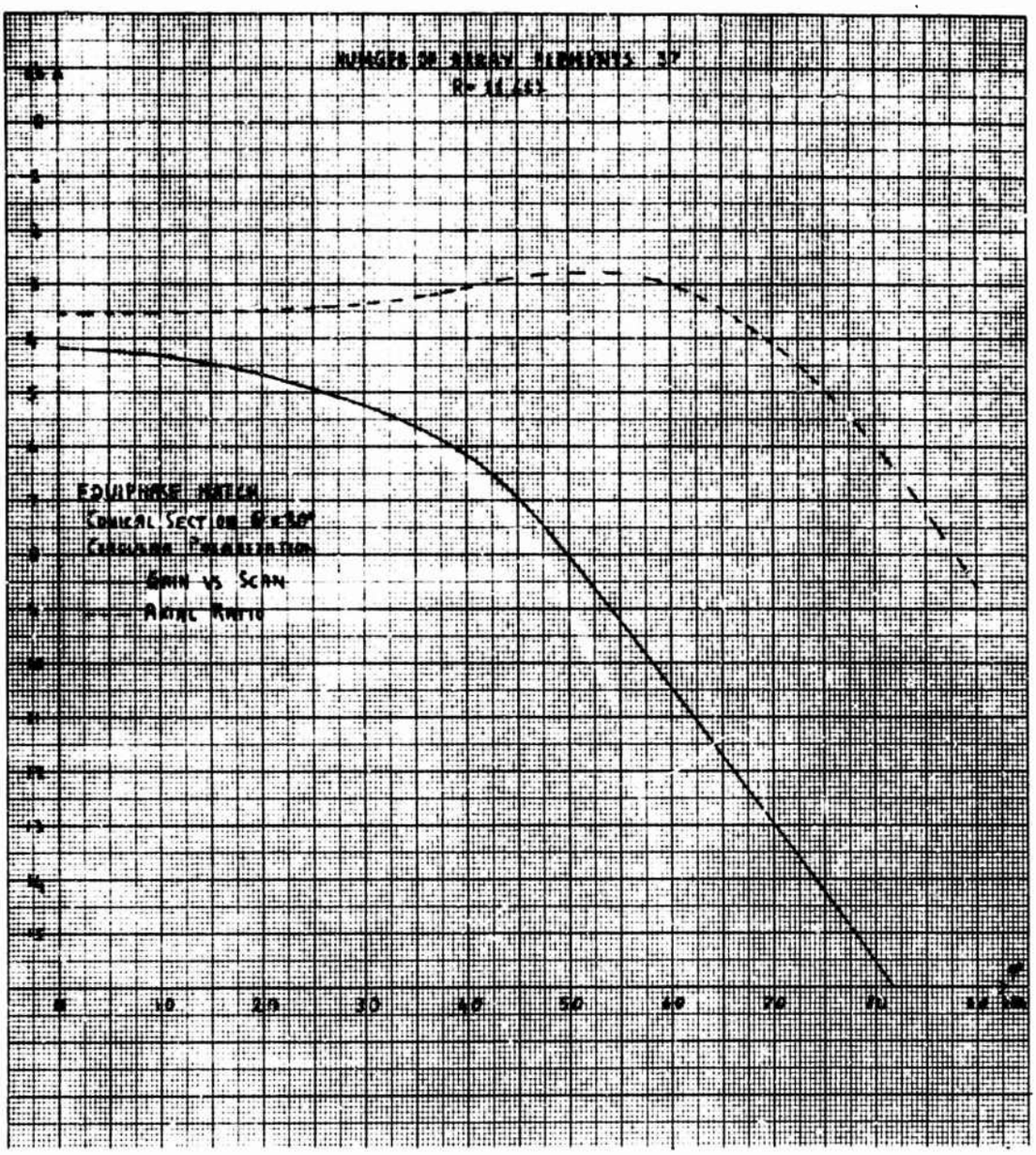


Figure 58 - Array Scan Coverage. Conical Section $\theta = 30°$. Circular Polarization. Equiphase Match. Number of Array Elements 37

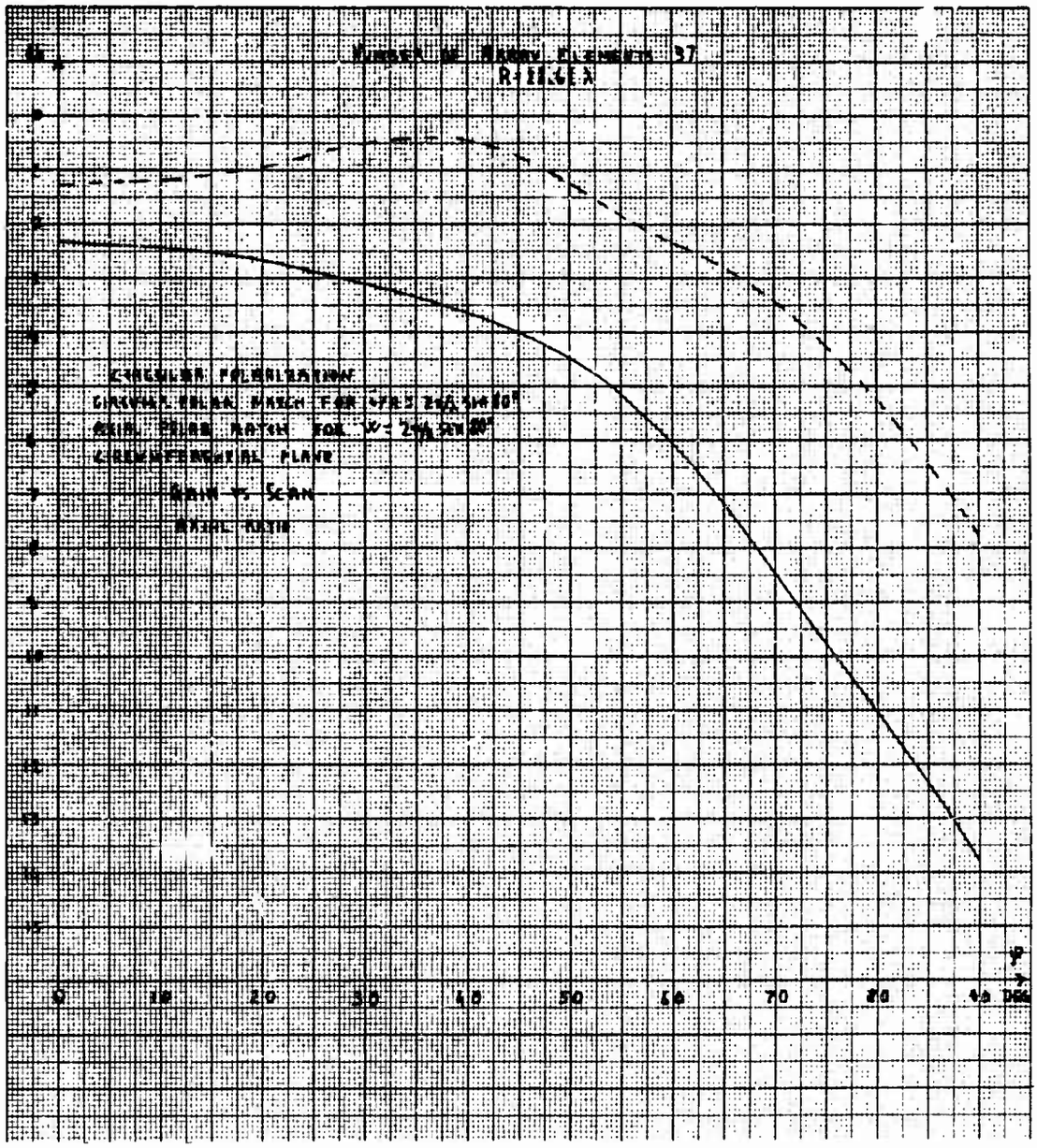


Figure 59 - Array Scan Coverage. Circumferential Plane. Circular Polarization. Number of Array Elements 37

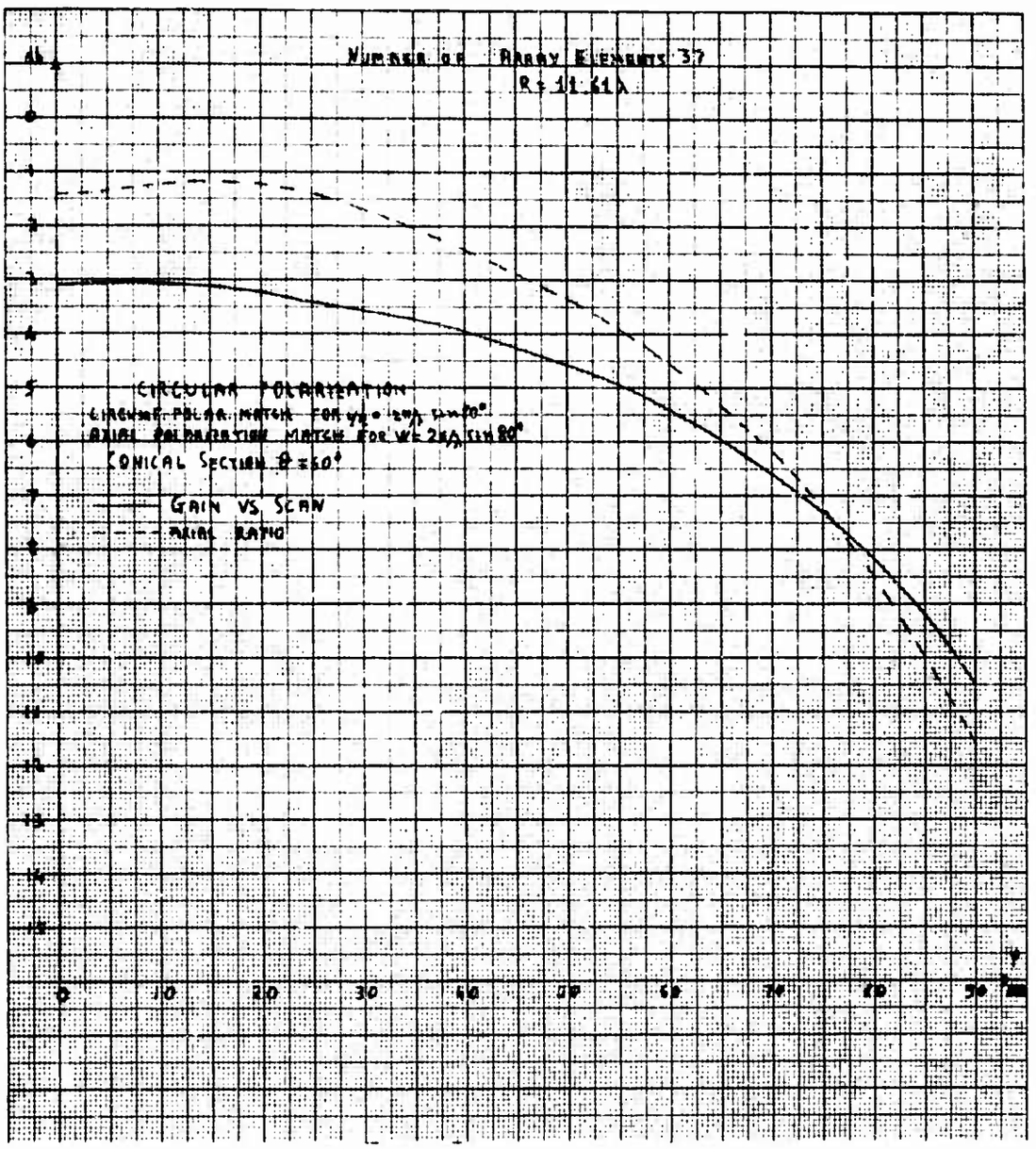


Figure 60 - Array Scan Coverage. Conical Section 6 = 60°. Circular Polarization. Number of Array Elements 37

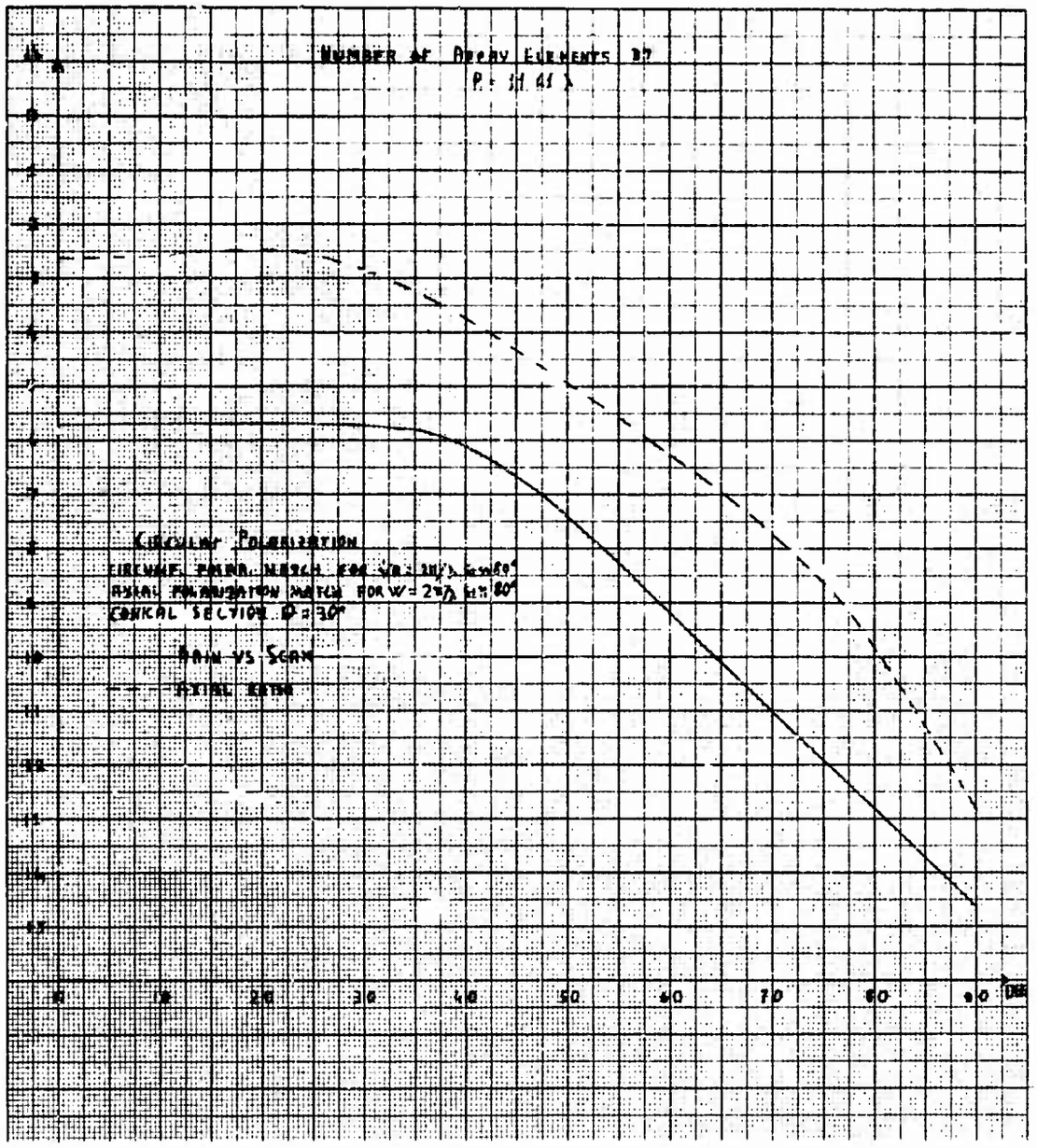


Figure 61 - Array Scan Coverage. Conical Section θ = 30°. Circular Polarization. Number of Array Elements 37

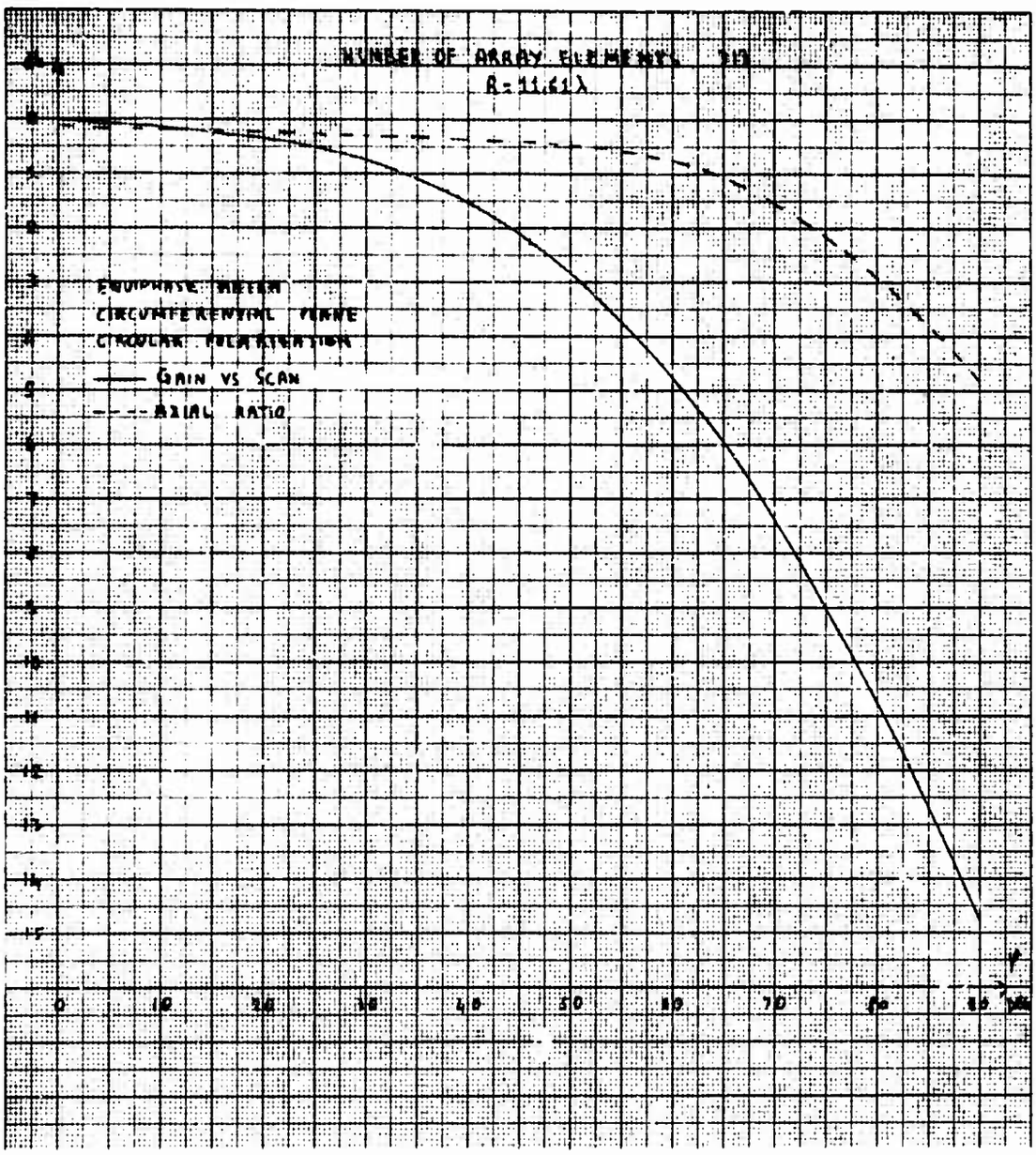


Figure 62 - Array Scan Coverage. Circumferential Plane. Circular Polarization. Equiphase Match. Number of Array Elements 313

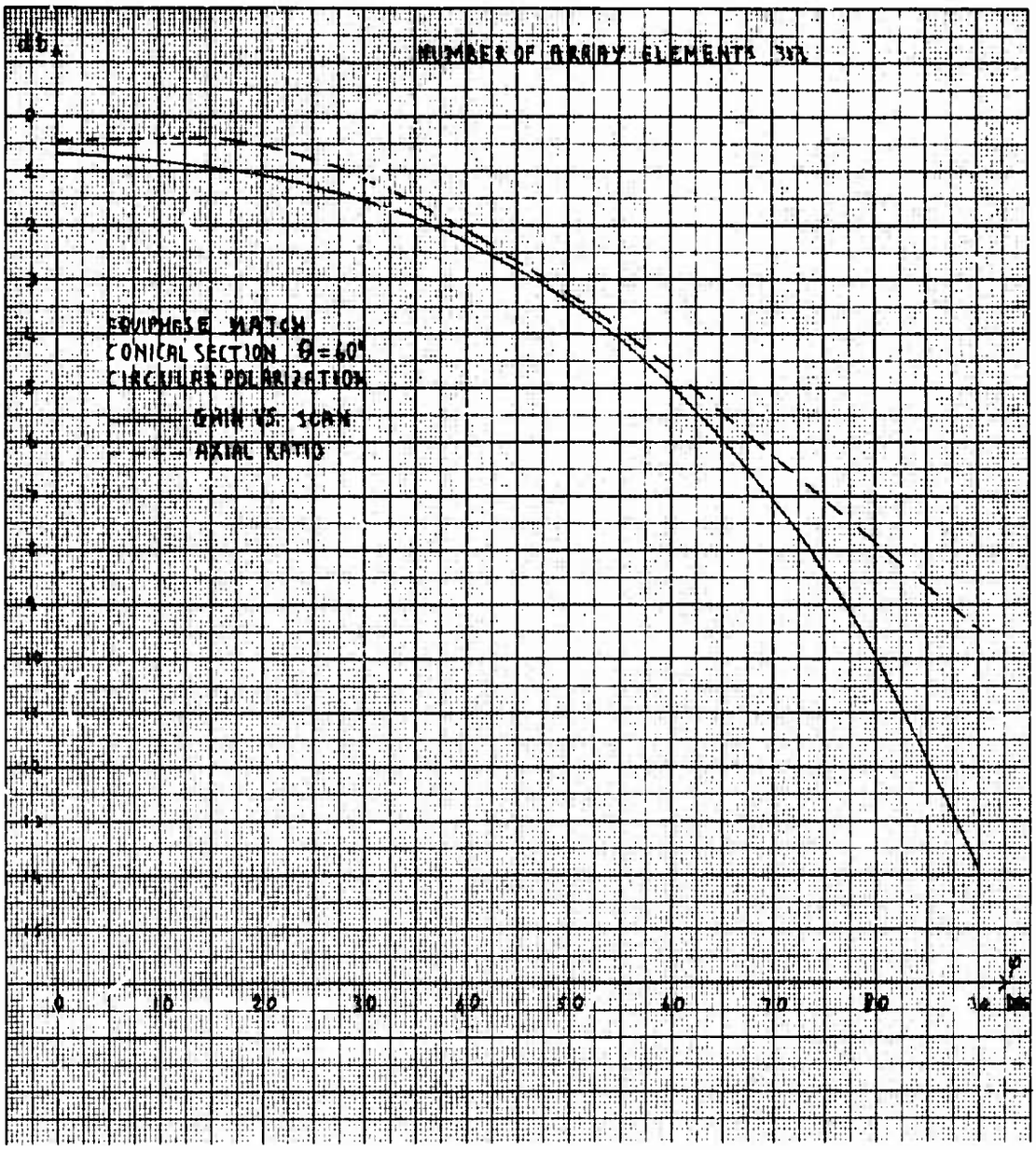


Figure 63 - Array Scan Coverage. Conical Section θ = 60°. Circular Polarization. Equiphase Match. Number of Array Elements 313

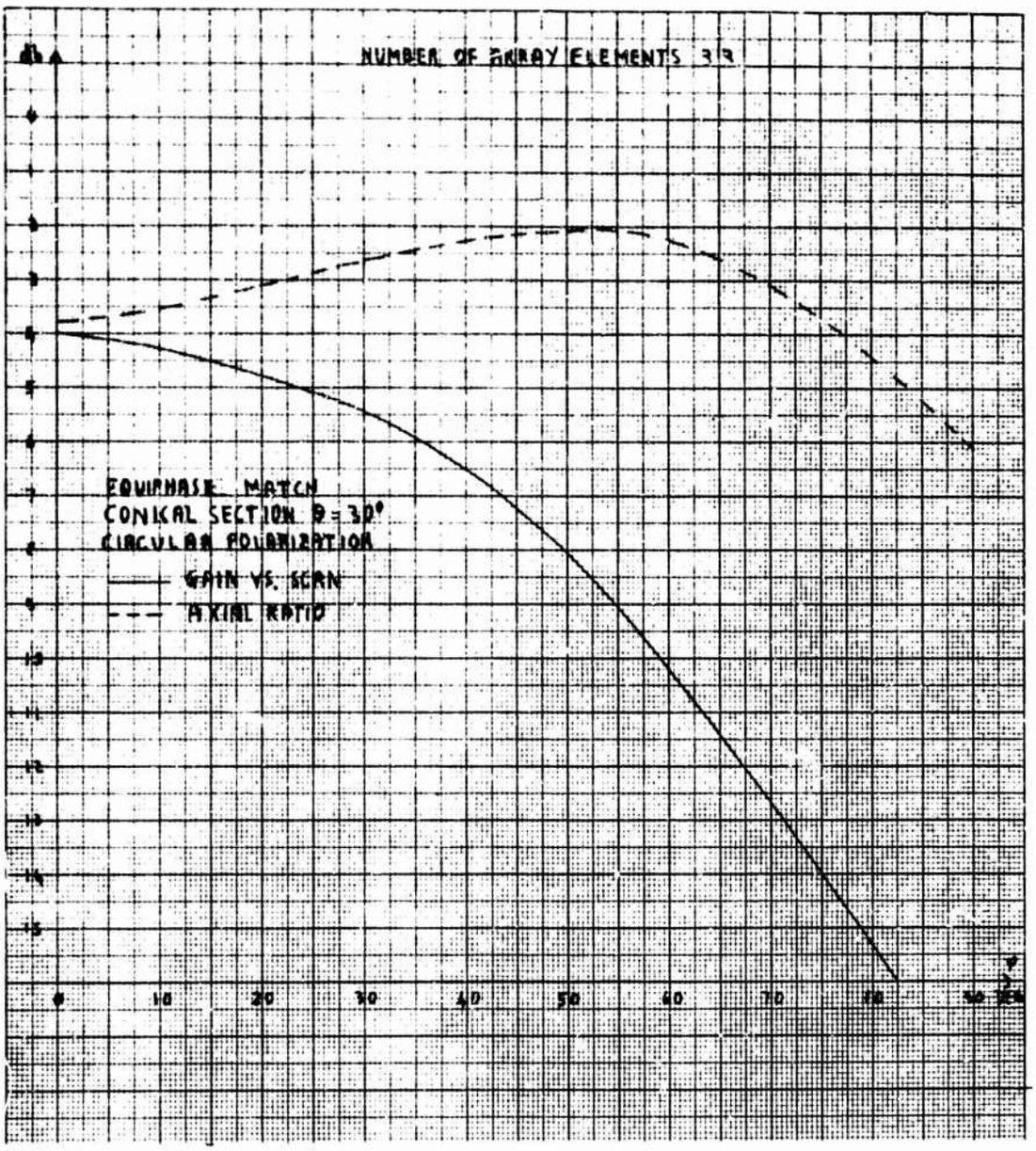


Figure 64 - Array Scan Coverage. Conical Section θ = 30°. Circular Polarization. Equiphase Match. Number of Array Elements 313

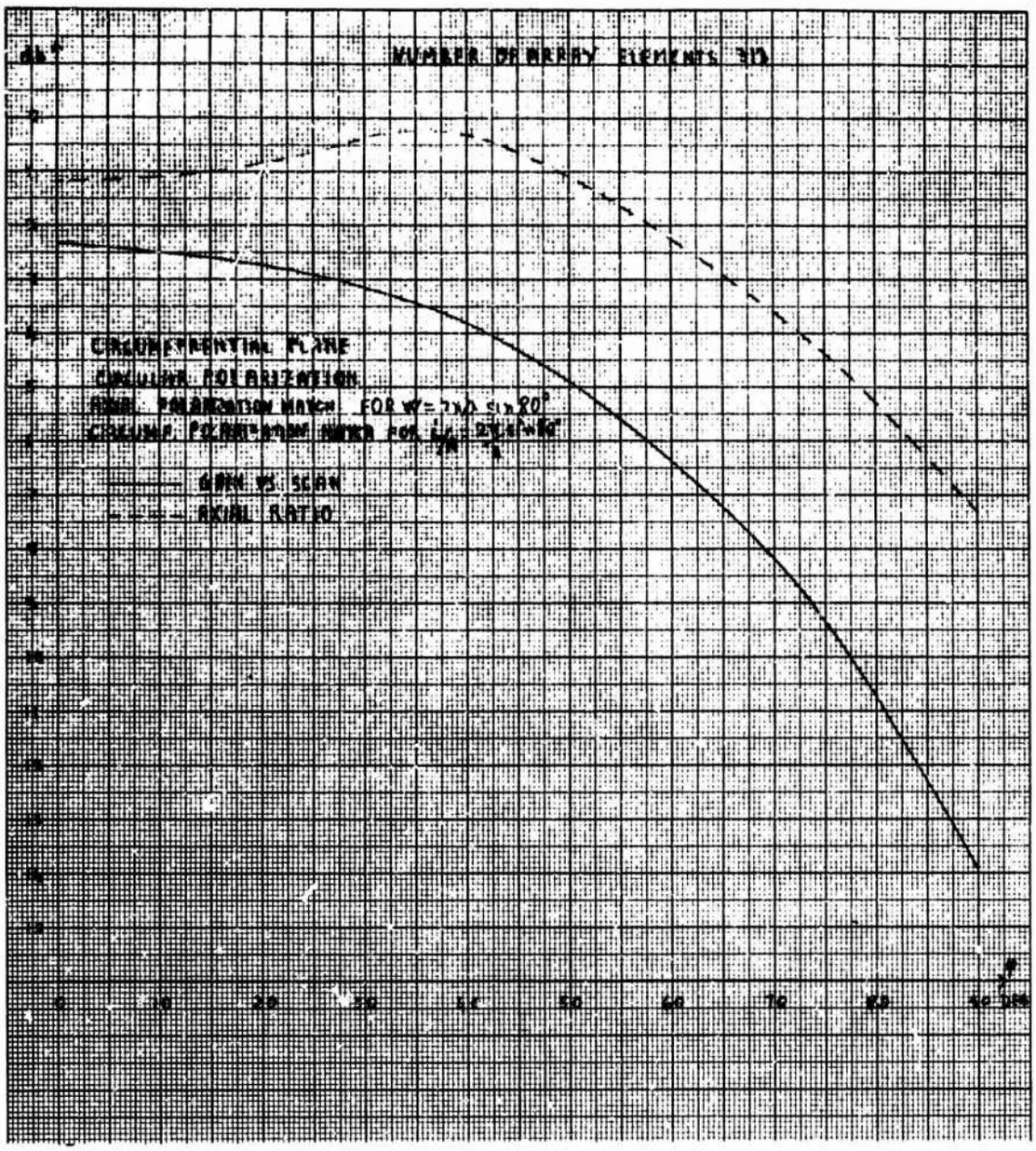


Figure 65 - Array Scan Coverage. Circumferential Plane. Circular Polarization. Number of Array Elements 313

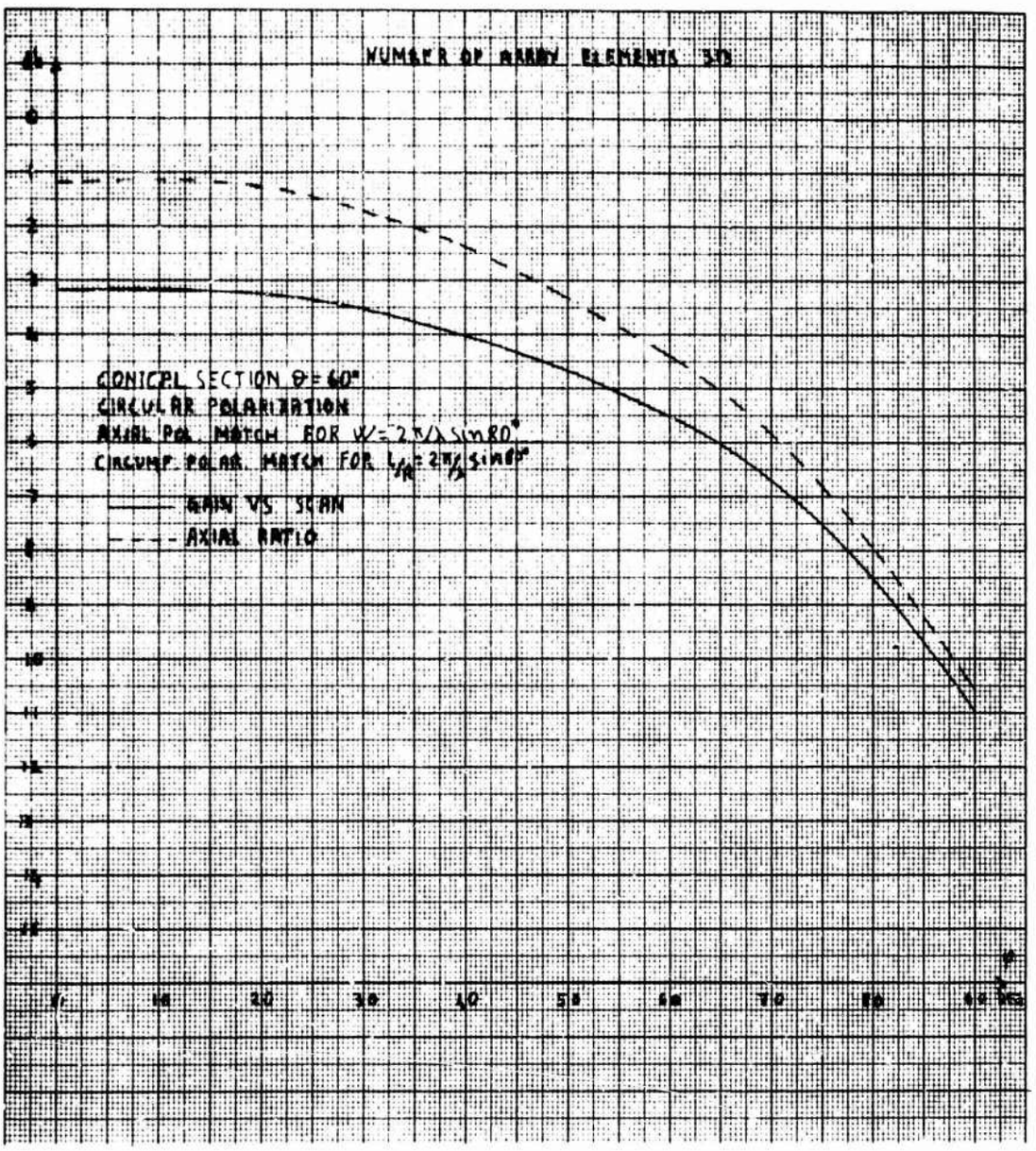


Figure 66 - Array Scan Coverage. Conical Section 1 = 60°. Circular Polarization. Number of Array Elements 313

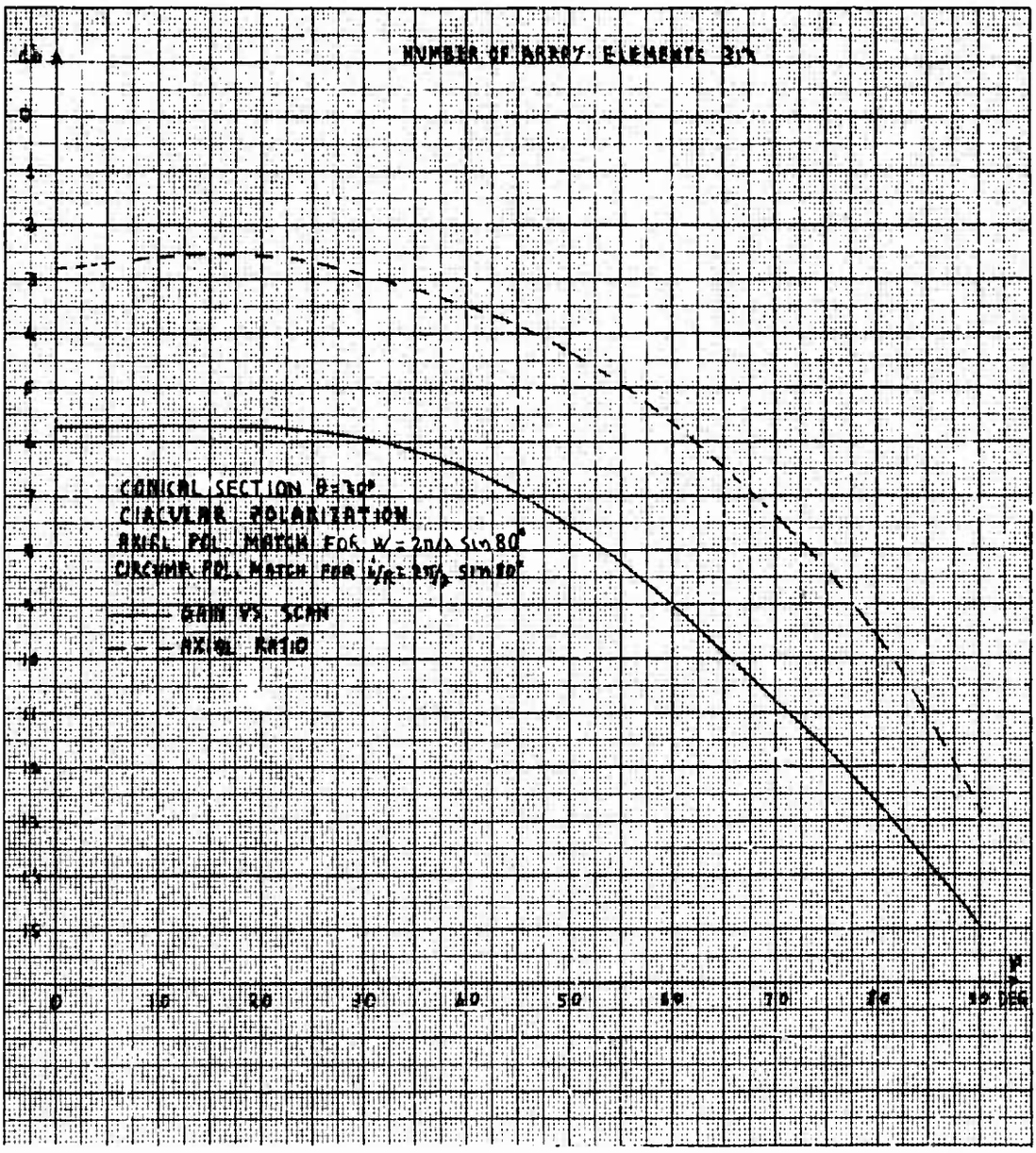


Figure 67 - Array Scan Coverage. Conical Section θ = 30°. Circular Polarization. Number of Array Elements 313

APPENDIX A
ORTHONORMALIZED EIGENEXCITATIONS

The eigenexcitations could be found from the inspection of the form of the scattering matrix (analytical counterpart of the symmetries of the physical structure). The method has been described elsewhere for cylindrical arrays with a finite number of element rings [6]. For the infinite array the procedure is different only for analytical details and therefore will not be discussed here. It can be, however, promptly checked that (7) are in fact eigenexcitations, by observing that any congruence represented by $p\underline{s}_1 + q\underline{s}_2$ with p and q integers have the effect of multiplying (7) by the constant (i. e. independent of m and n)

$$\sqrt{\frac{h}{2\pi N}} \exp[-j\underline{u}_0 (p\underline{s}_1 + q\underline{s}_2)]$$

and recalling that the scattering and symmetry matrices commute. The normalization constant in (7) is determined from the formal statement of completeness, which in this case is written:

$$\sum_{m=0}^{N-1} \sum_{n=-\infty}^{+\infty} e^{+}_{mn} \left(\frac{i}{R}, w_0\right) e_{mn} \left(\frac{k}{R}, w_1\right) = \delta_{ik}\, \delta(w_0 - w_1) \qquad (A1)$$

Introducing into (A1) the expressions (7) of the eigenexcitations, with an undetermined multiplicative constant D, the following relationship is easily obtained:

Preceding page blank

$$D^2 \sum_{n=-\infty}^{+\infty} e^{j(i-k)\frac{\pi}{N}n} e^{j(w_0 - w_1)nh} \sum_{m=0}^{N-1} e^{j(i-k)\frac{2\pi}{N}m} \tag{A2}$$

$$= D^2 \sum_{n=-\infty}^{+\infty} e^{j(w_0 - w_1)nh} N\delta_{ik} = D^2 \frac{2\pi}{h} \delta(w_0 - w_1)\, \delta_{ik} N$$

where the last equality is established by considering the expansion of a periodic delta function and by taking into account the fact that all the longitudinal numbers are obtained by having w wandering in the interval $-\pi/2h \leq w \leq \pi/2h$. This last assertion can be easily justified by considering the reciprocal lattice of points (9) on the plane u, w depicted in figure 3 for $u_o = 0$. It is clear that a "repetive" cell is represented by the rectangle B shadowed in figure 4, i.e. every point of the plane scan belonging to it can be obtained by translating a point of B by $pt_1 + qt_2$ with p and q integers. This shows that every eigenexcitation (7) is uniquely characterized by a point u_o in B. It is to be noticed however that while w can take a continuous range of real values, u_o is limited to take the discrete set of values represented by the integers between -N and N-1.

APPENDIX B
EXPRESSION OF TRANSFORMS OF VECTOR MODE FUNCTIONS

From the expressions of the polar components of the Fourier Transform of the axial and circumferential fundamental modes, given in [10], the rectangular components are easily calculated. They are given below for reference.

Let us consider the wave number plane u, w and let us put

$$t = \sqrt{u^2 + w^2}\ ;\ \cos\mu = \frac{u}{t}\ ;\ \sin\mu = \frac{w}{t}$$

then the u, w components of the Fourier Transform of the fundamental TE_{11} mode circumferentially polarized are given by:

$$\mathcal{E}_{cu} = A\left[-\frac{\cos^2\mu}{t} J_1(at) - \frac{a \sin^2\mu}{1 - \left(\frac{at}{x'_{11}}\right)^2} J_1'(at)\right] \tag{B1}$$

$$\mathcal{E}_{cw} = A\left[-\frac{J_1(at)}{t} + \frac{a J_1'(at)}{1 - \left(\frac{at}{x'_{11}}\right)^2}\right] \sin\mu \cos\mu \tag{B2}$$

For the axial mode, the corresponding components are:

$$\mathcal{E}_{au} = -\mathcal{E}_{cw} \tag{B3}$$

$$\mathcal{E}_{aw} = \left[A \frac{\sin^2 \mu}{t} J_1(at) + \frac{a \cos^2 \mu}{1 - \left(\frac{at}{x'_{11}}\right)^2} J'_1(at) \right] \qquad \text{(B4)}$$

In (B1)-(B4), "a" represents the radius of the radiating element, J_1 is the Bessel function of first kind and order, J'_1 is its derivative and x'_{11} is the first solution of the equation $J'_1(x) = 0$. The amplitude constant

$$A = \frac{\sqrt{\frac{2}{\pi}}}{\sqrt{x'^2_{11} - 1}}$$

is obtained by imposing the normalization condition:

$$\iint \underline{e}_i(\underline{s})\, \underline{e}_k(\underline{s}) dA = \delta_{ik} \qquad \text{(B5)}$$

δ_{ik} being the Kronecker's symbol, and i and k being in this case the subscript c and a.

APPENDIX C

DERIVATION OF THE EXPRESSIONS FOR THE REFLECTION AND MODE CROSS COUPLING COEFFICIENTS

First the expression (21) for the aperture transverse magnetic field will be derived. With reference to Figure 2 the reflection coefficient for the excited axial mode can be expressed through the terminal active admittance:

$$\Gamma_a(\underline{u}_o) = \frac{G_{ao} - \left[G_a(\underline{u}_o) + j\left(B_a(\underline{u}_o) - B_{ao}\right)\right]}{G_{ao} + \left[G_a(\underline{u}_o) + j\left(B_a(\underline{u}_o) - B_{ao}\right)\right]} \tag{C1}$$

The susceptance $-jB_{ao}$ shunts the aperture admittance $G_a(\underline{u}_o) + jB_a(\underline{u}_o)$ therefore the modal current for the axially polarized mode on the aperture section is given by:

$$I_a = \left[1 - \Gamma_a(\underline{u}_o)\right] G_{ao} - \left[1 + \Gamma_a(\underline{u}_o)\right]\left(-jB_{ao}\right) \tag{C2}$$

The modal current for the circumferentially polarized component is on the other hand given evidently by:

$$I_c = - \Gamma_{ac}(\underline{u}_o)\left(G_{co} - jB_{co}\right) \tag{C3}$$

where the minus sign depends upon the convention for the positive sense of current (consistent with C2). From (C2) and (C3), eq. (21) is promptly obtained.

To proceed further it is convenient to use (22-23) and to write the expressions of the z and φ components of the tangential magnetic field on the cylindrical surface as it follows:

$$H_z(R, \xi, z) = \sum_{p=-\infty}^{+\infty} \sum_{q=-\infty}^{+\infty} \left[a(\underline{u}_{opq})\, A_\varphi(\underline{u}_{opq}) + b(\underline{u}_{opq})\, A_z(\underline{u}_{opq}) \right] e^{-j\underline{u}_{opq}\underline{s}} \tag{C4}$$

$$H_\varphi(R, \xi, z) = \sum_{p=-\infty}^{+\infty} \sum_{q=-\infty}^{+\infty} \left[c(\underline{u}_{opq})\, A_\varphi(\underline{u}_{opq}) + d(\underline{u}_{opq})\, A_z(\underline{u}_{opq}) \right] e^{-j\underline{u}_{opq}\underline{s}} \tag{C5}$$

where the expressions for $a(\underline{u}_{opq})$, $b(\underline{u}_{opq})$, $c(\underline{u}_{opq})$ and $d(\underline{u}_{opq})$ are easily established, by comparison with (22) and (23):

$$a(\underline{u}_{opq}) = \frac{4\pi^2 \sqrt{k^2 - w_{opq}^2}}{j k \eta C} \frac{H^{(2)}_{i+pN}\left(R\sqrt{k^2 - w_{opq}^2}\right)}{H^{(2)'}_{i+pN}\left(R\sqrt{k^2 - w_{opq}^2}\right)} \tag{C6}$$

$$b(\underline{u}_{opq}) = \frac{4\pi^2 (i+pN)\, w_{opq}}{j k \eta C R \sqrt{k^2 - w_{opq}^2}} \frac{H^{(2)}_{i+pN}\left(R\sqrt{k^2 - w_{opq}^2}\right)}{H^{(2)'}_{i+pN}\left(R\sqrt{k^2 - w_{opq}^2}\right)} \tag{C7}$$

$$c(\underline{u}_{opq}) = \frac{j 4\pi^2 (i+pN)\, w_{opq}}{k \eta C R \sqrt{k^2 - w_{opq}^2}} \frac{H^{(2)}_{i+pN}\left(R\sqrt{k^2 - w_{opq}^2}\right)}{H^{(2)'}_{i+pN}\left(R\sqrt{k^2 - w_{opq}^2}\right)} \tag{C8}$$

$$d(\underline{u}_{opq}) = \frac{4\pi^2}{jC\eta} \left[\frac{-(i+pN)^2 w_{opq}^2}{k R^2 \sqrt{k^2 - w_{opq}^2}} \frac{H^{(2)}_{i+pN}\left(R\sqrt{k^2 - w_{opq}^2}\right)}{H^{(2)'}_{i+pN}\left(R\sqrt{k^2 - w_{opq}^2}\right)} + \right. \tag{C9}$$

$$\left. + \frac{k}{\sqrt{k^2 - w_{opq}^2}} \frac{H^{(2)'}_{i+pN}\left(R\sqrt{k^2 - w_{opq}^2}\right)}{H^{(2)}_{i+pN}\left(R\sqrt{k^2 - w_{opq}^2}\right)} \right]$$

It is convenient to write the expression of the transverse magnetic field in vector form, combining (C4) and (C5):

$$\underline{H}_t (R, \xi, z) = H_z (R, \xi, z)\, \hat{z} + H_\varphi (R, \xi, z)\, \hat{\varphi} \tag{C10}$$

Applying Galerkin's method, the difference between the expressions (C10) and (21) for the magnetic field is scalarly multiplied by the magnetic field vector mode function $\hat{\rho}_o \times \underline{e}_a(\underline{\varepsilon})$, and integrated over the reference element aperture A. The following equation is obtained:

$$\left[1 - \Gamma_a(\underline{u}_o)\right] G_{ao} + \left[1 + \Gamma_a(\underline{u}_o)\right] jB_{ao} = \iint_A (e_{a\varphi} H_z - e_{az} H_\varphi)\, dA \tag{C11}$$

where $e_{a\varphi}$ and e_{az} are the φ and z components of $\underline{e}_a$, and use has been done of the orthonormalization condition (B5).

In a totally analogous way the other equation is obtained:

$$-\Gamma_{ac}(\underline{u}_o)\,(G_{co} - jB_{co}) = \iint_A (e_{c\varphi} H_z - e_{cz} H_\varphi)\, dA \tag{C12}$$

By introducing (19) and (20) into (22) and (23), the integrals in (C11) and (C12) can be evaluated, making use of the expressions of the Fourier transforms of the vector mode functions, given in Appendix B. The following expressions are thus established:

$$1 - \Gamma_a(\underline{u}_o) = \left[1 + \Gamma_a(\underline{u}_o)\right] \left[L_{aa}(\underline{u}_o) - jB_{ao}\right] + \Gamma_{ac}(\underline{u}_o)\, L_{ac}(\underline{u}_o) \tag{C13}$$

$$-\Gamma_{ac}(\underline{u}_o) = \left[1 + \Gamma_a(\underline{u}_o)\right] L_{ac}(\underline{u}_o) + \Gamma_{ac}(\underline{u}_o) \left[L_{cc}(\underline{u}_o) - jB_{co}\right] \tag{C14}$$

where the coefficients L_{aa}, L_{ac} and L_{cc} are given by:

$$L_{aa}(\underline{u}_o) = \sum_{\underline{u}_{opq}} \left[a\, \mathcal{E}_{av}^2 + b\, \mathcal{E}_{au}\, \mathcal{E}_{aw} - c\, \mathcal{E}_{aw}\, \mathcal{E}_{au} - d\, \mathcal{E}_{aw}^2\right]_{\underline{u}_{opq}} \tag{C15}$$

$$L_{cc}(\underline{u}_o) = \sum_{\underline{u}_{opq}} \left[a \mathcal{E}_{cu}^2 + b \mathcal{E}_{cu} \mathcal{E}_{cw} - c \mathcal{E}_{cw} \mathcal{E}_{cu} - d \mathcal{E}_{cw}^2 \right]_{\underline{u}_{opq}} \tag{C16}$$

$$L_{ac}(\underline{u}_o) = \sum_{\underline{u}_{opq}} \left[a \mathcal{E}_{cu} \mathcal{E}_{au} + b \mathcal{E}_{cu} \mathcal{E}_{aw} - c \mathcal{E}_{cw} \mathcal{E}_{au} - d \mathcal{E}_{cw} \mathcal{E}_{aw} \right]_{\underline{u}_{opq}} \tag{C17}$$

In (C15-C17) the simplified notations used mean that the functions in the square brackets must be calculated in the points of the lattice (9) of the u, w plane. From (C13) and (C14), equations (24) and (25) are promptly established.

APPENDIX D
COMPUTATION OF CYLINDRICAL FUNCTIONS AND SPACE HARMONICS SERIES

As pointed out before, the computation of the radiation from an array over an infinite cylinder involves the evaluation of series representing the admittances of the fundamental modes eq. (24-25) and the array pattern eq. (39). The only difficulty presented by eq. (24-25) to computation arises from the presence of ratios of Hankel functions $\frac{H_n^{(2)}(x)}{H_n^{(2)'}(x)}$ for $|w_o| < k$ and ratios of modified Bessel functions $\frac{K_n(x)}{K_n'(x)}$ for $|w_o| > k$, since series of these functions are slowly converging. The array pattern eq. (35) consists of a series of $\frac{1}{H_n^{(2)}(x)}$ and $\frac{1}{H_n^{(2)'}(x)}$, which are of easier evaluation than the series mentioned before, since they converge very rapidly for $n > x$. On this basis, the only numerical problem one faces is the computer evaluation, with high speed and precision, of a very large number of $J_n(x)$, $Y_n(x)$ and $K_n(x)$ Bessel functions. This difficulty can be overcome by making use of the recurrence formulas peculiar of these kinds of functions.

For the $J_n(x)$ the recurrence formula is computationaly very stable, i.e. no precision is lost by repeated application, for decreasing values of n and for constant argument x. Since $J_n(x) \to 0$ for $n >> x$, the generation of the $J_n(x)$ can procede as follows. Set $J_m(x) = 0$ for $m \approx 2|x|$ and $J_{m-1}(x)$ equal to a small number; then by repeated use of the recurrence formula all $J_n(x)$ are generated except for a constant factor, computed by imposing $J_o(x) + 2\sum J_{2n}(x) = 1$.

The recurrence formula for $Y_n(x)$ is stable for increasing values of n. From the computation of the $J_n(x)$, the $Y_o(x)$ can be readily evaluated from the equation $Y_o(x) = \frac{2}{\pi}\left[\gamma + \log\frac{1}{2}x\right] J_o(x) - \frac{4}{\pi}\sum_K (-1)^K \frac{J_{2K}(x)}{K}$ (γ = Euler's constant) and $Y_1(x)$ through the Wronskian relations. Then by repeated use of the recurrence formula all desired $Y_n(x)$ are computed. A similar procedure is applied for the evaluation of the $K_n(x)$ functions.

The computational method just outlined enables the achievement of relative precisions of 10^{-16} and high speed. On the computer UNIVAC 1108 an estimated time of 20 μsec is required for the evaluation of a single Bessel function. The same computer time is necessary for the generation of a value of a sine or cosine function.

Given the convenience of computing Bessel functions for constant argument and variable order, the space harmonics of eq. (24-25) and (35) are generated for constant values of w and each series for the index i is then evaluated. Relative precision of 10^{-8} has been achieved all through the computations of $L_{aa}(\underline{u}_o)$, $L_{cc}(\underline{u}_o)$, $L_{ac}(\underline{u}_o)$ of (24-25) and of the radiation pattern of (35).

REFERENCES

(1) G. V. Borgiotti "Mutual coupling effects on arrays of slots on a cylinder" 1969 U.R.S.I. Spring Meeting - Washington, D.C., April 1969.

(2) J. C. Sureau and A. Hessel "Element pattern for circular arrays of axial slits on large conducting cylinder" IEEE Transactions on Ant. and Prop. vol AP. 17 n.6 pp 799-803 November 1969.

(3) G. V. Borgiotti and Q. Balzano "Mutual coupling analysis of a conformal array of elements on a cylindrical surface" IEEE Trans. on Ant. and Prop. Vol. AP-18, No. 1, pp 55-63, January 1970.

(4) B. R. Gladman "Mutual coupling on cylindrical array antennas" Proceedings of the Conformal Array Antenna Conference, Naval Electronics Laboratory Center, San Diego, California, January 13-15, 1970.

(5) J. C. Sureau and A. Hessel "Realized gain function for a cylindrical array of open-ended waveguides" 1970 Phased Array Antenna Symposium, Polytechnic Institute of Brooklyn, June 2-5, 1970.

(6) G. V. Borgiotti and Q. Balzano "Conformal arrays on surfaces with rotational symmetry" Phased Array Antenna Symposium, Polytechnic Institute of Brooklyn, June 2-5, 1970.

(7) R. C. Hansen (Editor) "Microwave scanning antennas" Academic Press, New York 1966, Chapter 3, pp 209 and foll.

(8) C. G. Montgomery, R. H. Dicke and E. M. Purcell "Principles of Microwave Circuits" Chapter 12.

(9) G. V. Borgiotti "Impedance and gain of a dipole in an infinite periodic phased array" Research Triangle Institute, Durham, N. C., Technical Report, RTI TMR-25, March 1966.

(10) G. V. Borgiotti "Modal analysis of periodic planar phased arrays of apertures" IEEE Proceedings, Vol. 56, No. 11, November 1968, pp 1881-1892.

(11) N. Amitay and V. Galindo: "The Analysis of Circular Waveguide Phased Arrays" Bell Syst. Tech. J. Vol. 47, pp. 1903-1932, November 1968.

REFERENCES (Cont.)

(12) G. V. Borgiotti and Quirino Balzano "Analysis of periodic phased arrays of circular apertures" IEEE Transactions on Antennas and Propagation Vol AP-17, No. 2, March 1969, pp 224-226.

(13) N. Amitay and V. Galindo, "On Energy Conservation and the Method of Moments in Scattering Problems", IEEE Trans, AP-17, pp 747-751, 1970.

(14) S. W. Lee, W. R. Jones and J. J. Campbell "Convergence of Numerical Solutions of Iris Type Discontinuity Problems", Hughes Aircraft Company, FR 70-14-594, 31 August 1970.

(15) R. Mittra "Relative Convergence of the Solution of a Doubly Periodic Infinite Set of Equations", J. Res. NBS, 67D, 1963, pp 245-252.

UNCLASSIFIED
Security Classification

DOCUMENT CONTROL DATA - R & D

(Security classification of title, body of abstract and indexing annotation must be entered when the overall report is classified)

1. ORIGINATING ACTIVITY (Corporate author)	2a. REPORT SECURITY CLASSIFICATION
Raytheon Missile Systems Division Radar Laboratory Bedford, Massachusetts 01730	Unclassified
	2b. GROUP

3. REPORT TITLE

ANALYSIS AND ELEMENT PATTERN DESIGN OF PERIODIC ARRAYS OF CIRCULAR APERTURES ON CONDUCTING CYLINDERS.

4. DESCRIPTIVE NOTES (Type of report and inclusive dates)

Scientific Interim

5. AUTHOR(S) (First name, middle initial, last name)

Giorgio V. Borgiotti
Quirino Balzano

6. REPORT DATE	7a. TOTAL NO. OF PAGES	7b. NO. OF REFS
November 1970	128	15

8a. CONTRACT OR GRANT NO.	9a. ORIGINATOR'S REPORT NUMBER(S)
F19628-70-C-0226	BR-6129 Scientific Report No. 1
b. Project, Task, Work Unit Nos. 4600-10-01 c. DoD Element: 62702F d. DoD Subelement: 674600	9b. OTHER REPORT NO(S) (Any other numbers that may be assigned this report) AFCRL-70-0632

10. DISTRIBUTION STATEMENT

This document has been approved for public release and sale; its distribution is unlimited.

11. SUPPLEMENTARY NOTES	12. SPONSORING MILITARY ACTIVITY
TECH. OTHER	Air Force Cambridge Research Laboratories (LZ) L. G. Hanscom Field Bedford, Massachusetts 01730

13. ABSTRACT

The analysis and the design of the elements of a large array of circular apertures on a triangular grid is approached by modeling the antenna as an infinite structure rotationally symmetric and periodic along the cylinder axis. Because of this particular symmetry every possible excitation is the superposition, with suitable weights, of a set of fundamental excitations having uniform magnitude and linear phase progression in the azimuthal direction and in the direction of the cylinder axis ("eigenexcitations"). Thus, by invoking superposition the electromagnetic analysis of the array is reduced to the solutions of the simpler boundary value problems pertinent to the set of eigenexcitations. This is done by expanding the field in normal modes in the region exterior to the cylinder and in the waveguides feeding the apertures, followed by a field matching at the cylinder surface (obtained approximately through Galerkin's method). The realized gain pattern of the radiators can be modified to a considerable extent by using an "element pattern shaping network" (in the radiator waveguides), serving the purpose of matching the array for a selected eigenexcitation. Criteria for the network design are given. A series of numerical examples illustrates the technique and shows that a "flat" element pattern can be thus obtained with a gain fall off with respect to the peak of less than 6 db at 80 degrees.

DD FORM 1 NOV 68 1473 REPLACES DD FORM 1473, 1 JAN 64, WHICH IS OBSOLETE FOR ARMY USE.

UNCLASSIFIED
Security Classification

14. KEY WORDS	LINK A		LINK B		LINK C	
	ROLE	WT	ROLE	WT	ROLE	WT
Conformal Arrays Element Pattern Design Wide Angle Coverage Phased Arrays						

INSTRUCTIONS TO FILL OUT DD FORM 1473 - DOCUMENT CONTROL DATA
(See ASPR 4-211)

1. ORIGINATING ACTIVITY: Enter the name and address of the contractor, subcontractor, grantee, Department of Defense activity or other organization *(corporate author)* issuing the report.

2a. REPORT SECURITY CLASSIFICATION: Enter the overall security classification of the report. Indicate whether "Restricted Data" is included. Marking is to be in accordance with appropriate security regulations.

2b. GROUP: Automatic downgrading is specified in DoD directive 5200.10 and Armed Forces Industrial Security Manual. Enter the group number. Also, when applicable, show that optional markings have been used for Group 3 and Group 4 as authorized.

3. REPORT TITLE: Enter the complete report title in all capital letters. Titles in all cases should be unclassified. If a meaningful title cannot be selected without classification, show title classification in all capitals in parenthesis immediately following the title.

4. DESCRIPTIVE NOTES: If appropriate, enter the type of report, e.g., interim, progress, summary, annual, or final. Give the inclusive dates when a specific reporting period is covered.

5. AUTHOR(S): Enter the name(s) of the author(s) in normal order, e.g., full first name, middle initial, last name. If military, show grade and branch of service. The name of the principal author is a minimum requirement.

6. REPORT DATE: Enter the date of the report as day, month, year; or month, year. If more than one date appears on the report, use date of publication.

7a. TOTAL NUMBER OF PAGES: The total page count should follow normal pagination procedures, i.e., enter the number of pages containing information.

7b. NUMBER OF REFERENCES: Enter the total number of references cited in the report.

8a. CONTRACT OR GRANT NUMBER: If appropriate, enter the applicable number of the contract or grant under which the report was written.

8b, 8c, and 8d. PROJECT NUMBER: Enter the appropriate military department identification, such as project number, task area number, systems numbers, work unit number, etc.

9a. ORIGINATOR'S REPORT NUMBER(S): Enter the official report number by which the document will be identified and controlled by the originating activity. This number must be unique to this report.

9b. OTHER REPORT NUMBER(S): If the report has been assigned any other report numbers *(either by the originator or by the sponsor)*, also enter this number(s).

10. DISTRIBUTION STATEMENT: Enter the one distribution statement pertaining to the report.

Contractor-Imposed Distribution Statement

The Armed Services Procurement Regulations *(ASPR), para 9-203* stipulates that each piece of data to which limited rights are to be asserted must be marked with the following legend:

> "Furnished under United States Government Contract No._____. Shall not be either released outside the Government, or used, duplicated, or disclosed in whole or in part for manufacture or procurement, without the written permission of _____, except for: (i) emergency repair or overhaul work by or for the Government, where the item or process concerned is not otherwise reasonably available to enable timely performance of the work; or (ii) release to a foreign government, as the interests of the United States may require; provided that in either case the release, use, duplication or disclosure hereof shall be subject to the foregoing limitations. This legend shall be marked on any reproduction hereof in whole or in part."

If the above statement is to be used on this form, enter the following abbreviated statement:

"Furnished under U. S. Government Contract No._____. Shall not be either released outside the Government, or used, duplicated, or disclosed in whole or in part for manufacture or procurement, without the written permission of_____, per ASPR 9-203."

DoD Imposed Distribution Statements *(reference DoD Directive 5200.20)* "Distribution Statements *(Other than Security)* on Technical Documents," March 29, 1965.

STATEMENT NO. 1 - Distribution of this document is unlimited.

STATEMENT NO. 2 (UNCLASSIFIED document) - This document is subject to special export controls and each transmittal to foreign governments or foreign nationals may be made only with prior approval of *(fill in controlling DoD office)*.

(CLASSIFIED document) - In addition to security requirements which must be met, this document is subject to special export controls and each transmittal to foreign governments or foreign nationals may be made only with prior approval *(fill in controlling DoD Office)*.

STATEMENT NO. 3 (UNCLASSIFIED document) - Each transmittal of this document outside the agencies of the U. S. Government must have prior approval of *(fill in controlling DoD Office)*.

(CLASSIFIED document) - In addition to security requirements which apply to this document and must be met, each transmittal outside the agencies of the U. S. Government must have prior approval of *(fill in controlling DoD Office)*.

STATEMENT NO. 4 (UNCLASSIFIED document) - Each transmittal of this document outside the Department of Defense must have prior approval of *(fill in controlling DoD Office)*.

(CLASSIFIED document) - In addition to security requirements which apply to this document and must be met, each transmittal outside the Department of Defense must have prior approval of *(fill in controlling DoD Office)*.

STATEMENT NO. 5 (UNCLASSIFIED document) - This document may be further distributed by any holder only with specific prior approval of *(fill in controlling DoD Office)*.

(CLASSIFIED document) - In addition to security requirements which apply to this document and must be met, it may be further distributed by the holder ONLY with specific prior approval of *(fill in controlling DoD Office)*.

11. SUPPLEMENTARY NOTES: Use for additional explanatory notes.

12. SPONSORING MILITARY ACTIVITY: Enter the name of the departmental project office or laboratory sponsoring *(paying for)* the research and development. Include address.

13. ABSTRACT: Enter an abstract giving a brief and factual summary of the document indicative of the report, even though it may also appear elsewhere in the body of the technical report. If additional space is required, a continuation sheet shall be attached.

It is highly desirable that the abstract of classified reports be unclassified. Each paragraph of the abstract shall end with an indication of the military security classification of the information in the paragraph, represented as *(TS)*, *(S)*, *(C)*, or *(U)*.

There is no limitation on the length of the abstract. However, the suggested length is from 150 to 225 words.

14. KEY WORDS: Key words are technically meaningful terms or short phrases that characterize a report and may be used as index entries for cataloging the report. Key words must be selected so that no security classification is required. Identifiers, such as equipment model designation, trade name, military project code name, geographic location, may be used as key words but will be followed by an indication of technical context. The assignment of links, roles, and weights is optional.